On the modeling of a bistable beam with application to energy harvesting

vorgelegt von
M. Sc.
Max-Uwe Noll

an der Fakultät V – Verkehrs- und Maschinensysteme
der Technischen Universität Berlin
zur Erlangung des akademischen Grades

Doktor der Ingenieurwissenschaften
– Dr.-Ing. –

genehmigte Dissertation

Promotionsausschuss:

Vorsitzender: Prof. Dr. rer. nat. Wolfgang H. Mueller
Gutachter: Prof. Dr.-Ing. Utz von Wagner
Gutachter: Prof. Dr.-Ing. Norbert Hoffmann

Tag der wissenschaftlichen Aussprache: 20.02.2020

Berlin 2020

Abstract

The term energy harvesting refers to various strategies to transform small amounts of ambient energy into a useful form. When the available energy is of a kinetic type, an energy harvester is often designed as a mechanical oscillator, made of a bending beam structure and attached piezoelectric patches to transform motion energy into electrical energy. One specific harvester has attracted a lot of attention, due to its potentially higher efficiency for energy harvesting purposes. It consists additionally of two permanent magnets near the free end of the beam, which is itself ferromagnetic. As a result, the system is nonlinear with two stable states for the deformed beam. When the piezoelectric part is neglected, the system is reduced to a bistable beam and its dynamics is most often described by the bistable Duffing oscillator equation with a cubic part in the restoring terms. This model has been extensively studied in literature. However, the assumptions which are necessary to reduce the reality of an experimental setup of a bistable beam to this type of model, have so far not been studied as extensively. Hence, the validity of the theoretical predictions for an actual experimental setup is often doubtful. Typically, the bistable Duffing oscillator is initially set to be a sufficient model and just adapted to an experimental setup by a heuristic method. A consequential drawback is that there is no direct connection between the model and the physical parameters of the setup. It is, therefore, not clear how the physical setup should be changed once the model parameters are changed, for example, when optimizing the model parameters in regards of its efficiency.

The thesis presented here is a step towards a more sophisticated modeling of such an experimental setup of a bistable beam. It is a cumulative dissertation based on three publications, each dealing with specific aspects of the model assumptions usually made in literature. Among these assumptions, the most important ones are that the influence of the magnetic field can be approximated by a single force, which is concentrated at the beam tip and is cubically dependent on the beam's displacement, and that the beam shape stays constant during vibrations, with only its amplitude changing over time.

In the first publication, the magnetoelastic force is of main interest. One of the article's goals is to present an alternative to the mentioned heuristic modeling by determining the magnetic force numerically. An analysis of the bifurcation behavior of the system's stable states for different magnet distances was conducted to compare the model with the experiments. At present, the accuracy of the achieved results is unsatisfactory, because the magnetic field cannot be sufficiently approximated through a two-dimensional simulation, as further investigations revealed. The second publication investigates the shape of the deformed beam during forced vibrations. An analysis of picture sequences of the beam taken by a high speed camera during forced vibrations and subsequent digital image processing shows that the assumption of one constant beam shape is sufficient in most cases. A second constant function is required only when superharmonic responses occur. The third publication compares the experimental setup's stationary response to the predictions of a corresponding Duffing model. A direct comparison of explicit solutions cannot be performed, since the steady state solution of the nonlinear system depends on the initial conditions, which cannot be controlled on the experimental setup. A comparison, conducted between a large amount of experiments and many time integrations shows that they are of good accordance, but a shift of the occurred type of solutions to higher frequencies is observed in the numerical case.

In conclusion, the predictions of a bistable Duffing model are, generally, in good agreement with the experimental results of the setup considered, and deviate only in some aspects, as this dissertation describes. This thesis thus constitutes a link between the heuristic modeling approach discussed in literature and a model that will enable an optimization of the underlying energy harvesting system in future.

Kurzzusammenfassung

Energy Harvesting ist ein Sammelbegriff für sämtliche Strategien, wie kleine Mengen bereits vorhandener Energie aus der Umgebung technisch nutzbar gemacht werden können. Wenn es sich um Bewegungsenergie handelt, sind Energy Harvesting Systeme oft aus einer schwingungsfähigen Balkenstruktur aufgebaut, an der zur Energieumwandlung Piezos angebracht sind. Ein spezieller Aufbau hat dabei in der Literatur viel Aufmerksamkeit erhalten, da er sich unter bestimmten Umständen als besonders effizient herausgestellt hat. Er hat die Besonderheit, dass in der Nähe der Balkenspitze zusätzlich zwei Permanentmagnete platziert sind, weshalb sich das System durch ein ausgeprägtes nichtlineares Verhalten kennzeichnet und zwei stabile Gleichgewichtslagen für den Balken aufweist. Für den Fall, dass die Piezos aus der Betrachtung ausgeschlossen werden, verbleibt ein sogenannter bistabiler Balken, dessen Dynamik in der Literatur zumeist durch die bistabile Duffinggleichung beschrieben wird, die durch eine kubische Nichtlinearität in der Rückstellung gekennzeichnet ist. Jedoch sind die Modellannahmen, die von einem realen Aufbau auf diese Duffinggleichung führen, nicht gleichermaßen abgedeckt. Daraus folgt, dass die Modellvorhersagen nicht uneingeschränkt auch für einen physischen Aufbau gelten. Darüber hinaus wird die Gültigkeit des bistabilen Duffings häufig einfach vorausgesetzt und dieses Modell heuristisch für den zu untersuchenden Aufbau angepasst. Das bedeutet im Umkehrschluss, dass das Modell nicht von den spezifischen Eigenschaften des Aufbaus abgeleitet wird und deshalb auch nicht klar ist, wie der physische Aufbau entsprechend zu ändern ist, wenn die Modellparameter verändert werden, beispielsweise im Zuge einer Optimierung.

Die vorliegende Arbeit ist der Versuch, die Modellierung eines solchen bistabilen Balkens zu verbessern. Es handelt sich um eine kumulative Arbeit, bestehend aus drei Veröffentlichungen, die sich jeweils verschiedenen Modellierungsaspekten des bistabilen Balkens widmen. Die wichtigsten davon sind, dass sich das Magnetfeld in seiner Wirkung auf eine Einzelkraft an der Balkenspitze reduzieren lässt, die kubisch von dessen Auslenkung abhängt. Außerdem wird angenommen, dass die Deformation des Balkens stets durch lediglich eine feste Funktion beschrieben werden kann.

In der ersten Veröffentlichung stehen die aus dem Magnetfeld resultierende Kraft und ihre numerische Bestimmung im Mittelpunkt. Das Ziel in dieser Publikation ist es, ein alternatives Verfahren zu der heuristischen Herangehensweise zu entwickeln. Die Ergebnisse aus Theorie und Experiment werden anhand des Verzweigungsverhaltens der Ruhelagen für verschiede Magnetabstände verglichen. Es muss konstatiert werden, dass die Ergebnisse soweit noch keine zufriedenstellende Genauigkeit aufweisen, da das Magnetfeld nicht zureichend durch eine zweidimensionale Simulation approximiert werden kann, wie in weiterführenden Untersuchungen festgestellt wurde. Die zweite Veröffentlichung behandelt die Frage nach der Schwingform des Balkens bei erzwungenen Schwingungen. Dafür wurden mit einer Highspeed-Kamera Aufzeichnungen gemacht, aus denen nach einer Bild-für-Bild Analyse ermittelt werden konnte, dass die Verformung des Balkens zum größten Teil durch eine feste Form beschrieben werden kann und eine weitere nur bei superharmonischen Antworten benötigt wird. In der dritten Veröffentlichung werden die Vorhersagen eines entsprechenden heuristischen Modells bezüglich der stationären Systemantworten für eine harmonische Anregung mit denen des experimentellen Aufbaus verglichen. Dazu wurden zahlreiche Experimente mit den theoretischen Zeitverläufen aus numerischen Zeitintegrationen verglichen. Die Ergebnisse stimmen großteils gut überein, jedoch besteht auf numerischer Seite eine Verschiebung der auftretenden Arten von Lösungen zu höheren Frequenzen.

Insgesamt stellt die Duffinggleichung in weiten Bereichen ein geeignetes Minimalmodell dar, aber kann in wenigen, oben beschriebenen, Details unzulänglich sein. Diese Arbeit stellt einen Zwischenschritt zwischen einem heuristischen Modell und einem zukünftigen Modell dar, das eine Optimierung des Systems anhand seiner spezifischen Eigenschaften ermöglicht.

List of publications

This cumulative dissertation is composed of the following three publications:

• [Noll et al., 2019a]: Noll, M.-U., Lentz, L., and von Wagner, U. (2019a). On the improved modeling of the magnetoelastic force in a vibrational energy harvesting system. *Journal of Vibration Engineering & Technologies*, Pp. 1-11.
doi: https://doi.org/10.1007/s42417-019-00159-4
status: 'published'

• [Noll et al., 2019b]: Noll, M.-U., Lentz, L., and von Wagner, U. (2019b). On the discretization of a bistable cantilever beam with application to energy harvesting. *Facta Universitatis, Series: Mechanical Engineering*, 17(2):125-139.
doi: https://doi.org/10.22190/FUME190301031N
status: 'published'

• [Noll et al., 2020]: Noll, M.-U., Lentz, L., and von Wagner, U. (2020). Comparison of the dynamics of a Duffing equation model and experimental results for a bistable cantilever beam in magnetoelastic energy harvesting. submitted for publication in *Technische Mechanik. Scientific Journal for Fundamentals and Applications of Engineering Mechanics.*
status: 'submitted'

Contents

1 Introduction

Energy harvesting is a term which refers to strategies for capturing ambient energy already available in the environment, which is simply lost for technical purposes if it remains unused. This technology is distinct from energy generation on large scales as renewable energy, since its goal is to convert only small amounts of energy into a useful form, usually electricity. The harvested energy is just sufficient to run small electric devices, which are currently most often powered by batteries [Shaikh and Zeadally, 2016; Tang et al., 2018], which are finite sources of energy. Energy harvesting techniques hold the potential, in many applications, to avoid battery replacements, which entail high cost and considerable chemical waste production. Typical applications of low power electronic devices powered by energy harvesting systems are animal tracking [Wu et al., 2014], environmental or structural health monitoring [Matiko et al., 2013; Park et al., 2008], or medical devices [Paulo and Gaspar, 2010]. An earlier overview of the versatile applications of energy harvesters was published more than a decade ago [Gilbert and Balouchi, 2008] and their relevance is still growing today [Adu-Manu et al., 2018; Safaei et al., 2019].

The principle of energy conversion in any energy harvester primarily depends on the nature of the ambient energy. Possible sources are temperature gradients, solar energy, electromagnetic waves or kinetic energy in the form of vibrations [Harb, 2011; Tang et al., 2018]. Strategies in the last case are comparatively new when contrasted with well-established applications like, for example, solar powered calculators, which are now known for 40 years [Brand et al., 2015]. One of the earliest mentions of the idea of vibration-to-electricity conversion appeared in [Williams and Yates, 1996]. Since then, motion-based energy harvesting approaches have been a major interest of international research, resulting in a well-established fundamental theory covered in many related introductory textbooks [Erturk and Inman, 2011a; Brand et al., 2015; Rafique et al., 2018].

There are three main transduction mechanisms for vibration-to-electricity energy conversion given in [Williams and Yates, 1996] as electromagnetic, electrostatic and piezoelectric transductions. A comparison of the number of publications which have appeared using each of these three transduction alternatives reveals that piezoelectric transduction has received the most attention [Toprak and Tigli, 2014]. Piezoceramics are made of special crystalline materials that accumulate electric charges in response to applied mechanical stress, which is called the direct piezoelectric effect. Piezoelectric materials are preferred because of their high energy density and their ease of application [Caliò et al., 2014]. When mechanical strain is applied, usable voltage output can be obtained directly from the piezoelectric material itself, which eliminates the need for an external voltage input.

A typical vibration-based piezoelectric energy harvester is a cantilever beam with attached piezoceramic layers [Anton and Sodano, 2007; Kim et al., 2011]. The harvester beam is located on an exterior vibrating host structure, that excites the system by its motion. Thereby, dynamic strain is induced in the piezoceramics by a temporally varying deformation of the bending beam, which results in an alternating voltage output across their electrodes. When a harmonic external excitation of known and fixed frequency is present, such energy harvesters show their best performance when they are designed as linear resonators with their base frequency tuned to the excitation frequency. However, real-world excitations are most commonly not mono-frequent, but show broadband frequencies, are partly stochastic or change over time [Roundy et al., 2003; Reilly et al., 2009; Lentz et al., 2017]. In these cases, where there is a mismatch between the excitation frequency and the resonance frequency of the system, their power output decreases drastically [Fakhzan and Muthalif, 2013; Wang and Meng, 2013; Lumentut and Howard, 2013].

To overcome this design bottleneck, many strategies are developed to widen the frequency range with high power outputs of primarily linear energy harvesting systems. Earlier reviews on strategies

to enlarge the applicable frequency range are [Ibrahim and Ali, 2012; Tang et al., 2010; Twiefel and Westermann, 2013], and this remains of high interest today [Yildirim et al., 2017; Wei and Jing, 2017; Maamer et al., 2019]. Right from the start, parallel to the improvements of energy harvesters that can be described by linear models, the ambitious approach was made to purposely introduce nonlinearities to the system to increase its efficiency, which can be done by many different mechanisms. The number of review papers summarizing the even larger number of individual publications are a proof of their diversity and the general interest in nonlinear vibrational energy harvesting systems [Pellegrini et al., 2013; Harne and Wang, 2013; Daqaq et al., 2014; Wei and Jing, 2017; Tran et al., 2018].

Clearly, nonlinearities exist, at least to some extent, in any real mechanical system, but can most often be dealt with by a linearization of the underlying equations, which, in many cases, yields a good approximation of the system. The linearization is done around a given point of interest, which is, in the case of vibrational energy harvesting systems with a beam structure, most often the undeflected beam position. This is an equilibrium, a state where all forces (and moments) cancel each other out, and the total force is zero. Hence, in this state, the beam is able to rest when no excitation is present. However, the nonlinear mechanisms in nonlinear energy harvesting systems are designed to be so distinct that more than one equilibrium position exist. In many cases a linearization cannot be performed to describe the overall behavior of the system in all regions. This so called multistability can differ in its degree, where two, three, or more stable equilibria may exist. Note that when more than one stable equilibrium exists, also unstable ones exist. In the past, most publications have been on bistable systems with two stable equilibria and one unstable equilibrium, but the interest in systems with more than two stable equilibrium positions is rising [Zhou et al., 2014; Cao et al., 2015; Zhou et al., 2016; Zhou et al., 2018; Zhou and Zuo, 2018].

Bistability in energy harvesting systems is often achieved through the use of permanent magnets, which primarily cause magnetic forces on the (necessarily ferromagnetic) beam that depend on the beam's deformation. In synergy with the pure mechanical force from the beam bending, the magnetic force changes the overall restoring force, which is the force that brings the system towards the stable equilibrium positions and vanishes in any equilibria, stable or non-stable. Magnets offer favorable characteristics in terms of a purposed design of the system's nonlinearity, simply by the choice (number, dimensions, strength) and positioning of the permanent magnets. Adding magnets to a primarily linear system potentially increases its efficiency, but a direct comparison of a nonlinear magnetoelastic system to its linear counterpart, where the magnets have simply been removed, lacks significance, since both systems perform best in different excitation scenarios. When the excitation is not harmonic but distributed in a certain range and is of a sufficient amplitude, a bistable system holds more potential for energy harvesting purposes. Especially when the beam tip orbits both stable equilibrium positions, a high power output is expected, due to frequent large deformations of the beam and the piezos respectively [Erturk and Inman, 2011b].

The aspect of optimization and performance enhancement is omnipresent in literature concerning energy harvesting systems, since the scope of applications increases with more power generated by any energy harvester. The design of an energy harvesting system can be considered equivalent to the problem of an optimization in which the harvested energy is the target for maximization. Although appropriate sources of energy are modeled to be endless, they are limited in the rate of energy they provide; more precisely, in their power. Therefore, the harvester's efficiency, as the ratio of input to output power, is a key factor. The optimal design of an efficient energy harvesting system requires configurational options to be adapted specifically, with a specific application in mind depending on the energy demand of the device and the invariable external excitation process. The crucial question is how to design the energy harvesting system in order to achieve the largest electric power output for an existing excitation. For nonlinear systems, this optimization problem cannot be solved

exactly due to the lack of closed forms to describe the system's responses, in contrast to linear systems [Kim et al., 2015]. When optimizing the design of a given nonlinear magnetoelastic energy harvesting system to achieve a high efficiency, most approaches are to purposefully manipulate the restoring force of the system, which can simply be accomplished through a targeted positioning of the magnets. Therefore, various magnet arrangements have been proposed, with attracting or repelling magnetic forces. The aim is to ensure frequent changes of the system between the stable equilibria through small force barriers between them [Lan and Qin, 2017]. In this way, attempts are made to change the nonlinear restoring force to find beneficial configurations as regards the efficiency, as for example done in [Zhou et al., 2013] by trial and error on an experimental setup.

If not optimized experimentally, most publications follow a standard modeling approach. It is noteworthy that the modeling approaches to describe the mechanical part of each individual bistable energy harvesting system in all publications known to the author finally end in the same type of model, known as the Duffing oscillator. In the field of nonlinear dynamics, it is a popular equation with a nonlinearity due to a cubic term in the restoring force. The sheer variety of bistable energy harvesting systems that are modeled by a Duffing type equation with a cubic term as the only source of nonlinearity underlines the approximative character of these models. Many simplifications may result due to the topic being spread over numerous different fields of study, and early attempts to develop minimal models of predictive character [Erturk and Inman, 2011a]. Often, the bistable Duffing equation is simply stated as a suitable model for the mechanical subsystem of the energy harvester e.g. [Litak et al., 2010; Martens et al., 2013; Lentz and von Wagner, 2015; Lentz et al., 2017]. In such cases, an optimization of the model with respect to the model parameters is possible. In this regard, the Duffing equation offers certain degrees of freedom, in specific the two parameters for the linear and cubic restoring terms, which can be influenced, at least theoretically, just by the choice of the magnet positioning. In this way, [Martens et al., 2013] has investigated the Duffing equation for a good choice of model parameters. However, since the model is found heuristically in the first place, there is no direct relation to the physical setup anymore once the model parameters are adjusted. It is not known how to build or to change the existing setup to realize a configuration that leads to the corresponding optimal model parameters. The only possibility to enable a modeling where there is a direct relation between the physical setup and a model is to model each element of the setup with its underlying physical laws. This is the key step towards an optimization process, where many modifications of one setup are compared to one another by their model.

Since a wide variety of different systems and configurations of energy harvester concepts with proven potential to harvest energy have already been presented in existing literature, the next step is to take a closer look at the detailed modeling of a specific harvester. Only in this way a targeted design and adaption of any harvester to a specific application is possible. The thesis here presented is intended to be a link between the approximative models in literature and a refined model, which will enable an optimization of a specific energy harvesting system in future. The harvester which is the focus of this thesis is one early concepts towards magnetoelastic bistable energy harvesting and was introduced in the year of 2009 in [Erturk et al., 2009]. Its explicit configuration and corresponding state-of-the-art modeling is a key interest and, therefore, the next section is dedicated to it. The following sections outline reasons for revising the modeling methods described in existing literature, and, in doing so, will lead to the motivation for this dissertation. The thesis then moves on to present the preliminary investigations forming a basis for the three papers (two already published, one submitted) of this cumulative dissertation, which are detailed investigations of the model for the energy harvester.

This study was funded by Deutsche Forschungsgemeinschaft (DFG, German Research Foundation) - WA 1427/23-1,2.

2 The considered energy harvesting system and its treatment in literature

The main objective of this thesis is the modeling of a particular energy harvesting system that was introduced in 2009 in [Erturk et al., 2009]. It is schematically shown in figure 1. Broadly speaking, it comprises three main basic features: first, a slender beam structure that bends when it is excited by its base; second, two symmetrically-placed permanent magnets near the beam's free end; and third, piezoceramics attached at the beam clamping. The piezos are connected to an ohmic resistor to assemble an energy harvesting system with the simplest electric load possible. In the aforementioned first appearance of this particular energy harvesting system, the equation of motion is stated by citing the paper of [Moon and Holmes, 1979] from 1979, in which Moon and Holmes investigated a bistable beam that can be considered as sub-system of the energy harvester in figure 1, shown in figure 2. At the time when this system – which will be referred to as the considered sub-system in this thesis – was first investigated, the focus was on chaotic oscillations in a mechanical system. The authors state that they believe they were the first to observe experimental evidence of the existence of a so-called strange attractor undergoing chaotic motions in structural mechanics. The ability to exhibit chaotic motions implies that it is a non-linear system that's characteristics cannot satisfyingly be modeled by linearized equations.

Although the present thesis is motivated by investigations into the modeling of the energy harvesting system of Erturk, for the sake of simplicity the piezoceramics are neglected here, despite their mechanical and piezoelectrical influence, which is described in detail e.g. in [Lentz, 2018]. Hence, the investigations are thematically closer to the sub-system in figure 2. However, the following investigations are made without a loss of generality of the results for a system with piezoceramics, because they can be added to the model later, once the more challenging modeling of the mechanical sub-system is completed.

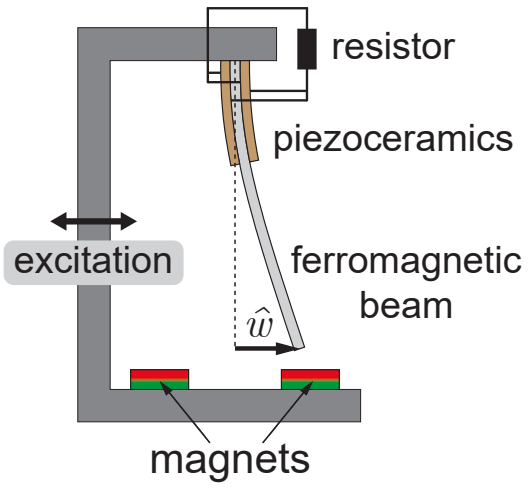

Fig. 1 Energy harvesting system by [Erturk et al., 2009]. Figure taken from [Noll, 2018].

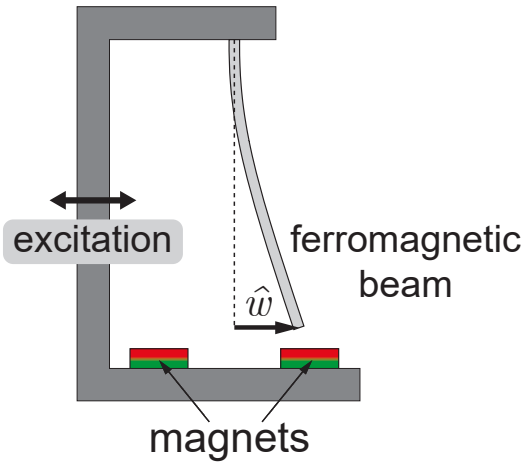

Fig. 2 Bistable beam (considered mechanical subsystem of the energy harvesting system in figure 1), first investigated in [Moon and Holmes, 1979]. Modified figure of [Noll, 2018] with removed piezoelectric part.

In the following, the literature regarding the modeling of the system in figure 1 and 2 respectively is described, now chronologically.

Moon: As previously mentioned, Moon and Holmes investigated the setup in figure 2. Prior to the work that introduces the setup, different other works of Moon [Moon and Pao, 1968; Moon and Pao, 1969; Moon, 1970] were published on the dynamics of thin plates in magnetic fields. Subsequently, in [Moon and Holmes, 1979] a one-degree-of-freedom model was developed in the form of an ordinary differential equation to describe the motion of the beam of the setup in figure 2. Therefore, the continuous beam structure is discretized in space, which corresponds to the assumption that the beam only deforms in a certain shape with a time-dependent amplitude. This shape function has to be chosen a priori under certain circumstances, pursuant to the Galerkin procedure used. It is a key issue in the modeling of the energy harvester system and its choice also holds main interest in this thesis. In [Moon and Holmes, 1979], the shape is chosen as the first eigenfunction of the associated linear setup without magnets, following the Euler-Bernoulli beam theory. The magnetic field is not computed. Although the forces in transverse and normal direction of the beam and an arising coupling are discussed, they are only mentioned and no calculation is presented. The shape of the system's potential energy – including the magnetic field influence – is found heuristically from observations of the occurring equilibrium positions of the beam tip. The equation of motion is derived after severe simplifications. It is simply stated that an even polynomial of sixth order is needed for its potential energy. Consequently, the restoring force is of fifth order with maximal five real roots corresponding to each of the equilibrium positions, according to the observed case where three stable and two unstable equilibrium positions exist. Later, it is argued that for cases where the system only shows bistable behavior with two stable and one unstable equilibrium positions, the fifth order term can be dropped since it does not alter the qualitative behavior of the system. The term of the largest order remaining is then cubic, yielding the equation of motion for the modal coordinate x, which is proportional to the beam tip displacement. In [Moon and Holmes, 1979], after a normalization is done, the equation is given as

$$\ddot{x}(t) + \gamma \dot{x} - \frac{1}{2}x(t) + \frac{1}{2}x^3(t) = f(t), \tag{1}$$

which is known as a Duffing oscillator. Besides the characteristic restoring terms, it also comprises a viscose damping with coefficient γ and on the right side an excitation f, representing a base excitation in most cases of vibration energy harvesting. This Duffing equation is popular in non-linear dynamics, and corresponding investigations are now filling entire books [Kovacic and Brennan, 2011].

Erturk: Motivated by the non-linear behavior, its bistability and the tendency to large beam tip displacements, Erturk has extended the setup in figure 2 to build the energy harvesting system in figure 1, equipped with piezos and an ohmic resistor. The initial paper [Erturk et al., 2009] introducing the energy harvesting system refers to the modeling undertaken in [Moon and Holmes, 1979] and extends the equation by a second differential equation for the voltage v, with an electromechanical coupling to the mechanical part of the system, given as

$$\ddot{x}(t) + \gamma \dot{x} - \frac{1}{2}x(t) + \frac{1}{2}x^3(t) - \chi v(t) = f(t) \tag{2}$$

$$\dot{v} + \lambda v(t) + \kappa \dot{x}(t) = 0. \tag{3}$$

For details of the coupling parameters see the original publication [Erturk et al., 2009]. Therein it is then shown that this energy harvesting system has a potentially higher efficiency compared with the system without magnets, in the case of excitation frequencies other than the resonance frequency

of the remaining setup, which is now linear. In conclusion, no separate modeling was conducted, and hence all model assumptions applied in [Moon and Holmes, 1979] are adopted by implication.

Tam: The modeling of the mechanical sub-system is revisited by Tam in several works [Tam, 2013a; Tam, 2013b; Tam and Holmes, 2014]. On the mechanical side, Tam followed Moon by assuming linear behavior of the beam as a Euler-Bernoulli beam, to be discretized with its first linear eigenfunction. In concerns of the magnetic field, the approach is made to determine the magnetic field by assuming that the cylindrical permanent magnets can be described by an ideal solenoid with given closed form of the magnetic field [Derby and Olbert, 2010]. The beam itself is not part of the magnetic field, which means that independent of the current beam deformation only one magnetic field simulation is to be performed. From the magnetic field without the beam, the magnetization of the beam is derived. This only works when making assumptions regarding the magnetization of the beam, which have already been described in [Moon and Holmes, 1979]. In Tam's works, the piezos are replaced by strain gauges, which are also used to measure the beam displacement. It is assumed that they have no influence on the static nor dynamic behavior of the beam. Concerning the magnetoelastic forces, a distinction between a transverse and longitudinal force and a mechanical coupling is made. All components of the static restoring force are accumulated to a single restoring force and reduced to a cubic force model found by a least square fit.

In conclusion: All three publications concur in most parts of the modeling and only differ in detail, as outlined above. The model parameters in [Moon and Holmes, 1979] and [Erturk et al., 2009] are only found heuristically. Therefore, the method used – which is referred to as the heuristic method in this thesis – is described in the following section. In [Tam and Holmes, 2014], it is found by a cubic fit of an approximative computed magnetoelastic force, which is then compared with the model found heuristically. The investigations by Tam are the most detailed concerning the modeling of the mechanical sub-system. They will be reproduced and subsequently taken to the next level of refinement in this publication.

When considering more recent corresponding literature, in the field of magnetoelastic energy harvesting there is now a tendency towards a magnet-to-magnet interaction determining the nonlinear restoring force, often achieved by an additional magnet, which is attached to the free end of the beam [Kim et al., 2015; Kumar et al., 2015; Kumar et al., 2016; Leng et al., 2017; Zhou et al., 2018; Zhou and Zuo, 2018]. This allows a modeling where certain simplifying assumptions are made, as the dipole magnet assumption, where all magnetic properties are lumped in a single point regardless of the magnet's geometric shape (cylindrical, cubical, etc) or their size. This might allow a more convenient modeling in many cases and prompts the question whether changing the system's setup is legitimate to allow a simpler modeling. In the author's opinion, this seems like a strong restriction in design options of energy harvesting systems in general and can be overcome by an in-depth insight into the underlying physical laws of any energy harvesting system. Nonetheless, in this thesis the early setup presented in [Erturk et al., 2009] is considered, where there is no tip magnet present and the whole ferromagnetic beam is magnetized.

3 The heuristic method to derive the restoring force of a model

In order to develop a model for the energy harvesting system a heuristic method can be used. It is applicable when, for the bistable beam, a one degree of freedom model is sought, and an experimental setup is present. Then the stable equilibria of the beam tip $\hat{w}_{1/2}$ and the corresponding frequency with $f_1 = f_2$, provided that the setup is symmetric, of oscillations with small amplitude in the stable states give the information necessary to uniquely adapt a cubic restoring force.

At this point it is important to make a distinction between the physical parameters of the beam and the modal coordinates of a model. The equation of motion for the beam dynamics is usually described by x, which is a modal coordinate and not the physical beam tip displacement, even though it is directly proportional to it and implied in many existing figures of the energy harvesting system, as in [Erturk et al., 2009; Litak et al., 2010; Martens et al., 2013]. Unlike in other contexts, here the beam coordinate is named ξ instead of x, which is as mentioned already used for the modal coordinate. Accordingly, and pursuant to the Galerkin scheme for the beam displacement w, the ansatz

$$w(\xi, t) = \phi(\xi)\, x(t) \tag{4}$$

is chosen. Consequently, the connection between the beam tip displacement $\hat{w}$ and the modal coordinate x is given by

$$\hat{w}(t) = \phi(L)\, x(t) \tag{5}$$

where ϕ is the shape function to discretize the beam in space and L the total length of the beam, giving the position of the beam tip.

In most publications, the potential energy of the considered energy harvesting system, here named U, is assumed to be a symmetric, so called double well potential of 4th order, which is shown in figure 3. There is one unstable equilibrium x_0 in the middle and the two stable equilibria $x_{1/2}$, one on each side of the undeflected state of the beam. The restoring force R, which is defined to be directed towards displacements of smaller absolute values when it is positive in sign, results from U as the spatial derivative $R = \mathrm{d}U/\mathrm{d}x$. The model is then of the bistable Duffing type, having a nonlinear restoring term with negative linear term, a vanishing quadratic term due to the setup's symmetry and a positive cubic restoring term. In a general form with no excitation, the equation of motion, when α and β are both positive, is given by

$$\ddot{x}(t) + \gamma\dot{x} - \alpha x(t) + \beta x^3(t) = 0 \tag{6}$$

Let x_s (s for static) be a system state with vanishing restoring force, in which the beam is able to rest still, thus $\ddot{x}_\mathrm{s} \equiv 0$ and $\dot{x}_\mathrm{s} \equiv 0$. Applying these conditions to equation (6) the remaining terms are given by

$$-\alpha x_\mathrm{s} + \beta x_\mathrm{s}^3 = 0, \tag{7}$$

which is fulfilled for the following three solutions, giving the equilibria x_i for $i = 0, 1$ and 2 as

$$x_0 = 0 \qquad \text{and} \qquad x_{1,2} = \pm\sqrt{\frac{\alpha}{\beta}}. \tag{8}$$

Further, when applying initial conditions that just slightly differ from one of the stable equilibrium state, the system undergoes small oscillations around this equilibrium position. Due to the nonlinearity the frequency depends on the amplitude, but for very small oscillations it can be linearized sufficiently. The restoring force is then approximatively given by a Taylor expansion that is stopped after the second term, which is linear in x. The linear restoring Term R_lin, in the vicinity of the equilibrium x_i, is given by

$$-\alpha x(t) + \beta x^3(t)\,|_{x=x_i} \approx \left(-\alpha + 3\beta x_i^2\right) x(t) - 2\beta x_i^3. \tag{9}$$

For the case where x_i is the positive equilibrium x_1, according to equation (8), the linearized restoring force R_lin is shown in figure 4.

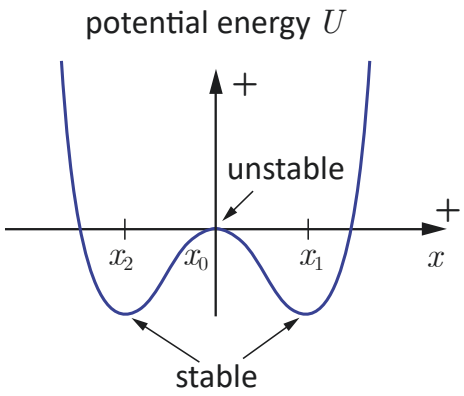

Fig. 3 Model of the double potential well of the bistable energy harvesting system as assumed in literature.

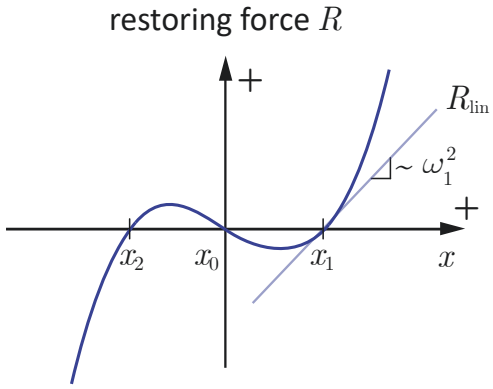

Fig. 4 Cubic model of the restoring force R with corresponding linearization R_{lin} in the equilibrium state x_1.

Its slope is proportional to the square of the circular frequency ω_1^2 of free oscillations of small amplitude in the equilibrium x_1, which can approximately be described by a linearized equation of motion. For small displacements $\bar{x}$ of the equilibrium position x_1, defined as $\bar{x}(t) = x(t) - x_1$, it can be found by a coordinate transformation of the form $x(t) = \bar{x}(t) + x_1$ inserted into the linearized equation of motion, which yields

$$\ddot{\bar{x}}(t) + \gamma \dot{\bar{x}}(t) + 2\alpha \bar{x}(t) = 0. \tag{10}$$

Hence, the circular frequency of oscillations of the system that is linearized with respect to the equilibrium position x_1 is given by $\omega_1 = \sqrt{2\alpha}$. If $\hat{\omega}_1$ and f_1 are known from measurements, or are arbitrarily set, and further the setup is assumed to be symmetric, the model parameters α and β are defined by

$$\alpha = 2\pi^2 f_1^2, \tag{11}$$

$$\beta = 2\pi^2 \left(\frac{f_1 \, \phi(L)}{\hat{\omega}_1} \right)^2 . \tag{12}$$

This way, a minimal model is determined, which is in this thesis referred to as heuristic model, since it is found based on observations on an existing experimental setup of the system. It fulfills the two conditions of matching equilibrium positions and frequencies of small oscillations around each stable equilibrium. Once the parameters are distinguished, the equation (6) can be transformed to the form of equation (1).

Vice versa, for given model parameters α and β corresponding equilibria and frequencies can be computed by inverting equation (11) and (12). The crucial key question is, in the case where it is desired to realize a system with arbitrarily given model parameters α and β, how is the physical setup to be built, other than by trial and error, in order to realize the theoretical equilibrium positions with corresponding frequency. This is particularly necessary to enable an optimization of a corresponding energy harvesting system. Thus the possibility of a targeted manipulation of the nonlinear restoring force with known resulting equilibria and frequencies of the system is desired and gives the motivation and the goal of this thesis in the following section. Later it is then shown how this can be achieved to predict the number of existing equilibria and also their approximate values.

4 Motivation and goal

The goal of this thesis and the presented publications is to contribute to a more sophisticated modeling of the energy harvesting system described in section 2. The attempt is made to establish an alternative method that is preferable to the heuristic method outlined in section 3 to model the system. The goal is to perform a direct modeling based on the respective physical properties of an experimental setup to take a step towards an optimization procedure, where the specific physical properties of the physical setup are adapted, and a resulting model is known. Hence, it is necessary to find a model that is sufficient to represent all significant aspects of the setups reality, but is still comprehensive to be manageable mathematically. Therefore, the basic assumptions made in literature regarding the systems physics are to be revisited in this work. Even though the results of this thesis will not be a complete optimization of the considered energy harvesting system, it is a step towards the possibility of influencing its non-linearity in a targeted manner.

5 Preliminary work

5.1 The considered experimental setup and related student theses

In order to perform a modeling of the energy harvesting system with corresponding explicit computations, a concrete system is to be considered. All relevant details of the investigated setup are described in each corresponding publication. An existing experimental setup, designed and built up by the coworkers of the chair Huy The Nguyen and Lukas Lentz, was used and further adapted for the actual work.

Within the framework of this dissertation, related student theses were elaborated, which contributed to the topic. In [Vanegas Müller, 2018] experiments of magnet-magnet and magnet-beam force interaction have been made. Measurements of real-world excitations and their reproduction at the experimental setup are the focus of [Overbeck, 2018]. In [Pankratov, 2019] the control of the shaker to generate a harmonic excitation is described. In [Kienz, 2019] dynamic measurements of the bistable beam for harmonic excitations are performed, which are later in this thesis reinvestigated. In [Bard, 2019] the path integral method has been applied to determine the probability density function of the energy harvesting system for an excitation of a white noise type. If relevant, the corresponding theses are referred later in this thesis in the respective parts.

5.2 Modeling of the beam

A key aspect of the energy harvesting system is the bending structure, which is a slender cantilever beam made of steel. Its modeling is usually done according to the Euler-Bernoulli beam theory, which is only valid under certain circumstances, as detailed in many mechanics textbooks as [Hagedorn and DasGupta, 2007; Wauer, 2014]. Its applicability in the considered case is shown in the following.

In geometric concerns, the Euler-Bernoulli beam theory starts with the assumption that all planar cross-sections of the undeformed beam remain planar after the beam undergoes a deformation. This only holds true when the ratio of the height of the beam is much smaller compared with the radius of curvature of the neutral fiber in the deformed state. In terms of forces, this is fulfilled if the beam experiences no significant shear or torsional stress relative to the bending stress, which becomes relatively large when the beam is large in height and short in length. In other words, the theory is only admissible in the opposite case where the beam is slender (low in height, large in length) and only small displacements of the beam compared with its total length occur. In the considered case,

this is fulfilled as the beam is 250 times larger in length than in height (250 to 1 mm) and the largest displacements arising at the beam tip are significantly smaller than a tenth of the total beam length, which means the beam itself is not a cause for any non-linearities.

An experiment is conducted to show the linearity of the beam. Consider the case where the beam is bent by a single transverse force located at the beam tip. The static elastic restoring force of the beam – which is the force that is directed towards the undeflected beam position – is in total value equal to the external force. A string is attached to the beam tip to apply different forces, which are determined by a spring scale. The resulting displacement is measured by a laser triangulation sensor. The setup is shown in figure 5 and the corresponding results in figure 6.

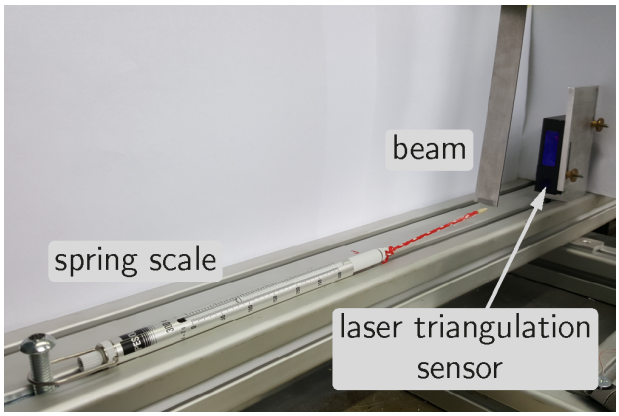

Fig. 5 Experimental setup to measure the elastic restoring force of the beam by a spring scale and the displacement of the beam tip by a laser triangulation sensor.

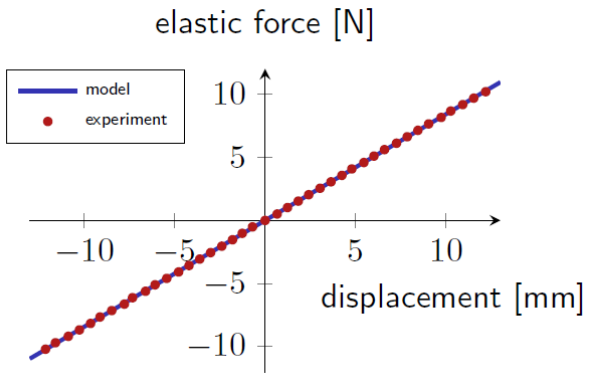

Fig. 6 Results of the measurement of the pure mechanical restoring force of the beam and comparison to the linear elastic restoring force according to the Euler-Bernoulli beam model.

These experimental results have already been published in [Lentz, 2018] and are recalled here, since they have been found in cooperation as mentioned there and are equally fundamental for both theses. It can be seen that the static elastic restoring force of the beam is indeed linear with respect to displacements in the considered range. The static equilibra of the experimental setup with magnets is in most realizations around ± 7 mm. This was also an essential result for the three publications and there applied accordingly: In the first paper [Noll et al., 2019a] the beam's mechanical elastic restoring force, which is besides the forces originating from the magnetic field one component of the overall restoring force, assumed to be linear. Further, the Euler-Bernoulli beam theory is applicable in dynamic cases, as long as oscillations of a frequency in the range of low order natural frequencies of the beam are considered. This holds interest in the second and third publications, where dynamic measurements of the beam during harmonic excitations are made. All occurring beam oscillations are of frequencies lower than the second eigenfrequency of the beam, and hence the use of the theory is suitable in this concern.

Note that – according to the Euler-Bernoulli beam theory – there is a difference between the static and dynamic case when it comes to the shape of the beam deformation. In static cases, it can be shown that the general deformation of the beam is of polynomial type. More specifically, in the case of a cantilever beam with a single load at the free end, the bending line of the beam is a polynomial of third degree [Gross et al., 2011]. By contrast, when the beam's dynamics is considered, linear oscillations are in the shape of the eigenfunctions, which are of trigonometric type. This is a contradiction in so far that a model of the beam – which is found after a discretization is performed – is suitable to model either the static or dynamic case, but not both at the same time. The stiffness of the model – which is related to the beam shape of deformation – differs between

the two cases. Hence, a single-degree-of-freedom model cannot cover static as well as dynamic cases equally well. For the sake of simplicity, this distinction is not made and only the dynamic case is modeled (except for the static investigations in figure 5 and 6), because the error is small and manageable. The consequences are a slight change of the linear elastic restoring force and the magnetoelastic forces, which indeed changes the position of the equilibria and the corresponding frequencies of a linearization. This is kept in mind throughout all investigations performed and is seen as a possible source of deviations between the theory and experiment, but it never shows strong potential to change the observed qualitative behavior.

5.3 On the modeling of the distribution of the magnetoelastic force

When reconsidering the paper of [Moon and Holmes, 1979], which gives the fundamentals of the modeling of the considered mechanical sub-system of the energy harvesting system, different mechanical and magnetoelastic influences on the beam are mentioned, although the model is ultimately found by the heuristic method (see section 3). One advantage of this heuristic method is that regardless of the relevance of each effect, all contributions to the overall system's dynamics are taken into account by the nature of the approach. When seeking a more detailed model, an explicit computation of the physics is needed. At this point, the question arises concerning which models are to be used and which effects are significant and need to be respected. The beam model is addressed in section 5.2. When now taking a look at the magnetoelastic influences, the following questions emerge: Which force components are to be considered? Are the forces of a distributed type or is an approximation valid, where the forces are accumulated to a single force? The answers to these questions depend on the respective realization of the sub-system and can only be answered when the force components are explicitly modeled. This is undertaken within this thesis in several steps.

The first step towards an improved modeling was taken in the master thesis of the author [Noll, 2016], and its results were presented by the author at a conference with a corresponding conference proceeding published as [Noll and Lentz, 2016]. To regard the distributional character of the magnetoelastic transverse force, its distribution is explicitly determined. Therefore, the external magnetic field caused by the magnets in both works was found by a semi-analytic approach. For detailed steps of the modeling of the magnetic field and the modeling of the magnetoelastic force, see these sources. The method outlined in both followed the line of argument regarding the magnetization of the beam that was already proposed in [Moon and Holmes, 1979] and later applied in [Tam and Holmes, 2014]. In contrast to the latter, in [Noll, 2016; Noll and Lentz, 2016], the force distribution was displayed over the length of the beam prior to an accumulation for each beam displacement according to the Galerkin modeling procedure applied. Note that this is simply undertaken to visualize the force distribution, since [Tam and Holmes, 2014] and [Noll and Lentz, 2016] ultimately result in the same model, only with different model parameters. However, the detailed distribution of the force indeed holds interest to assess the extent of its influence on the model. As can be seen in [Noll, 2016; Noll and Lentz, 2016] the force is – at least according to this model – of a distributed type, and its distribution will have an influence on the final model, compared with a case where the force is first accumulated to a single load at the beam tip. This particularly applies in cases where for one beam displacement, a force distribution with positive as well as negative sign along the beam occurs. In these cases, the force cannot be simplified to a single force without loss of accuracy, since a mechanical coupling also arises. The results found are plausible, although their accuracy is not satisfying when comparing the equilibrium positions predicted by the model with the positions measured on the experimental setup (results not shown in this thesis), yielding the motivation for further improvements and questioning the model assumptions regarding the magnetoelastic forces.

Further potential given by the underlying arguments and assumptions made exists to increase the accuracy of the force modeling. The aforementioned approach performed in [Tam and Holmes, 2014; Noll, 2016; Noll and Lentz, 2016] is convenient, since – by neglecting the influence of the beam on the magnetic field – only one magnetic field simulation is required. However, this enforces simplifying assumptions regarding the magnetization of the beam. The most substantial weak point in the multiple assumptions regarding the beam's magnetization is that the beams free end is not modeled, or – put differently – the boundary effects arising at the beam tip are neglected. This is a contradiction to the fact that the beam's free end is close to the magnets and the magnetic field is strong in its vicinity, hence probably generating the major proportion of the forces. Taking a closer look at the influence of the beam's free end – especially on the magnetic field and subsequent magnetoelastic force computation – entailed potential for an improved modeling and led to the work presented on a conference poster [Noll and Lentz, 2017], which can be found in the appendix of this work. The main goal was to compute the distributed magnetic forces on the beam regarding the influence of the beam itself on the external magnetic field. Further, in addition to the transverse force, a longitudinal force component is considered. Now, in order to regard the beam's influence on the magnetic field, it needs to be included in the magnetic field simulation and subsequently a new force model is needed to retrieve the force from the magnetic field simulation.

Computing the distribution of the force on the beam is an ambitious challenge, since appropriate methods are rarely discussed in textbooks on electromagnetism. In general, in terms of methods to compute forces in magnetized matter, there is no common agreement about the correct method to compute the electromagnetic forces, and several equations, methods and equivalent formulas are discussed and compared. A distinction is to be made between a total force computation on a whole body that is completely surrounded by air and the even more challenging attempt to find the distribution of the forces within the body volume. Overviews of different techniques can be found in [Carpenter, 1960; Lefevre et al., 1988; Reyne et al., 1987; De Medeiros et al., 1998b; Makarov and Rukhadze, 2009]. To the author's best knowledge, to date there is no single, widely-accepted approach to determine the force within magnetized matter. Their rich diversity can be explained by the need for constitutive laws that summarize microscopic phenomena in magnetized matter. Although the force on a single electric charge is well known by the Lorentz force, the number of charges in matter is unmanageably large. Different models to summarize their behavior yield the different existing force models. At least most of them agree on the total force on a body that is completely surrounded by air (see [Reich, 2017]). An overview demonstrating their disagreements regarding the force distribution inside a body due to their different assumption at the microscopic level can be found in [De Medeiros et al., 1999].

Given the variety of methods, the most convenient to choose once the magnetic field is known is the Maxwell stress tensor. It is a tensor expression in terms of the magnetic field only, and hence it does not depend on state variables of the mechanical compartment and is given by

$$T_{ij} = \frac{1}{\mu_0} B_i B_j - \frac{1}{2\mu_0} \boldsymbol{B}^2 \delta_{ij}, \tag{13}$$

which is an alternative expression to the tensor defined on the conference poster [Noll and Lentz, 2017] (see appendix). For the derivation of the tensor from the Maxwell equations, the reader is advised to consult a textbook on electromagnetic dynamics; for example [Griffiths and Reeves, 1999]. To find the total force on a body, the Maxwell stress tensor is determined, and its divergence is integrated over the body volume V, by

$$\boldsymbol{F} = \oiiint_V \operatorname{div} T \, \mathrm{d}V, \tag{14}$$

or for numerical reasons, it is possible to transform the volume integral to an integral over an enclosing surface O using the divergence theorem of Gauss, which yields the equation for the force $\boldsymbol{F}$ given on the poster (see appendix, left column next to poster-figure 3). It is noteworthy that different Maxwell stress tensors exist, although all of them coincide for linear isotropic materials and lead to the same values of the total force [Bermúdez et al., 2016]. Note also that the Maxwell stress tensor is not a stress tensor in the sense of a mechanical Cauchy stress tensor and therefore its applicability is different [Rinaldi and Brenner, 2002]. For further details of the application of the Maxwell stress tensor to compute the magnetoelastic force, see for example [Lefevre et al., 1988; De Medeiros et al., 1998a].

The validity of its use concerning total force predictions is undoubted, although its suitability for local force distributions discussed controversially in literature. In [Bossavit, 2011; Bossavit, 2014] it is differentiated, and the case is described in which the Maxwell stress tensor is indeed applicable and provides the correct result of local force distributions. It is stated that when the local magnetic properties such as permeability or magnetization do not depend on the local deformation of the body, the Maxwell stress tensor is applicable. Taking note of these requirements for this method – which are no limitations for the considered case of a quasi static magnetic field with no regard of local mechanical beam deformation within each simulation – the distribution of the force is computed. The method applied to find the force distribution on the beam mostly follows the argumentation outlined in [Bermúdez et al., 2016], where discontinuities of magnetic field properties and the Maxwell stress tensor respectively are regarded in the domain of interest. Hence, only parts of the beam can be considered.

The force distribution is found by dividing the beam in a finite number of beam elements, where the force is determined for each of the beam elements. Hence, the distribution is only approximately found, and its resolution depends on the size of the beam elements. The force is determined by the integral according to the equation given on the poster next to poster-figure 3 (see [Noll and Lentz, 2017] in appendix), along the boundary $\delta\Omega$, which is completely enclosing the considered beam element. Since the magnetic field simulation is in two dimensions, $\delta\Omega$ is a closed contour, as exemplarily shown in poster-figure 3. The result of a magnetic field simulation can be seen in poster-figure 3, where the color refers to the absolute value of the magnetic flux density $\boldsymbol{B}$. It is noteworthy that the Maxwell stress tensor undergoes discontinuities at material jumps between the steel beam and the surrounding air. For details concerning the mathematical details regarding how this is handled, see [Bermúdez et al., 2016]. For each beam element, enclosed by a path $\delta\Omega$, the Maxwell stress tensor $\boldsymbol{T}$ is evaluated and the force is determined. This procedure is undertaken for all beam elements and this is then repeated for many beam displacements. Hence, a spatial distribution of the force is found. More precisely, the force is determined for each beam element at the position where it is located when the beam is deformed in the first eigenfunction of a certain amplitude, which is the reason for the graph of the force distribution having its shape, as presented in poster-figure 4. There it can be seen that the force is indeed mostly concentrated at the beam tip. An accumulation seems valid, since the major part of the force acts in the vicinity of the free end of the beam.

This was an essential result for the first publication, as the forces there are reduced to a single force at the beam tip, which is sufficient and time-saving. It is noteworthy that this is contrary to the force distribution found earlier in [Noll, 2016; Noll and Lentz, 2016], where the beam's influence on the magnetic field is neglected. In the first publication, the results that are so far found numerically only, will be compared with experiments.

6 Overview of publications and their connection

All three presented publications address the modeling of the mechanical sub-system of the underlying energy harvesting system in general but have different emphases. There are different aspects of the overall system that can be – at least to a certain extent – analyzed separately but are always related to each other, which gives the connection between the publications. They can be seen as the continuation of the research undertaken by others author found in literature described in section 2, as well as the works by the author presented in [Noll, 2016; Noll and Lentz, 2016] and the poster [Noll and Lentz, 2017] shown in section 5.3.

In the first paper [Noll et al., 2019a], the main focus is on computing the magnetoelastic forces with the goal of enabling a more comprehensive determination of the restoring force compared with the heuristic method. It can be seen as a subsequent investigation to [Tam and Holmes, 2014] and [Noll, 2016; Noll and Lentz, 2016] in so far that the beam's influence on the magnetic field is now taken into account. The results of section 5.3 are respected as the magnetoelastic force is accumulated at the beam tip. All of these findings were considered in the first publication. Finally, the resulting model is compared with experimental results.

In general, whenever the magnetic field is to be computed by a numerical simulation, it can only be undertaken for fixed parameters, given geometric dimensions and chosen boundary conditions. This means that when the beam is to be considered, it is to be modeled with its geometric shape, although, since its deformation is changing over time, it cannot be computed by a single magnetic field simulation. In fact, a simulation is necessary for every possible beam deformation, however, since the mechanical beam model is found by a discretization of the beam using its first eigenfunction, it is only consistent to assume a deformation of the beam accordingly. Therefore, only beam deformations in the shape of the first eigenfunction with different amplitudes are modeled, and the force is assumed to be linear between two close adjoining simulations. This is not only a simplification for the resulting forces on the beam – which depend on the beam shape – but also the beam's dynamics in general, which is what led to the subsequent second publication [Noll et al., 2019b]. There, the assumption concerning the beam's deformation being solely in the shape of the first beam eigenfunction is addressed. The geometric shape of the beam is experimentally analyzed during driven oscillations of different harmonic excitations. The beam is filmed using a high-speed camera. In the videos taken, the positions of distinct applied markers on the beam are tracked over time to determine the beam's shape during vibrations. In conclusion, the discretization of the beam with one eigenfunction is indeed a good approximation and the second eigenfunction only has a small geometric influence on the beam shape in cases of super harmonic responses. It justifies the assumption in the first paper in hindsight in so far that the geometric influence of the second eigenfunction is so small – indeed smaller than the spatial discretization of the finite element simulation of the magnetic field – and hence does not affect the significance of their results.

The third publication can be seen as an extension to the investigations conducted in the first publication. Although the theoretical model is already compared with experiments in the first publication, the experiments are restricted to the stable equilibrium positions of the system and corresponding frequencies of small oscillations. Now, in the third publication, a more comprehensive comparison is presented, where not the static behavior but rather the stationary response to a harmonic excitation is investigated. Similar to the second publication, driven harmonic oscillations are realized and the stationary beam response is measured. Its responses are compared with the predictions of the Duffing model with a cubic restoring force, found by the heuristic method described in section 3.

Copyright notice

Journal of Vibration Engineering & Technologies
https://doi.org/10.1007/s42417-019-00193-2

CORRECTION

Correction to: On the Improved Modeling of the Magnetoelastic Force in a Vibrational Energy Harvesting System

Max-Uwe Noll[1] · Lukas Lentz[1] · Utz von Wagner[1]

Correction to:
Journal of Vibration Engineering & Technologies
https://doi.org/10.1007/s42417-019-00159-4

The original version of this article contains an error. In Table 1 "Magnetic material parameters" the value for the "relative permeability of steel" is 1000 (instead of 300).

The original article can be found online at https://doi.org/10.1007/s42417-019-00159-4.

✉ Max-Uwe Noll
max-uwe.noll@tu-berlin.de

[1] Chair of Mechatronics and Machine Dynamics, Technische Universität Berlin, Einsteinufer 5, 10587 Berlin, Germany

Published online: 17 December 2019

Journal of Vibration Engineering & Technologies
https://doi.org/10.1007/s42417-019-00159-4

ORIGINAL PAPER

On the Improved Modeling of the Magnetoelastic Force in a Vibrational Energy Harvesting System

Max-Uwe Noll[1] · Lukas Lentz[1] · Utz von Wagner[1]

Received: 29 December 2018 / Revised: 29 April 2019 / Accepted: 12 June 2019

Abstract

Objective The efficiency of vibrational energy harvesting systems that consist of a cantilever beam with attached piezoceramic layers can be increased by intentionally introducing nonlinearities. These nonlinearities are often implemented in the form of permanent magnets near the beam's free end. The influence of these magnets is typically assumed to be a single transverse force that depends cubically on the displacement of the beam tip. The coefficients of a corresponding single degree of freedom model are often found heuristically, without an explicit modeling of the magnetoelastic force.

Methods In this paper, we present and assess the validity of a procedure to determine the magnetoelastic forces acting on the beam from physical laws of the magnetic field with corresponding parameters. The paper outlines the method itself, describing initially how the magnetic field is computed by a Finite Element simulation. In the second step, the total transverse force on the beam is determined from the magnetic field by means of a numerical evaluation of the Maxwell stress tensor. The required minimum degree of a suitable polynomial force approximation of the numeric values is discussed briefly. The validity of this model is then considered by investigating its bifurcation behavior with respect to mono-, bi-, and tristability for different distances between the magnets and comparing the findings to results found by experiments.

Results While the model's predictions of the number of equilibrium positions for any magnet distance are generally in good agreement with results of experiments, there are deviations when it comes to the exact positions of the equilibria. With respect to these findings, the limitations of a two-dimensional magnetic field modeling with only linear material models are addressed.

Conclusion The paper concludes that the method outlined here is a step toward the deduction of a detailed model based on physical laws of the magnetic field with corresponding parameters replacing simple heuristic polynomial magnetic force laws.

Keywords Energy harvesting · Bistable oscillator · Magnetoelastic force · Maxwell stress tensor

Introduction

Over the past few years, the interest in power extraction from ambient energy sources has grown, as they allow the support, e.g., of autonomous sensor systems for structural health monitoring or in general autonomous microelectronics due to the steadily decreasing power consumption of such systems. Vibrational energy harvesting systems generate electrical energy from ambient mechanical vibrations, which energy would otherwise be lost. A review of existing research on this topic can be found, e.g., in [1–3].

An implementation, which has received great attention, is a cantilever beam with piezoceramic patches attached near its clamped end. Hereby the beam's base is attached to an external structure, whose motion excites the system. Such vibrational energy harvesting systems were extensively investigated in the past, e.g., in [4–7]. In cases when they are designed as a linear resonator, optimal performance with respect to energy harvesting is achieved by matching their resonance frequency to the frequency of the excitation. Nevertheless, the power output drops drastically when they are exposed to frequency varying or broad band excitations, as they appear in many practical applications. Purposely introduced nonlinearities can be used to successfully widen the range of excitation frequencies that lead to large amplitude responses with high power output, as is shown in [8–12].

✉ Max-Uwe Noll
max-uwe.noll@tu-berlin.de

[1] Chair of Mechatronics and Machine Dynamics, Technische Universität Berlin, Einsteinufer 5, 10587 Berlin, Germany

Published online: 24 June 2019

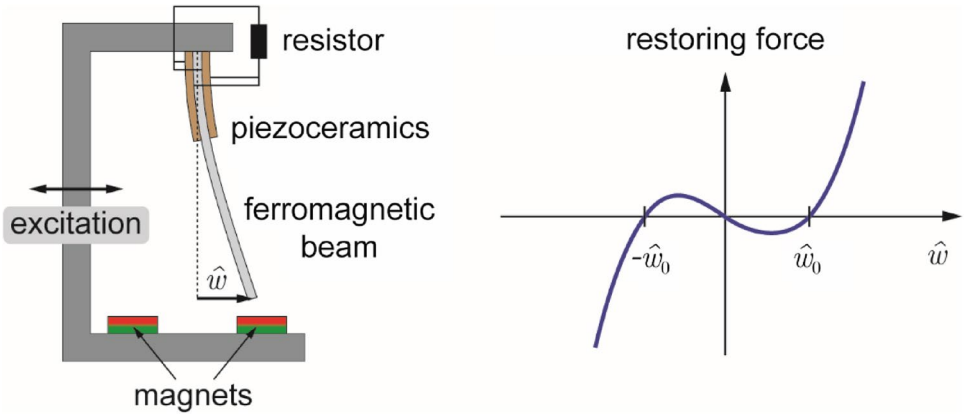

Fig. 1 Bistable magnetoelastic energy harvesting system (left) [39] and nonlinear restoring force (right)

To purposely introduce nonlinearities to a linear energy harvesting system consisting of a cantilever beam with piezoelectric patches, two permanent magnets are placed symmetrically near the free end of the ferromagnetic beam. This extension of the system by the magnets leads to a nonlinear restoring force. The earliest work known to the authors that investigates the dynamics of a mechanical system similar to the setup shown in Fig. 1 is [13], which analyzes the system without the piezoceramic layers under the aspect of chaotic vibrations in structural mechanics.

In [8], this setup was extended by piezoceramic patches connected to an ohmic resistor to design a simple model of an energy harvesting system. In many publications, the beam is modeled as an Euler–Bernoulli beam that is discretized in space by one modal ansatz function, as e.g., in [14]. Beside the purposely introduced nonlinearities by the magnets, the setup may contain several other potential sources of nonlinearities, for example, nonlinear material or damping behavior or geometrically nonlinear behavior of the beam. Usually all these effects are neglected and corresponding linear behavior is assumed as in [13, 15].

In recent investigations [16] of the authors of the present paper with the same experimental setup, operation vibration shapes in both intra- and inter-well solutions, i.e., vibrations around one or both of the stable equilibrium position, respectively, were recorded by a high-speed camera in the case of harmonic excitation close to the first eigenfrequency of the linear system. Expanding the operation shapes with respect to response frequencies (main- and superharmonics) and eigenshapes of the corresponding linear Euler–Bernoulli beam gives the result, that the part of the operation shape with the same frequency as the excitation, is very well represented by the first eigenshape of the Euler–Bernoulli beam and only small additions of the second Euler–Bernoulli eigenshape are necessary in the case of superharmonics. Therefore and as the focus of the present paper is on the modeling of the magnetic forces, we will restrict the modeling on just one modal ansatz function and the consideration of sources of nonlinearities on the magnetic forces only. Nevertheless, one conclusion of the work presented in this paper will be that the ferromagnetic beam material is indeed a source of nonlinearity.

Depending on positions and parameters of the magnets (while considering a symmetric setup), this can either result in a mono-, bi-, or tristable system, respectively (e.g., [13, 15]). For a mono-stable system with magnets close to each other, the properties of the system will not much differ from that of a linear one. For distinctly separated magnets, the straight equilibrium position of the beam becomes unstable resulting in a bistable characteristic of the restoring force, as sketched in Fig. 1 on the right. The bistable configuration has attracted the most attention within the last years (see e.g., the review paper [10]). Shifting the magnets further from the center, the straight position of the beam may become stable again resulting in a tristable system. There is a current trend toward considering such multistable systems, like tristable systems with two unstable and three stable equilibrium positions (see e.g., [7, 17, 18]), or even quadstable systems with four stable states [19], when more than three magnets are used. In general, all these nonlinear systems are more promising with respect to energy harvesting compared to their linear counterpart, as there is a broad range of frequencies possible with parallel existing solutions, where solutions with a periodical change between the potential wells lead to a higher energy output of the system [20, 21].

A multistability of an energy harvesting system can not only be achieved by adding magnets, but also by versatile mechanisms. Examples are snap through structures under preload (e.g., [21]), or systems with pronounced geometric nonlinearities as they arise, e.g., on an upright cantilever beam with tip mass [22]. Nevertheless, in many recent publications, magnets are used to purposely induce nonlinearities in the system without introducing additional mass or friction (e.g., [23–25]), which allows a targeted modification of the nonlinearity just by the positioning of the magnets. As a result, the corresponding modeling approaches in the literature of bistable systems finally result in a Duffing-like

oscillator with a double well potential that can be treated by corresponding standard techniques.

In basic heuristic models in the literature, the resulting nonlinear restoring force is simply introduced in the discretized equation of motion, without consideration of the actual form of the magnetic force (for example in [14]). It is not discussed where the force is exactly applied nor if the force is of a distributed type or of a concentrated type. Further, no distinction is made between the transverse component and the longitudinal component of the force. In the bistable case, the model's resulting restoring force, depending on the displacement of the beam, can simply be assumed to be of third order with a negative linear term, a vanishing quadratic term (due to the symmetry of the setup), and a positive cubic one. These assumptions lead to a minimal model for the bistable system, which possibly shows deficits in the accuracy of the force modeling due to its simplicity. The coefficients of the model are, in general, found in the following way: the parameters are chosen based on given stable equilibrium positions and corresponding eigenfrequencies of the therein linearized system (as in [26]). They can either result from the considered experimental setup or assumptions for the model. This has the advantage that the model is a good approximation in the vicinity of the stable equilibrium positions of the beam. However, it is impossible to find a representation from physical model parameters. To deduce a model for a specific practical realization of the energy harvesting system, the setup needs to be built physically to measure the mentioned quantities as the coefficients in the model by this way of modeling and parameter identification are not directly related to physical parameters of the setup with the magnets. Therefore, although it is possible to increase the efficiency of a model by an optimization of its parameters, as it was done in [27], it is not possible to find a real physical representation of a preferred model by directly reading out its parameters. The only way—if not trial and error is performed with a corresponding flexible experiment—is to directly model the magnetoelastic forces and get from this a model of the setup.

Therefore, the objective of this paper is to describe a method to directly compute the magnetic force. Most publications that deal with an explicit computation of the restoring force, particularly for systems with nonlinearities introduced by magnets, consider a magnet-to-magnet interaction. This allows a derivation of a closed form of the forces, mainly due to the simplifying dipole assumption, where all magnetic properties of each magnet are lumped in one single point [23–25]. The most recent publications known to the authors that deal with the magnetic interaction between a magnetic field of a set of various magnets and an elongated ferromagnetic beam structure corresponding to the considered energy harvesting system in Fig. 1 are [15, 28]. The similarities and differences of the presented approaches are described in detail in the next section. In [29], a soft magnetic stripe has been applied at the tip of the nonmagnetic beam to realize a concentrated force.

The magnetic force is usually determined in the discretized model of the beam, where, as already described above, only one ansatz function is used. Based on our results from [16], this seems to be sufficient for our setup and this allows to find the force solely based on the displacement of the tip of the beam. If more than one ansatz function and corresponding modal coordinates are used, the uniqueness of the shape of the deformed beam in the magnetic field for a defined beam tip displacement is lost.

To determine the magnetoelastic force, the magnetic field is computed. The focus is on the determination of the magnetic field and the magnetoelastic force on the beam. For this reason, the piezoceramic layers are, despite their mechanical and electro-mechanical influence, not part of the model in this first step, but could be added to the model later on, once the magnetoelastic force is computed. For this, the beam is to be divided into two sections with different mechanical properties according to the additional mass and bending stiffness due to the applied piezoceramic patches [30] and the model is to be extended by an additional equation describing the properties of the electric circuit coupled with the piezoceramics [8, 30].

To validate the numerical results, the model is compared to experimental investigations of the system's bifurcation behavior for different distances between the magnets with respect to the number and positions of the stable equilibria and the corresponding frequencies.

Some prior steps of the current investigations and corresponding results have already been published in [28] or worked out in the master thesis of the fist author (2016) and have been presented as a conference poster presentation [31].

Magnetic Field

To determine the nonlinear magnetoelastic force on the ferromagnetic beam, the inhomogeneous magnetic field is required [32]. A stationary magnetic field of homogeneous magnetized permanent magnets of specific shapes can be found analytically (e.g., cuboidal magnets [33] or cylindrical magnets [34]). The magnetic field of the permanent magnets, in the absence of the beam, is here referred to as the initial magnetic field. When the ferromagnetic beam is placed in this initial magnetic field, the beam is magnetized and this magnetization causes a magnetic field superposing the initial magnetic field. For the general case of an arbitrarily deformed beam, no analytical solution of the magnetic field is known to the authors and is therefore computed numerically by the **F**inite **E**lement **M**ethod (FEM).

The magnetic field depends on the beam's velocity, as the beam is electroconductive and moves through an inhomogeneous magnetic field. According to Faraday's law of electromagnetic induction, a voltage is induced inside the beam causing an electrical current, which generates another proportion of the overall magnetic field. This aspect is neglected in this paper. The laws of magnetostatics are considered to be valid here due to the small velocity of the beam compared to the speed of the electromagnetic waves. In fact, the magnetic field is modeled as quasistatic, where the beam is considered with its current deformation, but has a vanishing velocity.

In [15], the magnetic field of the permanent magnets is determined by solving an integral that gives the magnetic field of an ideal solenoid, which produces a magnetic field equivalent to the magnetic field of the cylindrical magnets (see [35]) used. This approach is restricted to magnet shapes with a known solution for the magnetic field and is furthermore not suitable to consider the change of the magnetic field due to the presence of the magnetized beam. In the works [15, 28], a method is described to determine the magnetoelastic force where only the initial magnetic field of the permanent magnets, without consideration of the beam, is required; fundamental laws of the magnetic flux density and the magnetic field strength on the material discontinuities between the air and the steel beam are used to approximate the magnetization of the beam. This means that only one magnetic field computation is necessary. A drawback is that some accuracy might be lost, in particular due to the assumptions, which must necessarily be made: the height of the beam is assumed to be small so there is no change of the magnetization across it and the influence of the beam tip is neglected, as if the beam was infinitely long. This contrasts with the hypothesis inherent in most models that the force is concentrated at the tip of the beam.

In the work presented here, a different method is used, in the sense that the influence of the beam on the magnetic field is covered. A Finite Element approach is applied to compute the magnetic field of rectangular magnets. The beam is included in this simulation. The magnetoelastic forces are then found from the magnetic field through a numerical evaluation of the Maxwell stress tensor, as described in the next section.

For the two permanent magnets and a fixed deflection of the beam, the magnetic field is computed numerically using the open source software FEMM.[1] It is restricted to a two-dimensional simulation, and only linear magnetic material characteristics are taken into account. The definition of the magnetic materials in FEMM requires the relative permeability μ_r of the beam and the magnets, respectively. To characterize the permanent magnetization of the magnets, their coercivity H_c is additionally needed. However, usually the magnetic flux density produced by the magnets, called remanence B_r, is provided by magnet suppliers. The relation that connects these magnetic quantities in the linear case is

$$H_c = \frac{B_r}{\mu_0 \mu_r}, \tag{1}$$

where μ_0 is the permeability of vacuum. The values used in the simulation, given in the following Table 1, are chosen within the range of material properties provided either by the supplier, or by literature.

Table 1 Magnetic material parameters

Parameter	Value
Coercivity H_c of magnets	1.067×10^6 A/m
Relative permeability of magnets	1.023
Relative permeability of steel	300

The computed magnetic field is shown in Fig. 2. For the purpose of a better visualization, the system shown is an example and corresponds neither in sizes nor in proportions to the experimental setup as shown in Fig. 4. The frame, which supports the beam and the magnets, is completely made of aluminum, which has a negligible influence on the magnetic field. Thus, the frame is not a part of the simulation and only appears transparent in the simulation results. The magnetic north pole of both magnets is pointing upwards (cf. Fig. 1).

The consideration of the ferromagnetic beam in the simulation leads to a non-symmetric magnetic field, except for the case of a vanishing beam deflection. The essential result of the simulation is the magnetic flux density $\boldsymbol{B}$, which will be used to compute the magnetoelastic force.

Beam Model

The modeling of the mechanical system is divided into two parts: first, the modeling of the beam and second, the modeling of the magnets' magnetoelastic force. Note that the beam is assumed to be an Euler–Bernoulli beam based on the argumentation performed in the introduction section. Therefore, all nonlinearities in the model originate from the magnetoelastic forces caused by the magnetic field and the transverse force is assumed to be consistently perpendicular to the x-axis of the underlying coordinate system as shown in Fig. 3 (i.e., no follower force).

[1] D. C. Meeker, Finite Element Method Magnetics, Version 4.0.1, http://www.femm.info.

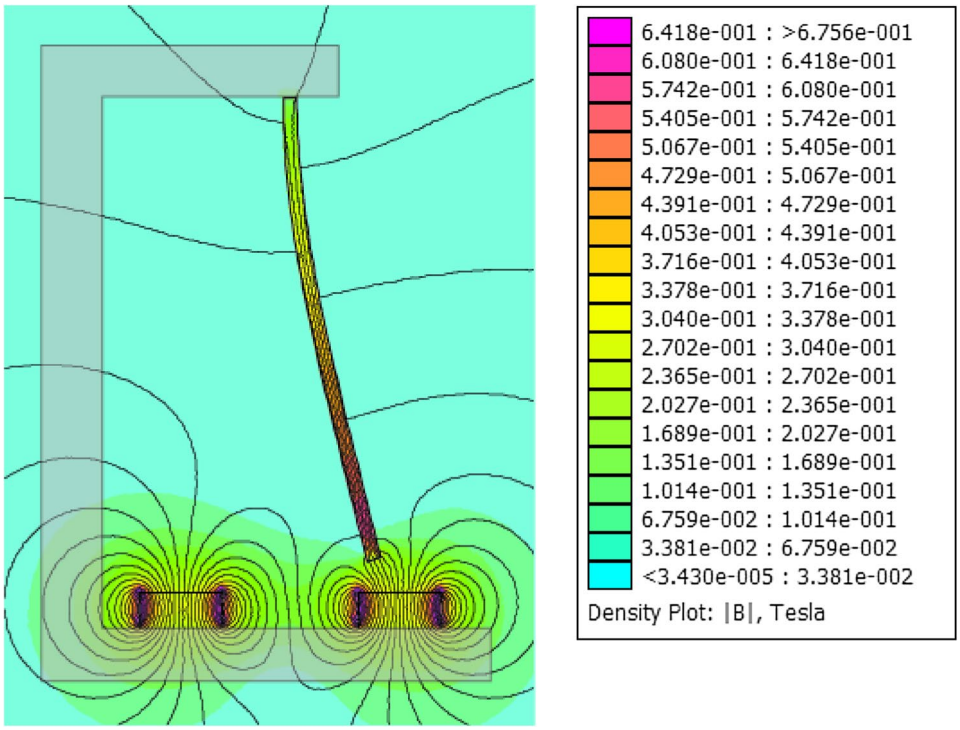

Fig. 2 Magnetic field of the permanent magnets with consideration of the ferromagnetic beam [40]

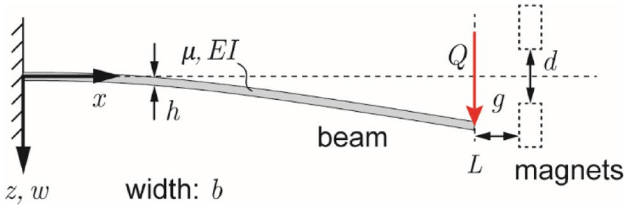

Fig. 3 Mechanical model of the cantilever beam

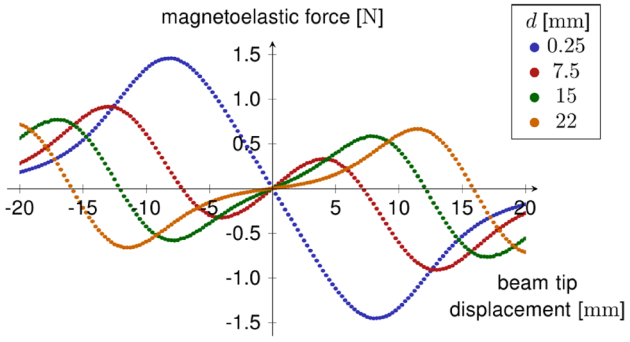

Fig. 4 Total magnetoelastic transverse force Q for different magnet distances d

In the presented work, the piezoceramic layers are not considered at this stage of the mechanical model, as it is assumed that they have an insignificant influence on the magnetoelastic force. The piezoceramics mainly damp the vibration due to the energy harvesting effect and only slightly increase the stiffness and the mass of the section of the beam to which they are attached, which is usually at the clamping. At this position, the largest mechanical strain is obtained, which leads to a large deformation of the piezoceramics. Additionally, they couple the beam with the electric circuit that is connected with the piezoceramics. The piezoceramics can be added to the model later, once the magnetoelastic force is known. For a detailed model that considers the piezoceramics, see e.g., [30].

The Euler–Bernoulli cantilever beam shown in Fig. 3 with the x-axis along the centerline has the length L and its mechanical characteristics are described by the constant mass per length μ, and the constant bending stiffness EI. $w(x,t)$ is the beam's lateral displacement at time t. The equation of motion, without external base excitation can be found in various textbooks and is given by

$$\mu\ddot{w}(x,t) + EIw''''(x,t) = q(x,w(x,t)), \tag{2}$$

where q is the distributed transverse force due to the magnetic field, which depends on the beam coordinate x and the current shape of the beam given by w at the actual time t. Since the force, which is distributed, is mostly concentrated around the tip of the beam and the shape function, which is used for the discretization, also has the largest values in this area, it seems reasonable to use a single force Q instead, which yields

$$q(x,w(x,t)) = Q(w(L,t))\delta(L), \tag{3}$$

with the Dirac distribution δ. The set of boundary conditions for the case of a clamped beam at $x = 0$ and free end at $x = L$, while the transverse force Q is considered in the field Eq. (3), is given by

$$w(0,t) = 0, \tag{4a}$$

$$w'(0,t) = 0, \tag{4b}$$

$$w''(L,t) = 0, \tag{4c}$$

$$w'''(L,t) = 0. \tag{4d}$$

To discretize the partial differential equation, a single mode ansatz

$$w(x,t) = a(t)\phi(x) \tag{5}$$

is introduced with a time-dependent modal coordinate a and a predefined ansatz function ϕ that depends on the x-coordinate only. The ansatz function is chosen to be the first eigenfunction of the beam without the influence of the magnets as addressed in the introduction, which satisfies the boundary conditions. The function ϕ is normalized in that way, that

$$\int_0^L \mu\phi^2(x)\mathrm{d}x = 1 \tag{6}$$

and

$$\int_0^L EI\phi''''(x)\phi(x)\mathrm{d}x = \omega_0^2 \tag{7}$$

hold where ω_0 is the first natural circular eigenfrequency of the beam without the magnets. Applying the Galerkin procedure by inserting Eqs. (5) into (2), multiplying both sides by ϕ, integrating over the length L of the beam and applying relations (6) and (7) yields the following one degree of freedom model

$$\ddot{a}(t) + 2D\omega_0\dot{a}(t) + \omega_0^2 a(t) = Q(\phi(L)a(t))\phi(L), \tag{8}$$

where an additional linear modal damping characterized by the damping ration D is added. Even though the influence of the magnetoelastic force appears on the right side, it is not an excitation, but a nonlinear term that depends on the modal coordinate a. The autonomous equation can be rewritten so that the former right side is now expressed as a polynomial of maximum degree $2N + 1$ and taken to the left side, which leads to

$$\ddot{a}(t) + 2D\omega_0\dot{a}(t) + \omega_0^2 a(t) + \sum_{i=1}^{N} \alpha_i a^{2i-1}(t) = 0, \tag{9}$$

where α_i are the polynomial coefficients of the nonlinear restoring force to be found from the computed magnetoelastic transverse force. Note that only odd polynomial coefficients α_i are considered, since the system including the magnets is symmetric, and therefore the restoring force is an odd function of the modal coordinate a. The error resulting from this approximation of the magnetoelastic force depends on N, which is so far usually set to two, resulting in a cubic restoring force.

Magnetoelastic Forces

The force, which depends nonlinearly on the displacement of the beam, is computed from the magnetic field, which itself depends on the current beam displacement. Consequently, it is necessary to compute the magnetic field and the resulting force for every possible beam deformation, but since the beam is discretized by a single mode shape ϕ, the shape of the beam in the magnetic field for any beam tip displacement is given. The magnetoelastic force is computed for a large number of uniformly distributed beam tip displacements. Due to the symmetry of the system, only positive displacements need to be considered.

Computing the magnetoelastic force is challenging, due to the large number of methods and force models with different underlying hypotheses about the macroscopic material properties in magnetoelastics. An overview of different approaches can be found in [36]. In the actual paper, the Maxwell stress tensor $\boldsymbol{T}$ is used to determine the magnetoelastic force, which depends in the magnetostatic case (no electric field) on the magnetic flux density and the permeability of vacuum μ_0, given by

$$\boldsymbol{T}_{ij} = \frac{1}{\mu_0}\boldsymbol{B}_i\boldsymbol{B}_j - \frac{1}{2\mu_0}\boldsymbol{B}^2\delta_{ij}. \tag{10}$$

The Kronecker delta δ is defined as 1 for $i = j$ and as 0 otherwise. When the magnetic field is known, the Maxwell stress tensor can be used to determine the force on a body with the volume V by the integral over the divergence of the Maxwell stress tensor by (e.g., [37])

$$\boldsymbol{F} = \iiint_V \mathrm{div}\ \boldsymbol{T}\mathrm{d}V. \tag{11}$$

The resulting force $\boldsymbol{F}$ is obviously a vector and as such has more components than just transverse to the beam axis. Hence, the beam is also under the influence of a longitudinal force. This results in a prestress on the Euler–Bernoulli beam that depends on the beam tip displacement. This aspect is neglected in the presented work but shall be the subject of further investigations.

The numerical evaluation of the integral in Eq. (11) in FEMM can be done with an implemented function called 'Weighted Maxwell Stress Tensor'. It is based on a method

proposed in [26, 38], respectively, in which a formulation for the force computation in a FE discretization by an integration over the volume is stated. This method is only capable of finding the force acting on an enclosed volume and requires the body to be totally placed in air. Neither the actual distribution of the force inside the body, nor the point of application of the equivalent resulting single force is known. Since a partial volume of the beam will always be connected to the remaining part of the beam and is not completely free, it is not possible to use this approach to find the distribution of the force with the provided function. Note that, so far, there is no widespread method to compute the distribution of magnetoelastic forces in a body, because although all common models agree on the total force on a whole body, they differ in the prediction of the distribution of the forces within the body [13]. For now, it will be assumed that the force is exclusively acting at the beam tip at $x = L$, as considered in Eq. (3). This reduction of the force to a single force, without consideration of its distribution along the beam, might cause erroneous predictions of the beam's dynamics and is to be investigated by further investigations.

The magnetic field is computed for a large number of beam displacements in the shape of the eigenfunction ϕ. Next, the total magnetoelastic force on the beam is determined by the implemented force function in FEMM. Its component in transverse direction for a variation of the magnet distance d (cf. Fig. 3) is shown in Fig. 4, where the results are in agreement with other investigations of such systems like in [15].

The graph shows the total nonlinear magnetoelastic force Q, where a positive sign indicates a force in the same positive coordinate direction as the beam tip displacement. Therefore, a positive force for positive displacements does not mean a positive restoring force but a negative one! For a small distance d between the magnets, the force is directed toward the center of the symmetric system, since in this case the magnets cause the same effect as one large magnet would do. In the cases of distinctly separated magnets, the force increases initially for increasing beam tip displacements, but will later decrease in its absolute value and eventually switch sign, implying a change in the force direction. For very large displacements of the beam, the force will become zero in any case as the beam tip is too far away to be influenced by the magnets. Note that only the magnetoelastic force and not the linear mechanical restoring force is shown.

To filter the numerical results and to find a model in the form of Eq. (9), the force distribution is expressed in polynomials, which can be found by a least square fit. Since the force is symmetrical—as aforementioned—only odd coefficients of the polynomial approximation are non-zero. The minimal necessary degree of the polynomials to approximate the numerical values depends on the investigated characteristics. As already mentioned in the introduction, magnet distances exist that cause mono-, bi- or tristability of the system. The minimal degree to model bistability is a cubic restoring force. Another way to achieve bistability is to use a quintic polynomial with or without the cubic term, that has three real roots and two complex roots [30]. A full quintic polynomial, which includes both, a cubic as well as a quintic term, is required only when tristability of the system is to be modeled. Any higher polynomials can be used to further refine the model. In this work, no results concerning the quality of any polynomial fit are shown, since there is a strong dependency on the considered maximum beam displacements. In fact, no polynomial is capable of representing the vanishing magnetic forces for beam displacements far beyond the position of the magnets. Therefore, the residuum of any approximation depends on the considered maximum deflections. The contribution of this work is that, based on the actual results, higher polynomials can be taken into account and that their accuracy can be quantified.

The theoretical results from this section are validated by measurements described in the next section.

Experimental Validation

To compare the numerical results obtained to experimental measurements, the overall model is divided into two major aspects: the model of the beam, in particular its linear restoring force due to its elastic behavior according to the Euler–Bernoulli beam theory, and the nonlinear magnetoelastic force caused by the magnets. At first, the beam model is compared to experimental measurements of its eigenfrequencies. Second, the overall model including the beam model and the magnetoelastic force is investigated. Both parts of the model determine together the multistability behavior of the equilibrium positions, which was also discussed in [13, 15]. It is suitable to investigate the model's results concerning the equilibrium positions and the number of existing equilibrium positions for different magnet distances; hence, we take into account the type of stability (mono-, bi- or tristability). A so far neglected aspect in existing analyses is the consideration of the beam's free oscillation, with small amplitude around the stable equilibrium positions. These can be determined experimentally and compared to the eigenfrequency of a linearization of the model. The experimental setup shown in Fig. 5, with the geometric properties given in Table 2, is used.

The mass distribution μ of the beam is found by dividing the total mass of the beam by its total length. The bending stiffness EI, which is a product of its area moment of inertia, is given for the rectangular cross section by $I = h^3 b/12$, and the material's Young's modulus is, in the literature, stated to be $E = 210$ GPa for steel. Considering these quantities and using Eq. (7) for higher modes with corresponding

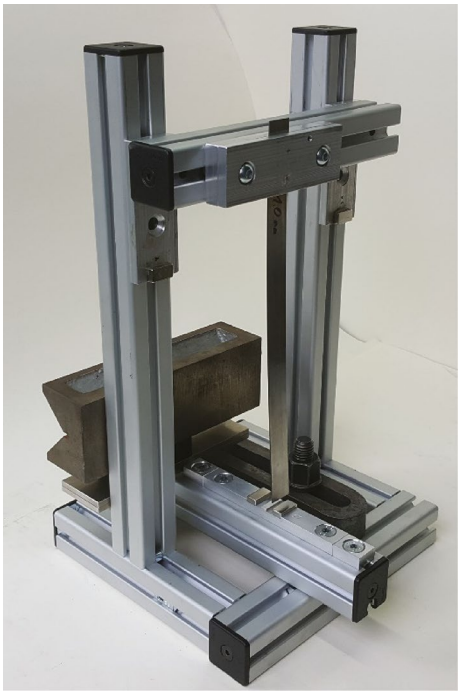

Fig. 5 Experimental setup [41]

Table 2 Geometric parameters (cf. Fig. 3)

Parameter	Dimension (mm)
Beam	
Length L	250
Width b	20
Height h	1
Magnets	
Length	5
Width	20
Height	10
Distances from edge to edge	
Beam tip to magnets g	6
Magnet to magnet d	5–21.5

eigenfunctions ϕ_i, the theoretical eigenfrequencies can be computed. They are experimentally determined by a laser vibrometer and a Fast-Fourier transformation of the beam's oscillation without magnets after applying small disturbances as initial conditions. To find an optimal agreement, the value E, which is the value with the highest uncertainty, is tuned to the corrected value $E = 208.8$ GPa in the model, which is still about 98% of the nominal value found in the literature. These mechanical parameters yield the results given in Table 3.

The results show a good agreement. The beam model can now be used for further investigations, in particular for the overall model of the entire system including the magnets. This is done with the experimental setup which was already used earlier by adding the magnet carriers shown in Fig. 6 on the right, all having different distances between the magnets.

Table 3 Comparison of theoretically and experimentally determined eigenfrequencies of the beam

Mode	Experimental (Hz)	Theoretical (Hz)	Deviation (%)
1	13.13	13.22	0.71
2	82.19	82.84	0.79
3	233.13	231.94	−0.51
4	456.56	454.56	−0.44
5	755.31	751.35	−0.53

The magnet carriers placed in the experimental setup can be replaced and their position with respect to the beam is set by two fixing blocks. The equilibrium positions of the beam are determined using a laser triangulation sensor and the frequency of the vibration around each of the stable equilibrium positions is determined by a Fast-Fourier transformation of the time signal measured by a laser vibrometer with a 2-m stand-off distance and a measuring range of 500 Hz (OptoMET Fixed Point Digital Laser Vibrometer). The results for positive and negative equilibrium positions are averaged and shown in Fig. 7 on the left. In [15], similar experimental investigations of the equilibrium positions can be found with comparable accordance with theory.

In Fig. 7, (left) the filled blue points show stable equilibrium positions, while the unfilled points show unstable equilibrium positions, which cannot be determined experimentally. The bifurcation behavior resulting from a change in the distance d between the magnets is clearly visible. For small d, the zero displacement (trivial) solution is the only stable one (monostable case). For increasing d, this solution becomes unstable and the system becomes bistable. For increasing d again—for values larger than 15.5 mm—the trivial solution becomes stable while additionally two unstable solutions exist, i.e., the system is now tristable. Finally, for theoretical values of d larger than 21 mm, the system becomes monostable again. Figure 7 (right) shows the frequencies that correspond to the linearization with respect to each stable equilibrium position.

The results show a good agreement and the numerical model represents the bistable as well as the tristable behavior that was found experimentally. Nevertheless, there are deviations which we attribute to the two main limitations of the modeling carried out. First: it seems to be necessary to determine the magnetic field through a three-dimensional simulation. Figure 8 shows another two-dimensional simulation of the magnetic field in a perpendicular plane of the coordinate system and it can be seen that there is a dependency of the magnetic field across the depth of the beam in

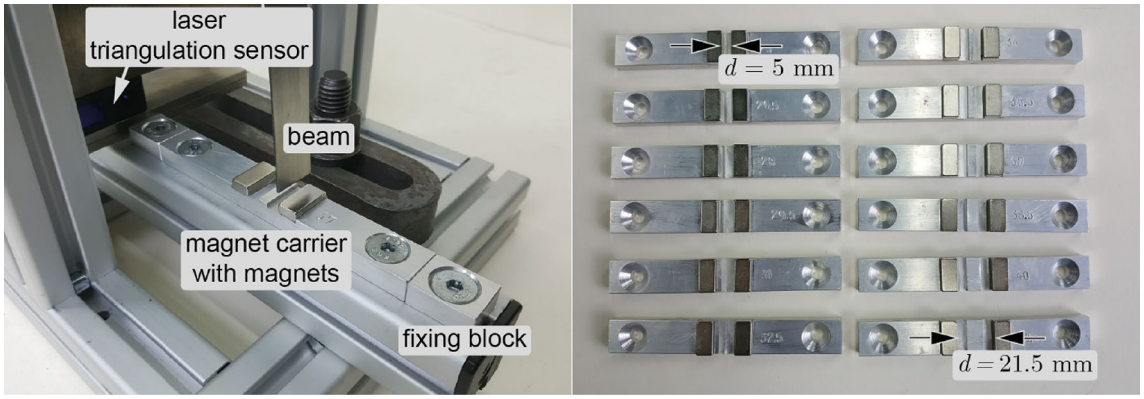

Fig. 6 Detail of the experimental setup (left) and interchangeable magnet carriers with varying magnet distances (right)

Fig. 7 Bifurcation behavior of the system for different magnets distances d: equilibrium positions and frequencies of free vibrations

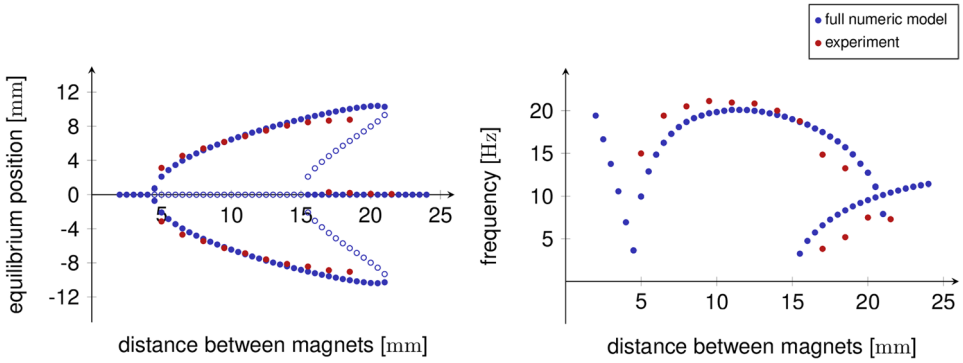

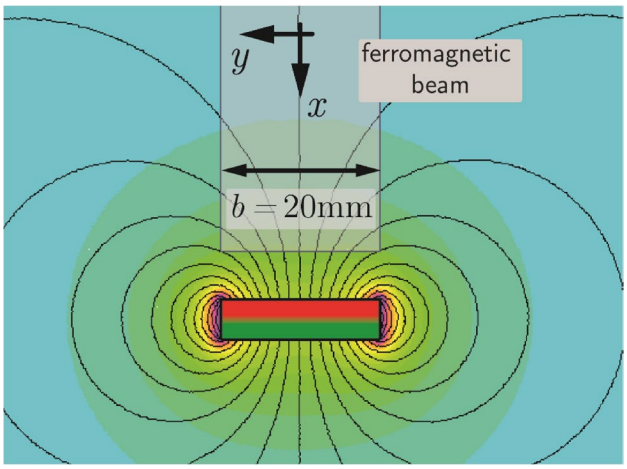

Fig. 8 Two-dimensional simulation of the magnetic field in the xy -plane instead of the xz-plane. The magnetic field is not constant across the depth b of the beam (y-direction), and therefore a three-dimensional simulation of the magnetic field is required

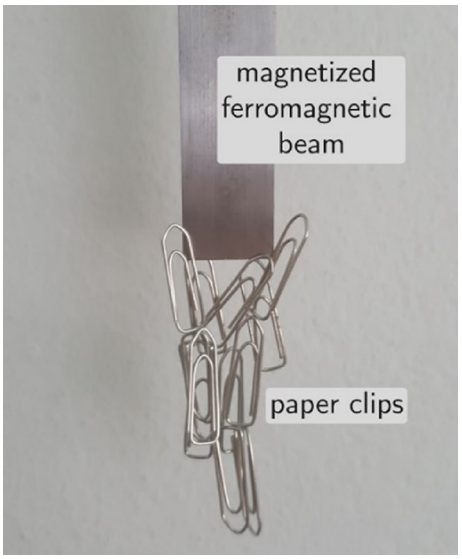

Fig. 9 Nonlinear material behavior of the magnetized beam in the absence of permanent magnets

the y-direction. Note that the position of the beam is shown but is itself not part of the simulation.

Second: another assumption made was a linear magnetic material behavior, which means that there is no magnetization of the beam when there are no magnets near the beam. Unfortunately, the contrary to this assumption can be seen in Fig. 9. There is a remaining magnetization, when

the magnets are removed. This means that there is a pronounced hysteresis of the magnetization of the beam. Therefore, its magnetization is also affected by the past, depending on how the beam was magnetized earlier. Both effects are not modeled, and corresponding further investigations are needed to improve the results.

Results and Conclusions

In this paper, the magnetoelastic force in transverse direction on the beam of the magnetoelastic energy harvesting system is computed. The approach outlined here provides the opportunity to deduce a model based on physical parameters to establish the possibility of designing a system from model parameters.

The total transverse force that acts on the beam was found by an evaluation of the Maxwell stress tensor, where the influence of the beam's magnetization on the magnetic field was considered by carrying out a large number of simulations of the magnetic field for different beam tip displacements. Not included in the modeling process is the longitudinal force component on the beam resulting in a prestress that depends on the beam's deformation. Also not covered is the distributional character of the magnetoelastic force. Furthermore, not included is any influence that originates from a magnetoelastic coupling, which additionally occurs in magnetic fields [13].

The beam is modeled according to the Euler–Bernoulli beam theory. Its linear elastic restoring force is compared to experiments by means of an investigation of the beam's eigenfrequencies without magnets. Through a slight tuning of the Young's modulus of the beam's material, a very good agreement to the measurements could be achieved, as given in Table 3. The overall model was examined experimentally by an investigation of the bifurcation behavior of the system on the experimental setup shown in Fig. 5, which allows a consideration of different magnet distances. The bifurcation behavior shows a generally good agreement, as can be seen in Fig. 7. Reasons for the remaining deviations are, as we believe, due to the limitations of a two-dimensional simulation of the magnetic field and the assumption of linear material behaviors, in particular concerning the ferromagnetic beam.

Future work will, therefore, concentrate on further refined modeling of the magnetoelastic forces and the investigations of the dynamic behavior of the entire energy harvesting system.

Funding This study was funded by Deutsche Forschungsgemeinschaft (Grant No. WA 1427/23-1,2).

Compliance with Ethical Standards

Conflict of Interest The authors declare that they have no conflict of interest.

References

1. Kim SK, Kim JH, Kim J (2011) A review of piezoelectric energy harvesting based on vibration. Int J Precis Eng Manuf 12(6):1129–1141. https://doi.org/10.1007/s12541-011-0151-3
2. Priya SJ (2007) Advances in energy harvesting using low profile piezoelectric transducers. J Electroceram 19:165–182. https://doi.org/10.1007/s10832-007-9043-4
3. Wei C, Jing X (2017) A comprehensive review on vibration energy harvesting: modelling and realization. Renew Sustain Energy Rev 74:1–18. https://doi.org/10.1016/j.rser.2017.01.073
4. Ajitsaria J, Choe SY, Shen D, Kim DJ (2007) Modeling and analysis of a bimorph piezoelectric cantilever beam for voltage generation. Smart Mater Struct 16(2):447–454. https://doi.org/10.1088/0964-1726/16/2/024
5. Erturk A, Inman DJ (2011) Piezoelectric energy harvesting. Wiley, New York. https://doi.org/10.1002/9781119991151
6. Sodano HA, Park G, Leo DJ, Inman DJ (2003) Model of piezoelectric power harvesting beam. In: ASME international mechanical engineering congress and expo, 15–21 Nov 2003, Washington DC, vol 40, no 2. http://dx.doi.org/10.1115/IMECE2003-43250
7. Yu S, He S, Li W (2010) Theoretical and experimental studies of beam bimorph piezoelectric power harvesters. J Mech Mater Struct 5(3):427–445. https://doi.org/10.2140/jomms.2010.5.427
8. Erturk A, Hoffmann J, Inman DJ (2009) A piezomagnetoelastic structure for broadband vibration energy harvesting. Appl Phys Lett 94:11–14. https://doi.org/10.1063/1.3159815
9. Gammaitoni L, Neri I, Vocca H (2009) Nonlinear oscillators for vibration energy harvesting. Appl Phys Lett 94:164102. https://doi.org/10.1063/1.3120279
10. Harne RL, Wang KW (2013) A review of the recent research on vibration energy harvesting via bistable systems. Smart Mater Struct 22:023001. https://doi.org/10.1088/0964-1726/22/2/023001
11. Tang L, Yang Y, Soh CK (2010) Toward broadband vibration-based energy harvesting. J Intell Mater Syst Struct 21:1867–1897. https://doi.org/10.1177/1045389X10390249
12. Daqaq MF, Masana R, Erturk A, Quinn DD (2014) On the role of nonlinearities in vibratory energy harvesting: a critical review and discussion. Appl Mech Rev 66(4):040801–040801-23. https://doi.org/10.1115/1.4026278
13. Moon FC, Holmes P (1979) A magnetoelastic strange attractor. J Sound Vib 65:275–296. https://doi.org/10.1016/0022-460x(79)90520-0
14. Litak G, Friswell MI, Adhikari S (2010) Magnetopiezoelastic energy harvesting driven by random excitations. Appl Phys Lett 96:214103-1. https://doi.org/10.1063/1.3436553
15. Tam JI (2013) Numerical and experimental investigations into the nonlinear dynamics of a magneto-elastic system. Final report, Department of Mechanical and Aerospace Engineering, Princeton University
16. Noll M-U, Lentz L, von Wagner U (2019) On the discretization of a bistable cantilever beam with application to energy harvesting. Facta Univ Ser Mech Eng (**submitted**)
17. Yan B, Zhou SX, Litak G (2018) Nonlinear analysis of the tristable energy harvester with a resonant circuit for performance enhancement. Int J Bifurc Chaos. https://doi.org/10.1142/S0218127418500920X

18. Zhou S, Cao J, Inman DJ, Lin J, Li D (2016) Harmonic balance analysis of nonlinear tristable energy harvesters for performance enhancement. J Sound Vib 373:223–235. https://doi.org/10.1016/j.jsv.2016.03.017
19. Zhou Z, Qin W, Zhu P (2017) A broadband quad-stable energy harvester and its advantages over bi-stable harvester: simulation and experiment verification. Mech Syst Signal Process 84:158–168. https://doi.org/10.1016/j.ymssp.2016.07.001
20. Erturk A, Inman DJ (2011) Broadband piezoelectric power generation on high-energy orbits of the bistable Duffing oscillator with electromechanical coupling. J Sound Vib 330:2339–2353. https://doi.org/10.1016/j.jsv.2010.11.018
21. Masana R, Daqaq MF (2011) Relative performance of a vibratory energy harvester in mono- and bi-stable potentials. J Sound Vib 330:6036–6052. https://doi.org/10.1016/j.jsv.2011.07.031
22. Friswell MI, Ali FS, Bilgen O, Adhikari S, Lees AW, Litak G (2012) Non-linear piezoelectric vibration energy harvesting from a vertical cantilever beam with tip mass. J Intell Mater Syst Struct 23(13):1501–1521. https://doi.org/10.1177/1045389X12455722
23. Lan C, Qin W (2017) Enhancing ability of harvesting energy from random vibration by decreasing the potential barrier of bistable harvester. Mech Syst Signal Process 85:71–81. https://doi.org/10.1016/j.ymssp.2016.07.047
24. Stanton SC, McGehee CC, Mann PB (2010) Nonlinear dynamics for broadband energy harvesting: investigation of a bistable piezoelectric inertial generator. Physica D 239:640–653. https://doi.org/10.1016/j.physd.2010.01.019
25. Wang H, Tang L (2017) Modeling and experiment of bistable two-degree-of-freedom energy harvester with magnetic coupling. J Mech Syst Signal Process 86:29–39. https://doi.org/10.1016/j.ymssp.2016.10.001
26. Henrotte F, Deliege G, Hameyer K (2002) The eggshell method for the computation of electromagnetic forces on rigid bodies in 2D and 3D. CEFC 2002, Perugia, Italy, 16–18 Apr 2002. https://doi.org/10.1108/03321640410553427
27. Martens W, von Wagner U, Litak G (2013) Stationary response of nonlinear magneto-piezoelectric energy harvester systems under stochastic excitation. Eur Phys J Spec Top 222:1665–1673. https://doi.org/10.1140/epjst/e2013-01953-5
28. Noll M-U, Lentz L (2016) On the refined modeling of the force distribution in a bistable magnetoelastic energy harvesting system due to a magnetic field. Proc Appl Math Mech 16(1):289–290. https://doi.org/10.1002/pamm.201610133
29. Kim P, Seok J (2014) A multi-stable energy harvester: dynamic modeling and bifurcation analysis. J Sound Vib 333(21):5525–5547. https://doi.org/10.1016/j.jsv.2014.05.054
30. Lentz L (2018) Zur Modellbildung und Analyse von bistabilen Energy-Harvesting-Systemen. Doctoral thesis, TU Berlin. https://doi.org/10.14279/depositonce-7525
31. Noll M-U, Lentz L (2017) On the modeling of the distributed force in a bistable magnetoelastic energy harvesting system. In: 4th Workshop in devices, materials and structures for energy harvesting and storage in Oulu, Finland
32. Moon FC (1997) Magneto-solid mechanics. Wiley, New York
33. Furlani EP (2001) Permanent magnet and electromechanical devices. Academic Press, New York
34. Reich F (2017) Coupling of continuum mechanics and electrodynamics—an investigation of electromagnetic force models by means of experiments and selected problems. Doctoral thesis, TU Berlin. http://dx.doi.org/10.14279/depositonce-6518
35. Derby N, Olbert S (2010) Cylindrical magnets and ideal solenoids. Am J Phys 78(3):229–235. https://doi.org/10.1119/1.3256157
36. de Medeiros LH, Reyne G, Meunier G (1999) About the distribution of forces in permanent magnets. IEEE Trans Magn 34:3560–3563. https://doi.org/10.1109/20.767168
37. de Medeiros LH, Reyne G, Meunier G (1998) Comparison of global force calculations on permanent magnets. IEEE Trans Magn 34:3560–3563. https://doi.org/10.1109/20.717840
38. McFee S, Webb JP, Lowther DA (1988) A tunable volume integration formulation for force calculation in finite-element based computational magnetostatics. IEEE Trans Magn 24(1):439–442. https://doi.org/10.1109/20.43951
39. Noll M-U (2018) Energy harvesting system. https://doi.org/10.6084/m9.figshare.7492208
40. Noll M-U (2018) Magnetic field. https://doi.org/10.6084/m9.figshare.7492469
41. Noll M-U (2019) Experimental setup of an energy harvesting system III. https://doi.org/10.6084/m9.figshare.7993115

FACTA UNIVERSITATIS
Series: **Mechanical Engineering** Vol. 17, N° 2, 2019, pp. 125 - 139
https://doi.org/10.22190/FUME190301031N

Original scientific paper

ON THE DISCRETIZATION OF A BISTABLE CANTILEVER BEAM WITH APPLICATION TO ENERGY HARVESTING

Max-Uwe Noll, Lukas Lentz, Utz von Wagner

Chair of Mechatronics and Machine Dynamics, Technische Universität Berlin

Abstract. *A typical setup for energy harvesting is that of a cantilever beam with piezoceramics excited by ambient base vibrations. In order to get higher energy output for a wide range of excitation frequencies, often a nonlinearity is introduced by intention in that way, that two magnets are fixed close to the free tip of the beam. Depending on strength and position of the magnets, this can either result in a mono-, bi- or tristable system. In our study, we focus on a bistable system. Such systems have been investigated thoroughly in literature while in almost all cases the beam has been discretized by a single shape function, in general the first eigenshape of the linear beam with undeflected stable equilibrium position.*

There can be some doubts about the suitability of a discretization by a single shape function mainly due to two reasons. First: In case of stochastic broadband excitations a discretization, taking into consideration just the first vibration shape seems not to be reasonable. Second: as the undeflected position of the considered system is unstable and the system significantly nonlinear, the question arises, if using just one eigenshape of the linear beam is a suitable approximation of the operation shapes during excited oscillations even in the case of harmonic excitation. Are there other, e.g. amplitude dependent, possibilities and/or should multiple ansatz functions be considered instead?

In this paper, we focus mainly on the second point. Therefore, a bistable cantilever beam with harmonic base excitation is considered and experimental investigations of operation shapes are performed using a high-speed camera. The observed operation shapes are expanded in a similar way as it is done in a theoretical analysis by a corresponding mixed Ritz ansatz. The results show the existence of distinct superharmonics (as one can expect for a nonlinear system) but additionally the necessity to use more than one shape function in the discretization, covering also the amplitude dependence of the observed operation shapes.

Key Words: *Bistable Beam, Energy Harvesting, Discretization, Vibration Shape Analysis via High Speed Camera*

Received March 01, 2019 / Accepted June 20, 2019
Corresponding author: Max-Uwe Noll
Chair of Mechatronics and Machine Dynamics, Technische Universität Berlin, Einsteinufer 5, 10587 Berlin
E-mail: max-uwe.noll@tu-berlin.de

1. INTRODUCTION

Harvesting of energy from ambient vibrations has attracted much interest and corresponding research in the past decades. A common method for transferring the mechanical energy into electric one is the usage of piezoceramics fixed on corresponding vibration structures. A survey of such systems gives, for example, the paper [1]. The classical setup in that case is a cantilever beam with piezoceramics bonded close to the clamping excited by ambient base vibrations. These systems perform well when they are designed as a linear resonator with its eigenfrequency tuned to the frequency of the excitation. A higher energy output, especially for broadband or stochastic excitations, can be realized in such systems, if nonlinearities are introduced by intention resulting in a broadband characteristic for large responses of excited vibrations compared to sharp resonance peaks of the linear system [2]. A common setup is to fix two magnets symmetrically close to the free end of the beam, as shown in Fig. 1.

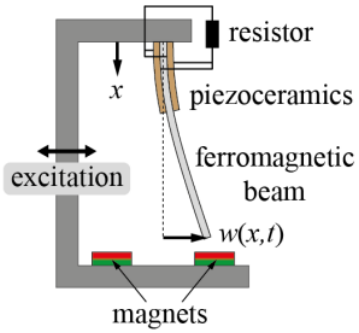

Fig. 1 Vibrational energy harvesting system [3]

Depending on strength and position of the magnets, this can either result in a mono-, bi- or tristable (e.g. [4, 5, 6] respectively) system. In this paper we investigate the bistable configuration and focus on the occurring vibration shapes during non-chaotic operation. In that case, there are two main types of solutions, namely so-called intrawell solutions around one of the two stable equilibrium positions and so-called interwell solution with large displacements covering both stable equilibrium positions. For the modeling of the system, knowledge is necessary for the discretization of the beam with respect to its longitudinal coordinate x, introducing a mixed (dependence on both x and time t) Ritz ansatz

$$w(x,t) = \sum_{i=1}^{n} W_i(x)\, p_i(t) \tag{1}$$

into the partial differential equation describing the continuum vibrations of the beam. Herein $w(x,t)$ is the lateral displacement of the beam relatively to the moving frame and n the chosen ansatz order. In this ansatz shape functions $W_i(x)$ shall be given (they must fulfill all the boundary conditions) while functions $p_i(t)$ can be calculated from the thereby discretized model equations e.g. by Harmonic Balance. This let arise the question of suitable shape functions $W_i(x)$ and ansatz orders n.

For the sake of simplicity and in order to concentrate on the question of how to discretize a bistable beam, the piezoceramics are neglected in the following. Only the

setup of the cantilever beam with magnets and base excitation is considered. The classical paper describing a corresponding modeling is that of Moon [7] discretizing the beam with the first eigenshape of the linear Euler-Bernoulli beam and modeling the magnetic forces by a third order polynomial. This discretization results in a Duffing-oscillator with negative linear and positive cubic restoring term. Most publications follow this model when adding the piezoceramics for the energy harvesting system, e.g. [8] where it was shown, that the nonlinear system performs better than its linear counterpart for a non-resonant excitation and [9] where the system was analyzed for the case of a stochastic excitation. Publications using more than one ansatz function are very rare. In [10] multiple ansatz functions are applied for a buckled beam system, nevertheless ending finally up again with a one-degree of freedom model.

There can be some doubts about the suitability of this discretization by a single shape function mainly due to two reasons. First: In the case of stochastic broadband excitation a discretization, taking into consideration just the first vibration shape, seems not to be reasonable. Therefore, the authors have in prior investigations [11, 12] added a second ansatz function in that way, that not just the first, but also the second eigenfunction of the linear beam is considered in the Ritz ansatz. Second: as the undeflected position of the considered system is unstable and the system significantly nonlinear, the question arises if using just the first eigenshape of the linear beam is a suitable approximation of the operation shapes during excited oscillations even in the case of harmonic excitation. Are there other, e.g. amplitude dependent, possibilities and should multiple ansatz functions be considered instead? In the work [13] and [14] this topic was already addressed, and it is shown how the usage of linear shape functions leads to erroneous results. Furthermore, a purely theoretical method to compute nonlinear, i.e. amplitude dependent shape functions, is presented. Later the concept of nonlinear normal-modes was transferred to the analysis of discrete nonlinear systems, see e.g. the review [15] and the references therein.

On the other hand in [16] it is shown, that for a bistable system, in that case a buckled beam, the two first modes coexist during the snapping process. In [17] exact solutions of postbuckling configurations of beams are calculated, but also the interaction between vibration modes is shown. Nevertheless, as already mentioned, it is state of the art in considering energy harvesting systems to use just one mode shape for discretization. An example for this is [18], where both the buckled beam as in the two papers mentioned before as well as the bistable cantilever beam, that is considered in the actual paper, is discretized by a single degree of freedom.

In this paper, the questions, if the mixed Ritz ansatz, Eq. (1), gives a suitable modeling as well as how many and which ansatz functions should be used, is discussed in the case of harmonic base excitation by analyzing experimental results. Therefore, operation shapes have been captured by a high-speed camera. The observed operation shapes are expanded into their frequency content and then the vibration shape corresponding to each frequency is analyzed.

2. Experimental Setup

The chosen setup for the experimental investigations is shown in Fig. 2. The steel cantilever beam is placed in an aluminum frame excited by a shaker and the bistability is realized by two magnets placed approximately symmetrical to the undeflected position of

the beam, therefore becoming unstable. The beam's static deflection, when there is no base excitation, as well as the dynamic displacement of the beam tip are measured using a laser triangulation sensor which is attached to the moving frame, hence directly providing the relative displacement of the beam tip from its undeflected position without the superposed movement of the supporting frame. The base excitation of the system is captured by a (nonmoving) laser vibrometer. Laptop I is used to process the data delivered by these two measurement devices with the software package vAnalyzer.

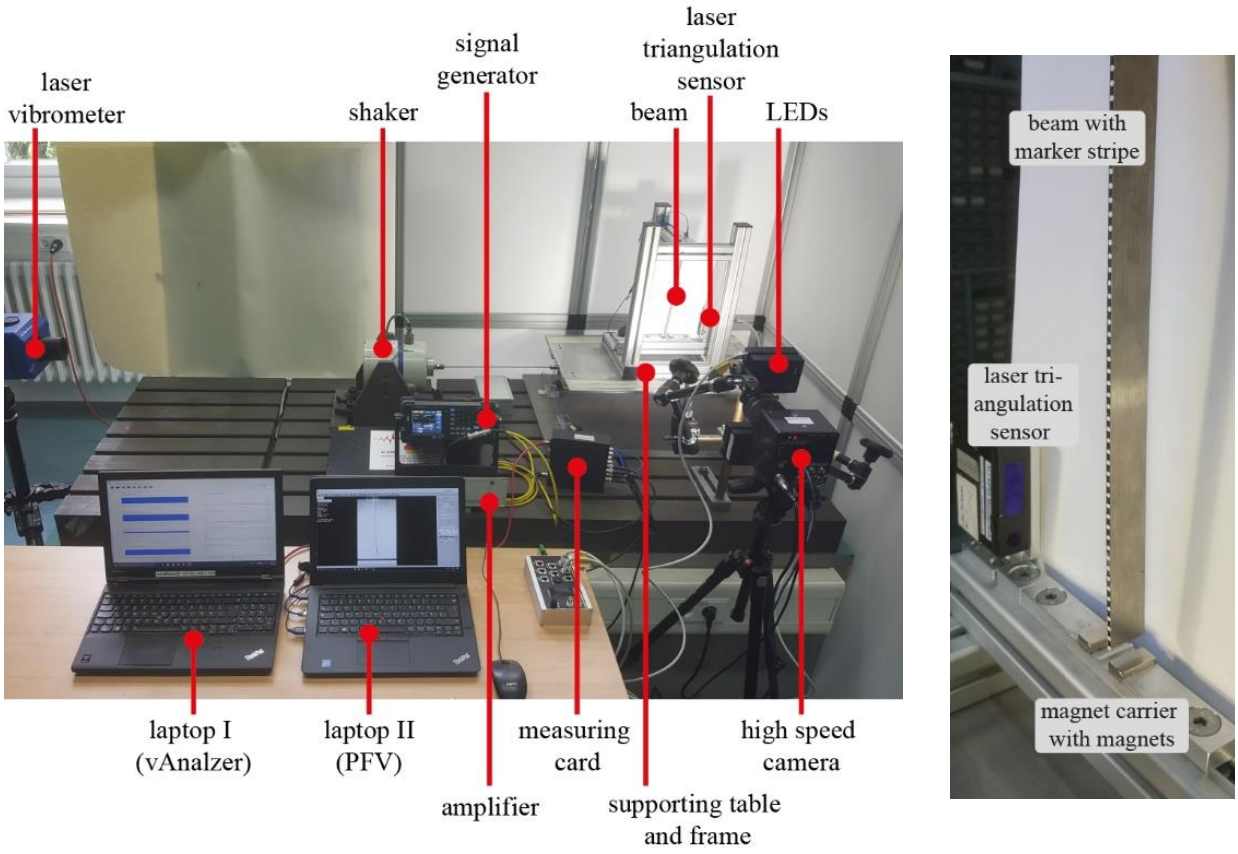

Fig. 2 Experimental setup with bistable cantilever beam excited by a shaker (left) and beam with magnets in detail (right) [19]

Laptop II is utilized to control the high-speed camera Photron Fastcam Mini AX100 by the software package **P**hontron **F**ASTCAM **V**iewer for high speed digital imaging. The dimensions of the cantilever beam together with its first natural frequency (without magnets) are given in Table 1.

Table 1 Properties of the cantilever beam

Property	Value
Beam length	250 mm
Beam width	20 mm
Beam thickness	1 mm
1st eigenfrequency	13.1 Hz

The magnets are intended to be placed symmetrically with respect to the undeflected position of the beam in order to realize an approximately equal distance of the two equilibrium positions from the undeflected beam position. The magnets are glued to a magnet carrier, also made of aluminum, which ensures a constant and reproducible distance between the magnets of approximately 14 mm. The exact placement of the magnet carrier with respect to the beam is however limited by the manual adjustment of the carrier with finite accuracy and reproducibility. The resulting distances of two realized experiments together with the frequencies of small free vibrations around the two stable equilibrium positions (intrawell solutions) are given in Table 2.

Table 2 Properties of bistable beam configuration (magnet distance approx. 14 mm)

	left	right
Setup I (static experiment in Fig. 6)		
Equilibrium position	-6.91 mm	7.13 mm
Frequency	15.1 Hz	14.5 Hz
Setup II (dynamic experiments)		
Equilibrium position	-7.01 mm	7.40 mm
Frequency	16.0 Hz	16.0 Hz

A paper stripe with geometry given in Fig. 3 is attached to the front side of the beam. The beam itself has a thickness of one millimeter, but for a higher detection rate of the markers their size is chosen to be two millimeters in diameter on an all-black background of the three millimeters wide paper stripe, which therefore exceeds the thickness of the beam.

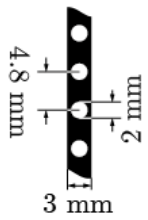

Fig. 3 Geometry of marker stripe

The camera was positioned manually in front of the beam setup with three goals regarding its arrangement. First: the camera was orientated orthogonal to the beam's plane of motion. Second: the camera was placed as far as possible from the beam to reduce errors due to perspective influences. Third: the camera was placed as close as needed so that the beam took up almost the full height of the pictures in order to use the full resolution to capture each marker.

The camera is taking monochrome black and white videos with a frame rate of 4000 frames per second and each frame has a resolution of 384×944 pixels. Each video has a duration of at least one second. To further reduce the amount of data and processing time only every second frame was considered for further evaluation. The authors are aware that taking a picture is a sampling like process of the time continuous movement of the markers. That means that not only the sampling rate needs to be at least two times the highest frequency that is expected to be occurring in the measured signal (Nyquist criteria), but

also needs to be filtered for even higher frequencies to prevent aliasing effects. Since there is no possible way to filter these analog signals, we have checked the results from the digital image analysis to the frequencies determined by the laser triangulation sensor, for which the signal has been aliasing filtered properly before sampling. Both results are in good accordance with each other.

The very first frame of each video is replaced by a frame showing the static, undeflected beam without magnets (Fig. 4 (left)), which was taken before the magnets were applied. This first frame is taken as the reference to determine the relative displacement of each marker on each frame from its position when the beam is undeflected. The software GOM Correlate is used to analyze each frame of the video and to detect the relative distance from its position on the reference frame. The calibration of the distance measurement from the frames is done using the known distance of the markers on the maker strip, which results in a resolution of roughly 3.5 pixel/mm.

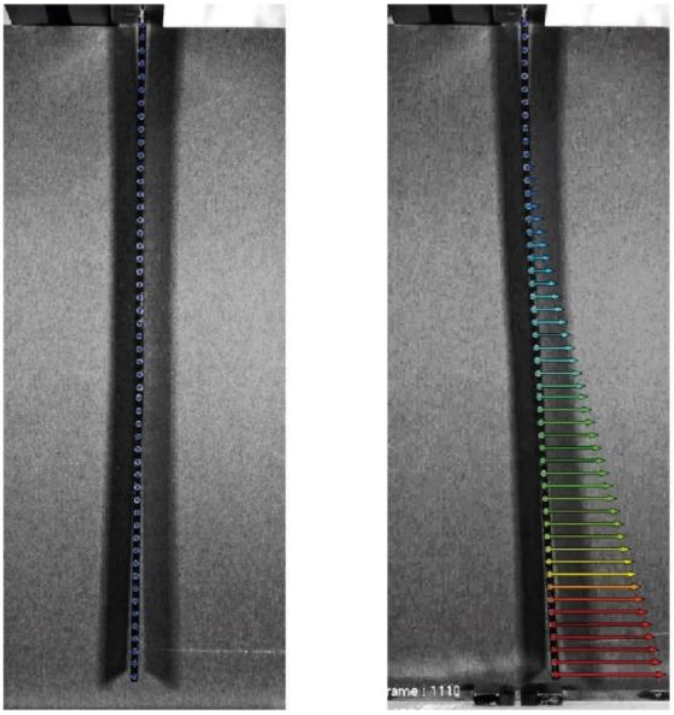

Fig. 4 Reference frame of undeflected beam without magnets (left) and marker detection and evaluation of marker displacement with GOM Correlate (right)

Further it is necessary to eliminate the relative movement of the supporting frame to the nonmoving camera in order to find the relative displacement of each marker. This is done by subtracting the current displacement of the marker that is the nearest to the beam clamping from all other marker displacements of that current frame.

3. Results of Experimental Investigations and their Analysis

The aim of the following investigations is to decide if the observed operational vibration shapes of the harmonically excited bistable beam can be expanded in the eigenshapes of the Euler-Bernoulli beam as well as how many ansatz functions are required according to the

mixed Ritz ansatz (Eq. (1)). Fig. 5 shows the first two eigenshapes ϕ_1, ϕ_2 of the beam together with the static bending line caused by a constant lateral tip force.

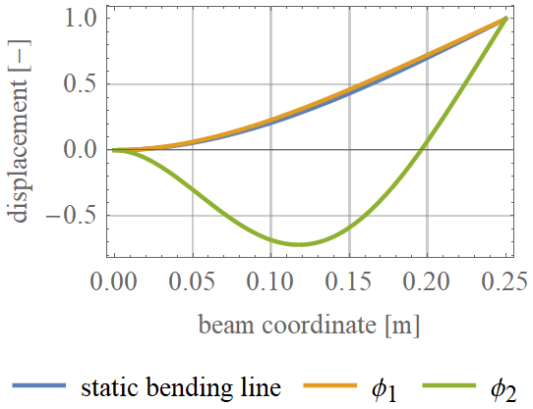

Fig. 5 Beam eigenshapes and static bending line according to the linear Euler-Bernoulli beam theory

In Fig. 6 the measured static bending line resulting in the "right" stable equilibrium (positive displacement according to Table 2) resulting from the magnets from the setup I is displayed. This measured bending line shows a high agreement with the theoretical static bending line.

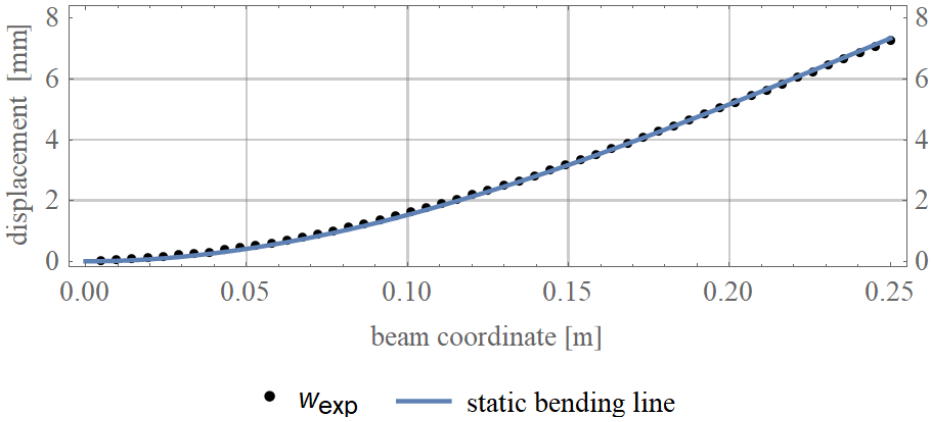

Fig. 6 Static bending of the beam in "right" equilibrium position (Table 2, setup I)

Now the operation shapes are measured with a high-speed camera. Fig. 7 shows typical examples of the two main types of solutions, namely the intrawell solution (left) and the interwell solution (right). The phase diagram of the last marker at the tip of the beam is shown, where the velocity has been determined by the time derivative of the displacement after filtering the signal by a Butterworth low pass filter.

Both solution types do not show any period multiplication in these tests, which restricts in the stationary case the occurring response frequencies to the excitation frequency and corresponding superharmonics while subharmonics do not occur.

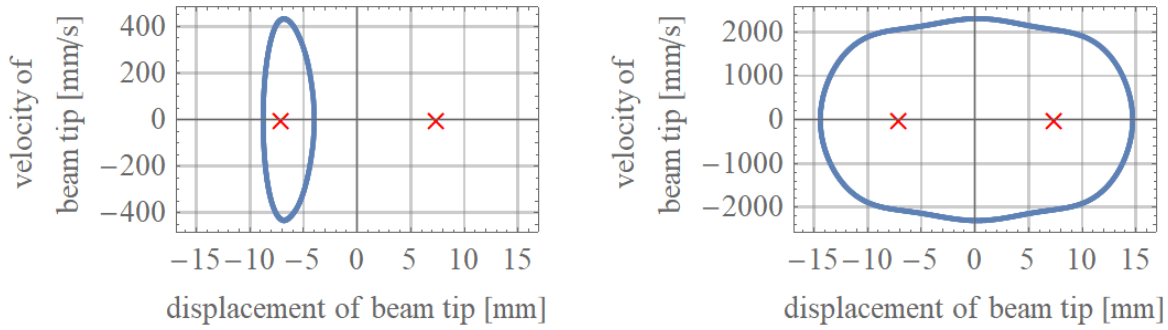

Fig. 7 Phase diagram of beam tip: intrawell solution (left) and interwell solution (right) (setup II)

For distinct points $\hat{x}_j$ time series for the displacement can be derived. A corresponding result is shown in Fig. 8 in the case of harmonic excitation with f_0=14 Hz.

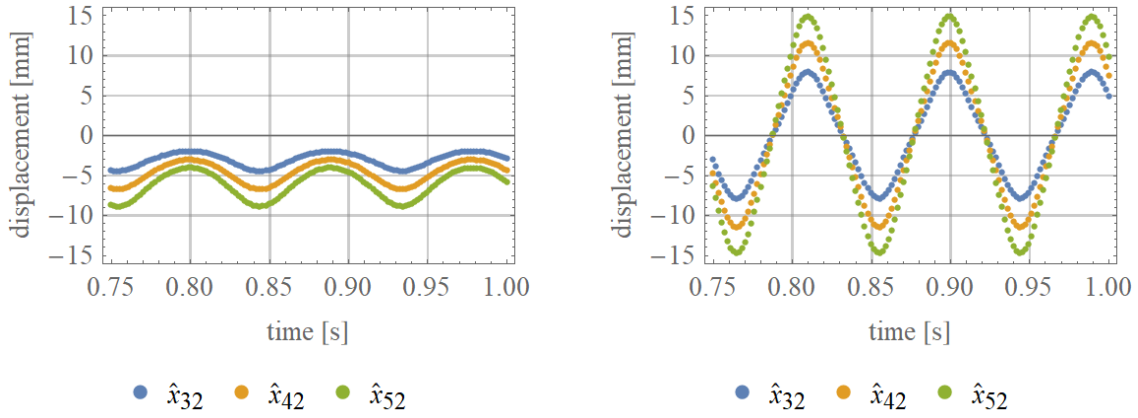

Fig. 8 Time series of three points x_j, j = 32,42,52 of the beam in case of an intrawell (left) and interwell solution (right) resulting from harmonic excitation with f_0=14 Hz (setup II)

Again in Fig. 8 on the left an intrawell solution is shown while an interwell solution is displayed on the right. An FFT (**F**ast **F**ourier **T**ransformation) analysis for each of the time series $\hat{x}_j(t_i)$ is performed. A corresponding result is shown in Fig. 9.

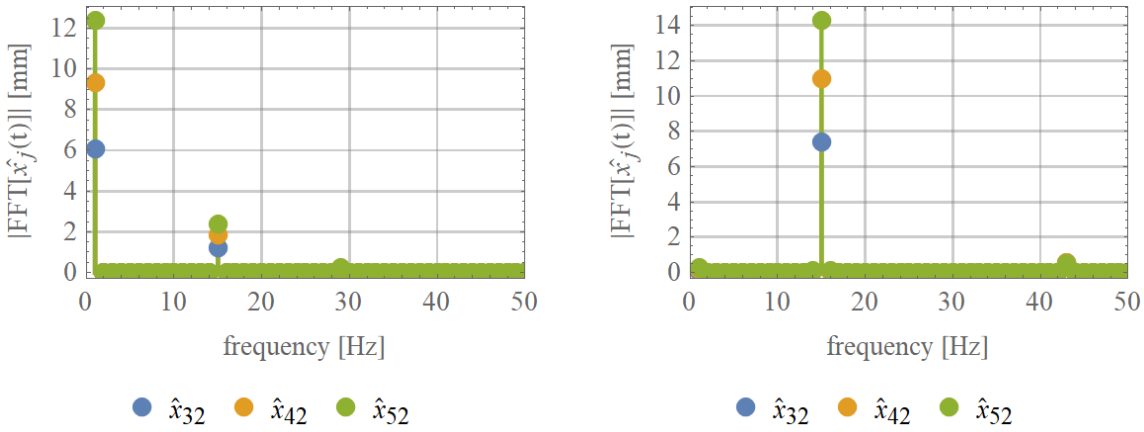

Fig. 9 FFT analysis of the time series in Fig. 8 (setup II)

According to the nonlinear character of the system, distinct superharmonics of the excitation frequency in the response can be expected. Due to the symmetric characteristic of the interwell solutions, odd superharmonics are expected while even and odd superharmonics can be expected in the intrawell case due to the asymmetric restoring characteristic around the stable equilibrium positions originating from the magnets. This is confirmed by the experimental results. Subharmonics do not occur, as there are no period multiplications.

Having considered these initial results, we will first reconsider the mixed Ritz ansatz (Eq. (1)) and the corresponding theoretical analysis. Using e.g. Harmonic Balance as solution method for the discretized system equations and considering an excitation being proportional to cosΩt with $\Omega=2\pi f_0$ where Ω is the circular excitation frequency, one can expect, that time function $p_i(t)$ in the mixed Ritz ansatz can be expanded as follows

$$p_i(t) = \sum_{k=0}^{m} A_{ik} \cos(k\Omega t + \varphi_{ik}) \tag{2}$$

where k=0,1,2,3, … in the case of the intrawell solution and k=1,3,5,7, … in the interwell case. The intrawell case contains both a constant solution part (k=0) due to the deflected stable equilibrium position as well as even superharmonics due to the non-symmetric magnet force characteristic. On the other hand, the interwell solution has in theory a zero mean value and is symmetric, which limits k to odd numbers. These considerations are almost fully confirmed by the results shown in Fig. 8 and 9. Only a small constant part of the interwell solution is possibly due to the non-perfect symmetry of the magnets (Table 2). Inserting the expansion (2) in the mixed Ritz ansatz results after sorting in

$$w(x,t) = \sum_{i=1}^{n} W_i(x) \sum_{k=0}^{m} A_{ik} \cos(k\Omega t + \varphi_{ik}) \,, \tag{3}$$

As already mentioned in the introduction, we are interested in the question which and how many shape functions $W_i(x)$ are necessary for a good representation of intra- and interwell solutions in our setup. Therefore, we will now do the same expansion with the experimental results. For the j-th distinct point $\hat{x}_j$ (position on the beam) the time series of its movement is expanded by a Fourier expansion

$$w(\hat{x}_j, t) = \sum_{k=0}^{m} \tilde{a}_{jk} \cos(k\Omega t + \tilde{\varphi}_{jk}) \tag{4}$$

with coefficients $\tilde{a}_{jk}$ and a phase shift $\tilde{\varphi}_{jk}$. While φ_{ik} in Eq. (2) describe the phase shift compared to the excitation, $\tilde{\varphi}_{jk}$ depend on the time sequence of the video to be analyzed, and are triggered by the starting of the measurement. As we are interested purely in vibration shapes this is not a restriction.

For each considered multiple k of excitation circular frequency Ω, from $\tilde{a}_{jk}$ a shape $\hat{w}_k(x)$ shall be formed, which is then expanded in considered shape functions $W_i(x)$. To do so, the following circumstances must be taken into consideration. $\tilde{a}_{jk}$ are taken from the absolute values of the Fourier expansion (which is performed in a complex notation), therefore they have positive values only. This means that in the cases where the beam vibration has vibration nodes it is to be considered that there is a phase shift of π between

$\widetilde{\varphi}_{jk}$, even for one fixed mode *k*. Therefore, applicability of Eq. (4) requires, that for each *k* all $\widetilde{\varphi}_{jk}$ are constant for all *j* with the exception that a jump with size π is possible in the case of nodes. If this is the case, subscript *j* can be neglected in the following and the final phase shift $\hat{\varphi}_k$ is described by

$$\hat{\varphi}_k = \widetilde{\varphi}_{1k} \tag{5}$$

while $\widetilde{a}_{jk}$ are replaced by $\hat{a}_{jk}$ following the scheme

$$\hat{a}_{jk} = \begin{cases} \widetilde{a}_{jk} \text{ if } \left|\widetilde{\varphi}_{jk} - \widetilde{\varphi}_{1k}\right| = 0 \\ -\widetilde{a}_{jk} \text{ if } \left|\widetilde{\varphi}_{jk} - \widetilde{\varphi}_{1k}\right| = \pi. \end{cases} \tag{6}$$

From $\hat{a}_{jk}$ the shape $\hat{w}_k(x)$ is formed, which is expanded as follows

$$\hat{w}_k(x) = \sum_{i=1}^{n} \hat{A}_{ik} W_i(x) \tag{7}$$

with coefficients $\hat{A}_{ik}$. In general, displacement *w*(*x*,*t*) from the experiments is therefore given by

$$w(x,t) = \sum_{k=0}^{m} \hat{w}_k(x) \cos(k\Omega t + \hat{\varphi}_k) \tag{8}$$

Inserting Eq. (7) in (8) results in

$$w(x,t) = \sum_{k=0}^{m} \sum_{i=1}^{n} \hat{A}_{ik} W_i(x) \cos(k\Omega t + \hat{\varphi}_k) \tag{9}$$

and after sorting in

$$w(x,t) = \sum_{i=1}^{n} W_i(x) \sum_{k=0}^{m} \hat{A}_{ik} \cos(k\Omega t + \hat{\varphi}_k) \tag{10}$$

which is almost equal to the theoretical result (3). The only differences are that subscript *i* is missing in $\hat{\varphi}_k$, i.e. if the expansion is possible as described, the phase shift for the *k*-th harmonic does not depend on the number *i* of the mode $W_i(x)$, and reference times for the phase shifts may differ as described above.

In the following, the steps (4)–(7) are performed with the experimental results. Fig. 10 shows a more detailed analysis of the frequency contents of the intrawell solution (left) and interwell solution (right) of the beam tip with a logarithmic scale. Constant parts (zero frequency) are not considered in the following as they are due to the static bending line, which is geometric almost similar to the first eigenshape ϕ_1 (Fig. 4) and therefore anyway covered by the following expansion in ϕ_1 and ϕ_2. In the case of the intrawell solution we limit our result in accordance with Fig. 10 (left) to *k*=1, 2 and 3, while we will take in the case of the interwell solution *k*=1, 3, 5 and 7 into consideration.

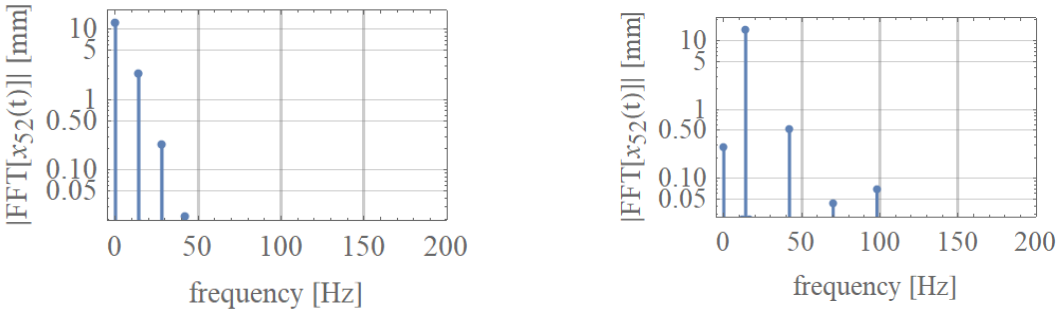

Fig. 10 FFT of beam tip displacement of intrawell (left) and interwell (right) oscillation (setup II)

Fig. 11 shows $\hat{a}_{j1}$ for the intrawell and interwell solution respectively, forming the corresponding shapes $\hat{w}_1(x)$. In the following these shapes shall be expanded according to Eq. (7), where coefficients $\hat{A}_{ik}$ are found from the experimental data using a least square approach. As shape functions $W_i(x)$ we take the first two eigenfunctions ϕ_1, ϕ_2 of the beam as sketched in Fig. 5, i.e. we limit n by 2, which means $i = 1, 2$. The corresponding expansion shows, that shapes $\hat{w}_1(x)$ are almost identical to $\hat{A}_{11}\phi_1$, and $\hat{A}_{21} \approx 0$ (red lines in Fig. 11 (top)).

Fig. 11 (bottom) shows the corresponding phases $\tilde{\varphi}_{j1}$, which should be equal, or only have a jump of π at a vibration node, for all j in order to allow the expansion (4). In fact, it can be seen that there are only small deviations occurring mainly close to the clamping, i.e. at points with only small displacements.

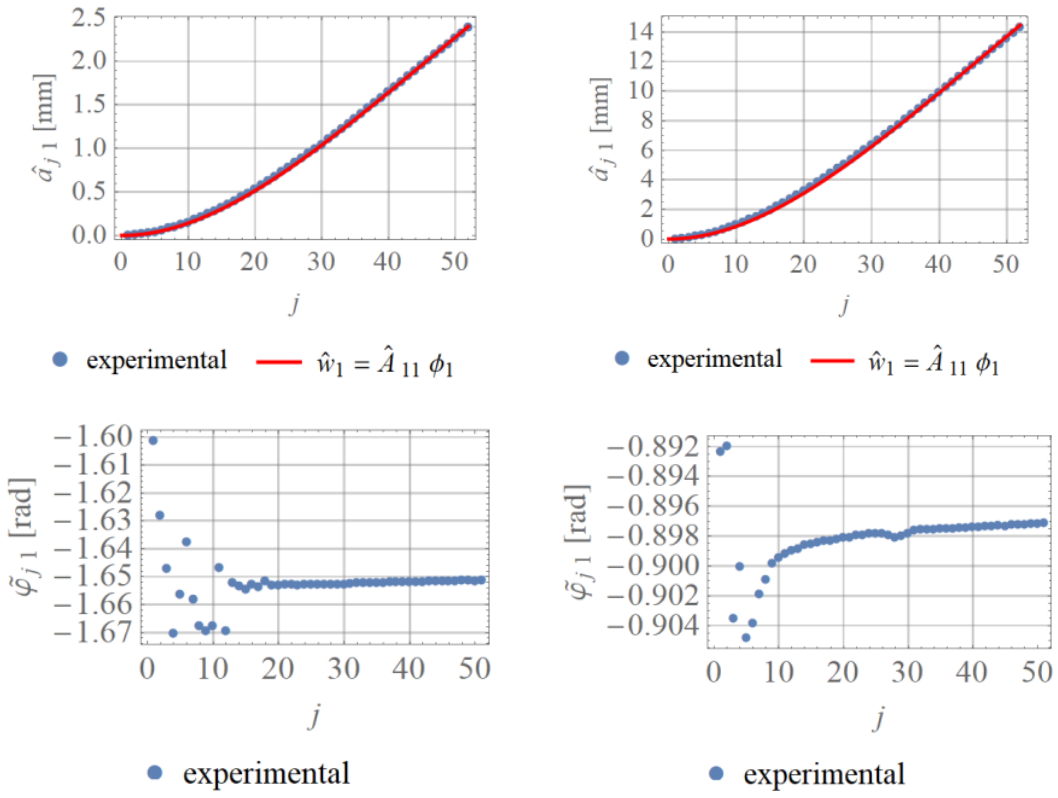

Fig. 11 Vibration shape $\hat{a}_{j1}$ of intrawell (top left) and interwell (top right) for frequency $f \approx f_0$ and corresponding phases $\tilde{\varphi}_j$ beneath (setup II)

For the intrawell solution Fig. 12 shows the $\hat{a}_{j2}$ and $\hat{a}_{j3}$ forming the shapes $\hat{w}_2(x)$ and $\hat{w}_3(x)$ corresponding to twice and three times excitation frequency $2f_0$ and $3f_0$.

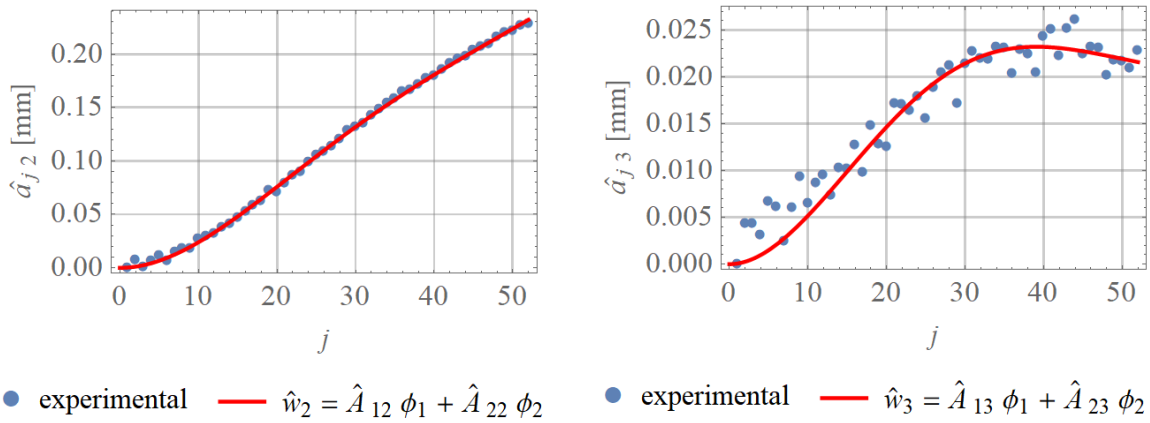

Fig. 12 Vibration shape of intrawell oscillation for frequency $f = 2f_0$ (left) and $f = 3f_0$ (right) (setup II)

While $\hat{w}_2(x)$ gives a somewhat smooth curve there are several small deviations in $\hat{w}_3(x)$ but the shapes of both functions can be expanded with the chosen ansatz functions ϕ_1 and ϕ_2.

Fig. 13 shows this step in the case of the interwell solutions for shapes $\hat{w}_3(x)$, $\hat{w}_5(x)$ and $\hat{w}_7(x)$. All shapes can be expanded in good approximation by ϕ_1 and ϕ_2.

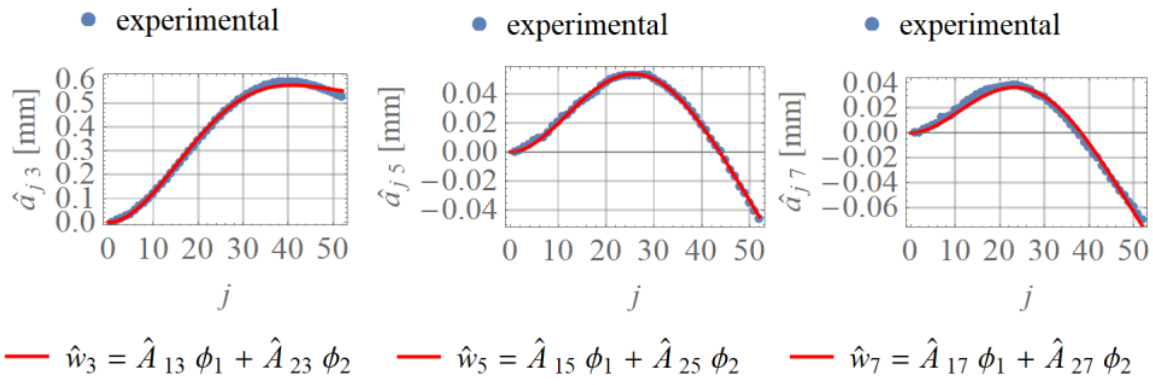

Fig. 13 Vibration shape for interwell oscillation for frequency $f = 3f_0$ (left), $f = 5f_0$ (middle) and $f = 7f_0$ (right) (setup II)

From these results it can be concluded that expansions (3) and (10), respectively, can give a good approximation of the experimentally observed shapes and that the beam eigenshapes are suitable functions for the expansion, which is in agreement to most used models in literature (cf. section 1).

On the other hand, the shapes corresponding to the superharmonics $k\Omega$ with $k>1$ can only be suitably expanded, when using at least two shape functions in the Ritz ansatz (1), while most publications restrict to a single one!

Finally, the amplitude dependence shall be discussed. Fig. 14 shows $\hat{a}_{j1}$ forming shape $\hat{w}_3(x)$ in the case of the intrawell (left) and the interwell solution (right) in the case of different excitation and, therefore, response amplitudes as well. The shapes are almost proportional and are represented for all excitation amplitudes in good approximation by ϕ_1. This changes for the higher harmonic shapes. In Fig. 15 and 16 the shapes for twice the excitation frequency in the case of the intrawell and three times excitation frequency in the case of the interwell solution are displayed. It can be seen especially in Fig. 15 that the corresponding shapes change with excitation amplitude, but all shapes can be very well approximated by ϕ_1 and ϕ_2.

From this it follows that the ansatz (1), (2) with $W_{1,2} = \phi_{1,2}$ can represent all the observed behavior in good approximation, but at least two ansatz functions are necessary while there is no need for amplitude dependent (nonlinear) ansatz functions in that case.

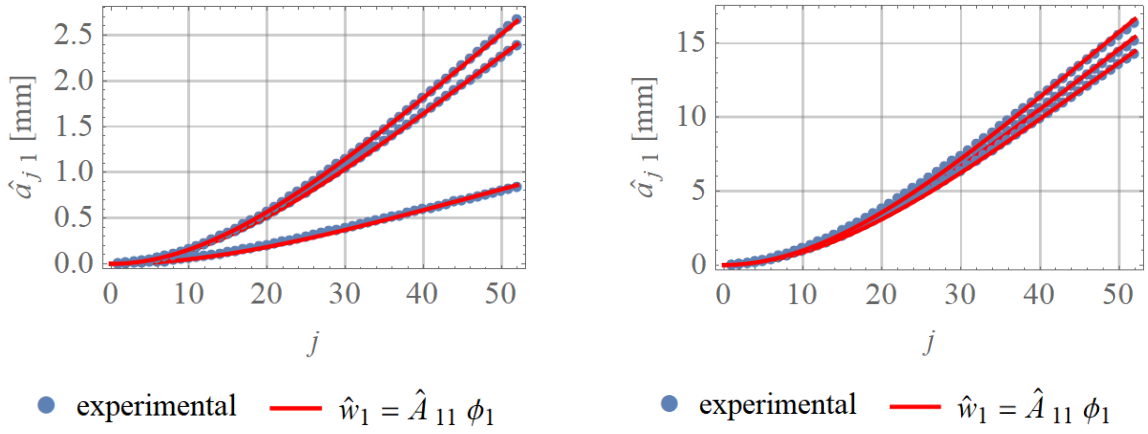

Fig. 14 Vibration shape for frequency $f=f_0$ for different amplitudes of the excitation (intrawell left, interwell right)

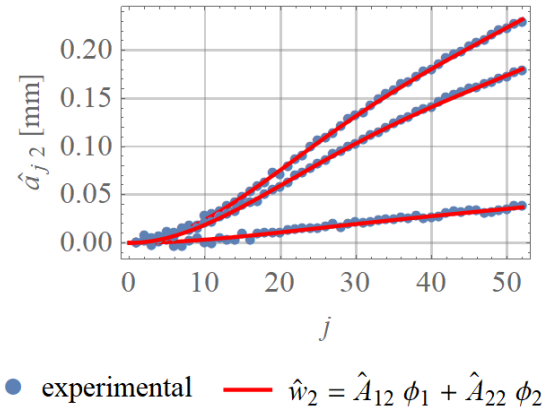

Fig. 15 Vibration shape for frequency $f=2f_0$ (intrawell) for different amplitudes of the excitation

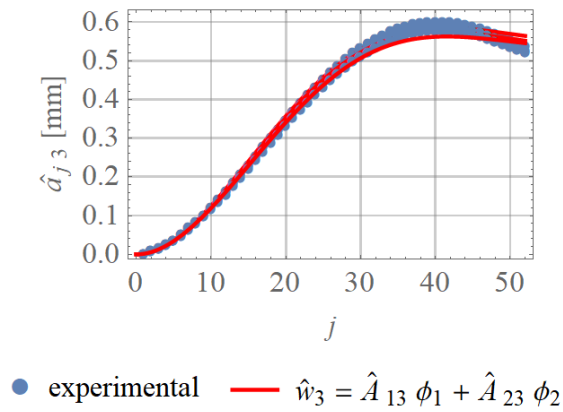

Fig. 16 Vibration shape for frequency $f=3f_0$ (interwell) for different amplitudes of the excitation

4. CONCLUSIONS

Energy harvesting performed by a bistable cantilever beam has attracted much attention. In general, the beam is in corresponding modeling discretized by the first eigenshape of the linear beam in a corresponding mixed Ritz ansatz. In this paper, this common assumption has been proofed for suitability. Therefore, the beam has been harmonically excited and corresponding response vibrations have been captured by a high-speed camera. Distinct markers have been applied to the beam and their positions were tracked over a series of frames. In accordance with the Ritz ansatz in theory the experimental results have been analyzed for both intrawell and interwell solution performing the following steps: first a Fourier expansion of the responses has been performed. As there was no period multiplication only the excitation frequency and superharmonics exist in the responses. For these harmonics, corresponding shapes could be identified which are afterwards expanded in the two first eigenfunctions of the undeflected cantilever beam.

The results show that the general ansatz to separate the solution of the beam vibration into a product of functions depending on t and x respectively is possible and sufficient. On the other hand, a good approximation of the experimentally observed shapes can only be reached if at least two ansatz functions are applied. Only for considering the excitation frequency in the response a single ansatz function is sufficient while for superharmonics a second ansatz function is needed to sufficiently approximate the observed vibration shapes. Further, the existing amplitude-dependence of the shapes due to the nonlinearities, can also be covered by the two ansatz functions.

Acknowledgements: *This work has been funded by Deutsche Forschungsgemeinschaft (DFG) by grant WA 1427/23,2.*

REFERENCES

1. Priya, S., 2007, *Advances in energy harvesting using low profile piezoelectric transducers*, Journal of Electroceramics, 19, pp. 165-182.
2. Erturk, A., Inman, D., 2009, *A piezomagnetoelastic structure for broadband vibration energy harvesting*, Applied Physics letters, 94, 254102.
3. Noll, M.-U., 2018, *Energy harvesting system*, doi:10.6084/m9.figshare.7492208.v1.
4. Mann, B. P., Owens, B., 2010, *Investigations of a nonlinear energy harvester with a bistable potential well*, Journal of Sound and Vibration, 329(9), pp. 1215-1226.
5. Harne, R., Wang, K., 2013, *A review of the recent research on vibration energy harvesting via bistable systems*, Smart Materials and Structures, 22, 023001.
6. Zhou, S., Cao, J., Inman, D. J., Lin, J., Li, D., 2016, *Harmonic balance analysis of nonlinear tristable energy harvesters for performance enhancement,* Journal of Sound and Vibration, 373, pp. 223-235.
7. Moon, F. C., Holmes, P. J., 1979, *A magnetoelastic strange attractor*, Journal of Sound and Vibration, 65(2), pp. 275–296.
8. Erturk A., Inman D., 2011, *Broadband piezoelectric power generation on high-energy orbits of the bistable Duffing oscillator with electromechanical coupling*, Journal of Sound and Vibration, 330(10), pp. 2339-2353.
9. De Paula, A., Inman, D., Savi, M., 2015, *Energy harvesting in a nonlinear piezomagnetoelastic beam subjected to random excitation,* Mechanical Systems and Signal Processing, 54-55, pp. 405-416.
10. Liu, W., Farmosa, F., Badel, A., Hu, G., 2017, *A simplified lumped model for the optimization of post-buckled beam architecture wideband generator*, Journal of Sound and Vibration, 409, pp. 165-179.
11. Lentz, L., Nguyen, H. T., von Wagner, U., 2017, *Energy harvesting from bistable systems under random excitation,* Machine Dynamics Research, 41(1), pp. 5-16.

12. Lentz, L., 2018, *On the modelling and analysis of a bistable energy-harvesting system*, PhD Thesis, TU-Berlin, Germany, 130 p.
13. Shaw, S., Pierre, C., 1994, *Normal modes of vibration for non-linear continuous systems*, Journal of Sound and Vibration, 169(3), pp. 319-347.
14. Szemplinska-Stupnicka, W., 1983, *Non-linear normal modes and the generalized Ritz method in the problems of vibrations of non-linear elastic continuous systems*, International Journal of Non-Linear Mechanics, 18(2), pp. 149-165.
15. Mikhlin, Y., Avramov, K., 2011, *Nonlinear normal modes for vibrating mechanical systems, review of theoretical developments*, Applied Mechanics Reviews, 63(6), 060802.
16. Cazottes, P., Fernandes, A., Pouget, J., Hafez, M., 2009, *Bistable buckled beam: modeling of actuating force and experimental validations*, Journal of Mechanical Design, 131(10), 101001.
17. Nayfeh, A. H., Emam, S. A., 2008, *Exact solution and stability of postbuckling configurations of beams*, Nonlinear Dynamics, 54, pp. 395-408.
18. Vocca, H., Cottone, F., Neri, I., Gammaitoni, L., 2013, *A comparison between nonlinear cantilever and buckled beam for energy harvesting*, Eur. Phys. J. Special Topics, 222(7), pp. 1699-1705.
19. Noll,M.-U., 2019, *Experimental setup of an energy harvesting system II*, doi:10.6084/m9.figshare.7764851.v1.

TECHNISCHE MECHANIK
an open access journal

journal homepage: www.ovgu.de/techmech

Tech. Mech., Vol. x, Is. x, (yyyy), bbb–eee

Received: dd.mm.yyyy
Accepted: dd.mm.yyyy
Available online: dd.mm.yyyy

Comparison of the dynamics of a Duffing equation model and experimental results for a bistable cantilever beam in magnetoelastic energy harvesting

Max-Uwe Noll[1]*, Lukas Lentz[1], and Utz von Wagner[1]

[1] Technische Universität Berlin, Institut für Mechanik, Einsteinufer 5, 10587 Berlin, Germany

Abstract: Nonlinear energy harvesting systems, consisting of a piezo cantilever beam with two additional magnets placed near the beam's free end, have received a lot of attention in the past decade. The most common approach to model this system is to discretize the beam in space with one modal ansatz function and to assume a cubic restoring force caused by the magnetic field. The magnets are positioned so that two stable equilibrium positions exist in addition to the unstable undeflected beam tip displacement, i.e. the system is bistable. This modeling procedure results in a Duffing equation with a negative linear and a positive cubic restoring term, which is capable to represent the bistability. However, its sufficiency is often just assumed without thorough experimental validation of the mentioned presumptions.
In this paper the authors present the results of broad experimental investigations into the sufficiency of the Duffing equation as the underlying model of the mechanical subsystem (beam and magnets, but for the sake of simplicity without piezos). Therefore, a model is developed accordingly, following the approach of most publications, where a heuristic method is used to determine the cubic restoring force of the system. The theoretical predictions of the Duffing like model concerning the dynamical response to different harmonic base excitations are compared to experimental measurements done on a physical setup of the investigated system. The results are generally in good agreement, however particular limitations regarding the model are observed, as there is a shift of the occurring solutions to higher frequencies in the theoretical model compared to the experiments.

Keywords: nonlinear dynamics, energy harvesting, bistable oscillator, Duffing equation, cubic restoring force

1 Introduction

The term energy harvesting describes specific strategies to derive small amounts of available energy from external sources, which would be otherwise lost. More specifically, vibrational energy harvesting systems use ambient vibrations to generate electric energy [Priya (2007), Kim et al. (2011), Erturk and Inman (2011b)]. Commonly, the mechanical energy is transferred into electric energy by the use of piezoceramics fixed on the corresponding bending structure. The tuning of such vibrating systems, as well as other strategies to increase their efficiency, have been addressed in many publications, e.g. [Adhikari et al. (2009), Erturk et al. (2009)]. Particularly due to the nature of real-world excitation processes [Lentz et al. (2017)], which can be partly stochastic or have broadband frequencies, approaches have been made to use more than the discrete base frequency of any foremost linear system [Pellegrini et al. (2013), Harne and Wang (2013), Daqaq et al. (2014), Wei and Jing (2017)]. About a decade ago [Erturk et al. (2009)] has proposed the setup in figure 1, which has received great attention.

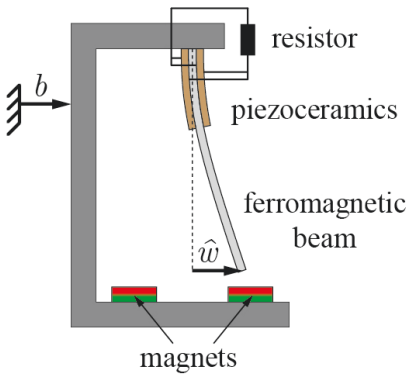

Fig. 1: Energy harvesting system. Modified figure of [Noll (2018)] with added coordinate b for the base excitation.

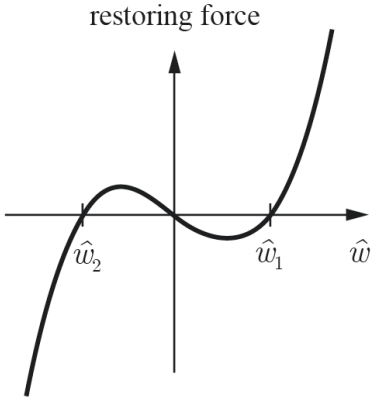

Fig. 2: Nonlinear restoring force with unstable trivial solution and two stable equilibria $\hat{w}_{1/2}$.

* E-mail address: max-uwe.noll@tu-berlin.de
doi: 10.1000/999

It consists of a base frame and a ferromagnetic cantilever beam that bends under base excitation b, with attached piezoceramic patches. The beam is clamped to an external structure, which excites the system by its motion. A characteristic feature of this particular system is its nonlinear behavior due to the magnets near the free end of the beam. In figure 2 the nonlinear restoring force is shown with its three equilibrium positions, at which the restoring force vanishes. Only the two non-zero equilibrium positions $\hat{w}_{1/2}$ are stable, which is the reason for the system to be called bistable. It has shown, as many other nonlinear systems, to be superior in efficiency to its linear counterpart when the excitation is not mono frequent but somehow distributed around the system's base frequency and when the beam orbits both stable positions ([Erturk and Inman (2011a), De Paula et al. (2015)]).
In order to model this energy harvesting system, it can be divided into three subsystems which are the bending beam structure, the restoring force caused by the magnetic field induced by the permanent magnets and the electrical part, which consists of the piezoceramics and the connected electrical circuit. The basic structure of the bistable cantilever beam with magnets, but without piezoceramics, was already described in [Moon and Holmes (1979)]. This part will be referred to as the mechanical subsystem in this paper. Hence, for the sake of simplicity, no piezoceramics are considered in the modeling and in the experiment in order to have the focus on the nonlinear magnetic restoring forces.
The key component of this mechanical subsystem is the cantilever beam, which is regularly modeled as an Euler-Bernoulli beam. The beam is discretized by its first linear eigenfunction (without magnets). This modeling has become the standard approach to describe its dynamics by a single second order ordinary differential equation, which has been applied many times (as in [Litak et al. (2010), Tam and Holmes (2014), De Paula et al. (2015), Noll et al. (2019a)]). The question if more than one ansatz function is necessary, is addressed in another paper by the authors [Noll et al. (2019b)]. Its conclusions are that the use of the first linear eigenfunction of the beam is suitable in most cases and the second linear ansatz function only has a small geometric share in cases of super harmonic responses. Following the standard modeling procedure, the magnets are replaced by a single transverse force that is applied at the tip of the beam and is assumed to be of a cubic polynomial type with vanishing quadratic term. This results in the Duffing equation with negative linear and positive cubic restoring force (see e.g. [Lentz (2018)]), which is a minimal model to describe bistability. A lot of varied systems with different arrangements of magnets (see e.g. Westermann et al. (2013); Lan and Qin (2017)]) or even other nonlinear mechanisms finally end in a Duffing equation. Most of the publications about comparable bistable configurations follow this approach, or simply state a Duffing equation as the underlying model, as in [Litak et al. (2010)] or [Lentz and von Wagner (2015)]. The model parameters are then found heuristically in a manner described in the following. The displacement of the nontrivial equilibrium positions and the corresponding frequency of free vibration of small amplitude are needed. They provide the necessary information to determine the restoring parameters. This can (only) be done when an experimental setup exists, or corresponding assumptions regarding the system are made.
In [Noll et al. (2019a)] the authors have tried to apply an alternative procedure, where no existing experimental setup would be needed to determine a model by a direct computation of the restoring force. Therefore, the magnetic field was simulated by a two-dimensional FEM-approach with subsequent numeric force computation, where linear magnetic material behavior (i.e. constant permeability) is assumed. However, the resulting model in that case could not satisfyingly meet the conditions of matching equilibrium positions and corresponding frequencies. In contrast, the agreement of the equilibrium positions and frequencies are always achieved when using the aforementioned heuristic method. It yields a model that is a good approximation when the beam tip is in the vicinity of the stable equilibrium positions. However, in other ranges of the beam tip displacement, as for example the unstable equilibrium with zero displacement, this might not be a good approximation.
In this paper, dynamic experiments are described, investigating the system's steady state response for different harmonic base excitations with varying frequency and amplitude. In the following section, the experimental setup is introduced. The results will be compared to predictions of a model that is found according to the heuristic method, described in the second next section.

2 Experimental setup

The main focus is on the mechanical subsystem (figure 3) of the energy harvesting system, that consists of a cantilever beam (dimensions: $250 \times 20 \times 1$ mm) and permanent magnets (dimensions: $5 \times 20 \times 10$ mm). No piezoceramics are considered in the presented investigations, as mentioned in the introduction. The distance between the beam tip in the undeflected state and the top side of the magnets is about 6 mm and the gap between the magnets is 12.7 mm. The beam made of ferromagnetic steel is modeled according to section 3 as an Euler-Bernoulli beam and therefore mechanically characterized by its mass per length μ and bending stiffness EI. Further it is magnetically characterized by its relative permeability. There are some indications that the material of the beam is not linear regarding its magnetic properties, i.e. it shows a distinct hysteresis depending on the strength of the applied external magnetic field [Noll et al. (2019a)]. The magnets are made of NdFeB (Neodymium) with remanence $B_\mathrm{r} = 1.35$ T. The overall system has the physical properties given in table 1.

Tab. 1: Physical properties of the experimental setup (cf. figure 3).

property	**value**
first circular eigenfrequency of the beam when no magnets are present ω_0	2π 13.4 Hz
displacement of the nonzero equilibrium positions $\hat{w}_{1/2}$	+6.97 mm
(distance from the undeflected position when permanent magnets are present)	−6.97 mm
circular frequency of the oscillation in equilibrium positions with small amplitude ω	2π 14.9 Hz
	2π 14.6 Hz
damping ration with magnets in equilibrium positions D	0.0013
	0.0019

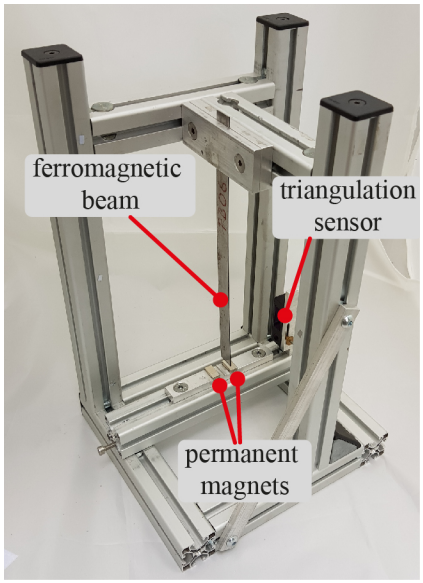

Fig. 3: Mechanical subsystem of the investigated energy harvesting system.

Note that in general there are two different circular frequencies ω for small vibrations in each stable equilibrium, due to an undesired but unavoidable asymmetry of the experimental setup. For the heuristic modeling later, the average will be taken. Same applies to the damping ratios D that are found by determining the logarithmic decrement from time signals of free beam vibrations. In order to measure the quantities in table 1, the setup shown in figure 4 is used. It consists of several devices to realize a harmonic base excitation and devices to measure the beam's response in form of its beam tip displacement. Also, the actual base excitation occurring at the base frame is measured. To determine the static (and later dynamic) displacement of the beam tip a laser triangulation sensor (ALLSENSE AM500-50) is used. It is attached to the moving base frame (cf. figure 3), hence directly provides the relative displacement of the beam tip with respect to the permanent magnets, which are fixed within the moving aluminum framework. The harmonic signal of the base excitation is generated by MATLAB R2018a and further processed by a measurement box (Datatranslation DT9837A) that provides the desired voltage signal for a shaker (LDS V406/8-PA100E) after amplification (LDS PA 100E Power Amplifier). The shaker is attached to a vibration table, containing four leaf springs as support, on which the system in figure 3 is placed. The vibration table has a notable dynamic of its own, which has an influence on the base excitation. The base frequency of the vibration table is about 6 Hz, which is not very far from the considered range of frequencies in experiments later. The range will be 7 Hz to 18 Hz and is chosen around the first eigenfrequency of the beam of 13.4 Hz. Hence, the transfer function of the vibration table is not constant within the considered range of frequencies and needs to be regarded. The measurement box provides a voltage signal that is amplified and provided to the shaker.

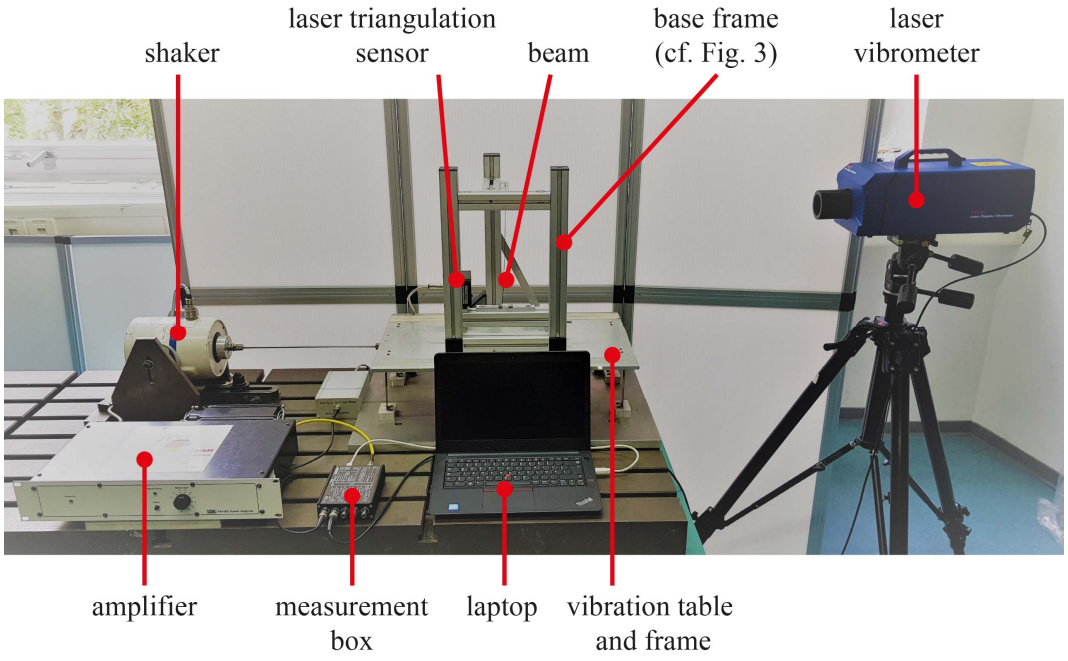

Fig. 4: Experimental setup of the energy harvesting system placed on a vibration table excited by a shaker, with measurement devices and related data acquisition tools.

The shaker generates a force proportional to this signal, to excite the vibrating table. Since a harmonic base excitation of a certain amplitude A is desired, that is independent of the circular excitation frequency Ω, the signal provided by the measurement box needs to regard the dynamics of the vibration table. To confirm that the specified signal of the excitation concurs with the actual base motion it is measured by a laser vibrometer (OptoMET Nova Basis), that determines the velocity $\dot{b}$ of the base frame. The base excitation, that is proportional to the acceleration $\ddot{b}$, is then found from this measurement by a numerical differentiation of the time signal of the discrete velocity values. The reason it is measured is that the base excitation occurring at the base frame is not always concurring with the specified signal generated in MATLAB. There is a bias in magnitude and a phase shift of roughly πrad originating from the dynamics of the vibration table. Also, the authors have observed that there are cases in which the beam, due to its inertia, has a retroactive effect on the actual base excitation. Especially when the beam tip exhibits large orbits around both of its stable equilibrium positions, deviations of the actual base excitation from the desired specified signal are probable. The measurements later to be shown in detail are chosen due to their fairly harmonic base motion.
All measurements are done in the steady state of the system, which is assumed to be reached after a 60 seconds transient response of the system. Subsequently the measurements are done for 10 seconds with a sample rate of 10 kHz. The sampling is performed after a suitable lowpass filter applied by the measurement box.

3 Modeling of the mechanical subsystem

The different aspects of the overall system can be, to a certain extent, modeled separately and in different levels of complexity. Two existing publications of the authors deal with particular parts of the energy harvesting system which are: first, the magnetic field, the thereby caused magnetic restoring force and the resulting corresponding stationary behavior of the system (equilibrium positions and corresponding frequencies of small free vibrations) in [Noll et al. (2019a)] and second, the spatial discretization of the beam using only the first linear eigenfunction of the beam in [Noll et al. (2019b)]. In both publications the beam has been modeled as an Euler-Bernoulli beam structure, that bends under excitation. The beam displacement is described by a partial differential equation for the beam displacement w depending on the beam coordinate ξ and time t as given in many continuum dynamics textbooks. Following the classical discretization process as in [Noll et al. (2019a)], the mixed Ritz ansatz

$$w(\xi,t) = x(t)\,\phi(\xi), \tag{1}$$

where x is the time dependent modal coordinate. ϕ is the first eigenfunction of the linear beam, $\xi \in [0, L]$ the beam coordinate and L the total length of the beam. ϕ is chosen to be 1 at $\xi = L$, hence x concurs with the beam tip displacement $\hat{w} = w(L,t)$ (cf. figure 1). It yields the ordinary differential equation of motion given by

$$\ddot{x}(t) + 2D\omega\dot{x}(t) - \alpha x(t) + \beta x^3(t) = g\ddot{b}(t). \tag{2}$$

Compared to [Noll et al. (2019a)] the term on the right-hand side is added, since in this paper dynamic experiments of the driven Duffing oscillator are performed considering a base excitation, while in [Noll et al. (2019a)] the static behavior and free vibrations were investigated. The coefficient g is determined accordingly and given by

$$g = -\frac{\int_0^L \phi(\xi)\,\mathrm{d}\xi}{\int_0^L \phi^2(\xi)\,\mathrm{d}\xi}. \tag{3}$$

The excitation is chosen to be a base excitation of a constant amplitude A of the form $\ddot{b}(t) = A\cos\Omega t$.
In order to get the specific kind of restoring term, that is $-\alpha x(t) + \beta x^3(t)$, the assumption has been made that the magnetic force is a cubic polynomial of the beam tip displacement. Further, a linear modal damping has been inserted with the damping ratio D. In cases where α and β are both positive, bistability is existent with the two nontrivial equilibrium positions $x_{1/2}$ on each side of the undeflected beam position

$$x_{1/2} = \pm\sqrt{\frac{\alpha}{\beta}}. \tag{4}$$

Further, if considering oscillations within these two equilibrium positions with small amplitude the circular frequency for free vibrations in each of the stable equilibrium position can be determined after linearization by

$$\omega = \sqrt{2\alpha}. \tag{5}$$

When a physical setup is available the model parameters can be determined and are given in table 2 for the setup in figure 3.

Tab. 2: Model parameters of corresponding experimental setup given table 1.

parameter	ω [1/s]	D [−]	α [1/s^2]	β [1/s^2]	g [1/m]
value	92.7	0.0016	4275.6	$8.8 \cdot 10^7$	−1.57

The parameter ω and D are found as the average of their values from an analysis of the time signals of free beam vibrations in each stable equilibrium when the magnets are applied. Even though the beams's circular eigenfrequency $\omega_0 = 2\pi 13.4$ 1/s has no direct significance for the setup with magnets, it is taken to define the frequency ratio η as

$$\eta = \frac{\Omega}{\omega_0}, \tag{6}$$

which is used later. α and β are found according to (4), (5) and g by equation (3). This approach is of a heuristic nature and therefore an experimental setup needs to be present first to find the according model parameters. This is an essential drawback of this approach, since these quantities need to be measured every time the setup is changed (e.g. the distance between the magnets). On the other hand, an advantage is that the model gives a good approximation of the physical setup when the beam tip is near one of the stable equilibrium positions. The approach ensures, that the equilibrium as well as the corresponding frequency of the model concur with those of the setup (except for possible asymmetries which cannot be covered by an uneven cubic force model). In the next section the experimental results are presented, and a comparison is done to the predictions of the Duffing model.

4 Experimental results and comparison to theory

In this section experimental results are shown and compared to the predictions provided by the corresponding Duffing model equation (2) with parameters in table 2. The setup is excited by different harmonic base excitations, which differ in acceleration amplitude and frequency. The beam tip displacement is measured, as well as the actual excitation. It is common to look at the phase diagram of the solution, which is a trajectory in the state space, that shows the velocity of the beam tip over the beam tip displacement (see figure 5). For that, the beam's velocity is to be determined from the measurement of the beam tip displacement, which is achieved by a numerical differentiation done using the central difference quotient. Since the signal of the beam tip displacement is noisy and a numerical differentiation increases noise, it is necessary to lowpass filter the signals. This is done using a Butterworth lowpass filter with cut-off frequency of 90 Hz (5 times the largest excitation frequency). This frequency is chosen as a compromise between a low cut-off frequency to get smooth results and a high cut-off frequency to remain the characteristics of the phase trajectory. Also, sub and super harmonics are to be expected. The super harmonics, which can be several multiples of the excitation frequency, could be eliminated by a filter with a too low cut-off frequency.
The solution that occurs depends on the initial conditions since the system is nonlinear, what means that for one excitation different types of solutions are possible. One approach to distinguish different solutions is to consider the turning points of the beam tip throughout the measurement time. In figure 5 the turning points are marked. More specifically: when the velocity changes in sign, the beam is changing the direction it travels. If all those occurring turning points (and therefore all beam tip displacements also) have the same sign (either all exclusively positive or negative) the solution is called intrawell (in blue). If the sign switches periodically with a period not being larger than a defined threshold, the solution is labeled as interwell solution (red). If there is a very large number of turning points (in this work set to be greater than 25) with positive and negative signs the solution is considered to be chaotic, even though it might be possible it is a periodic solution with a very large period.

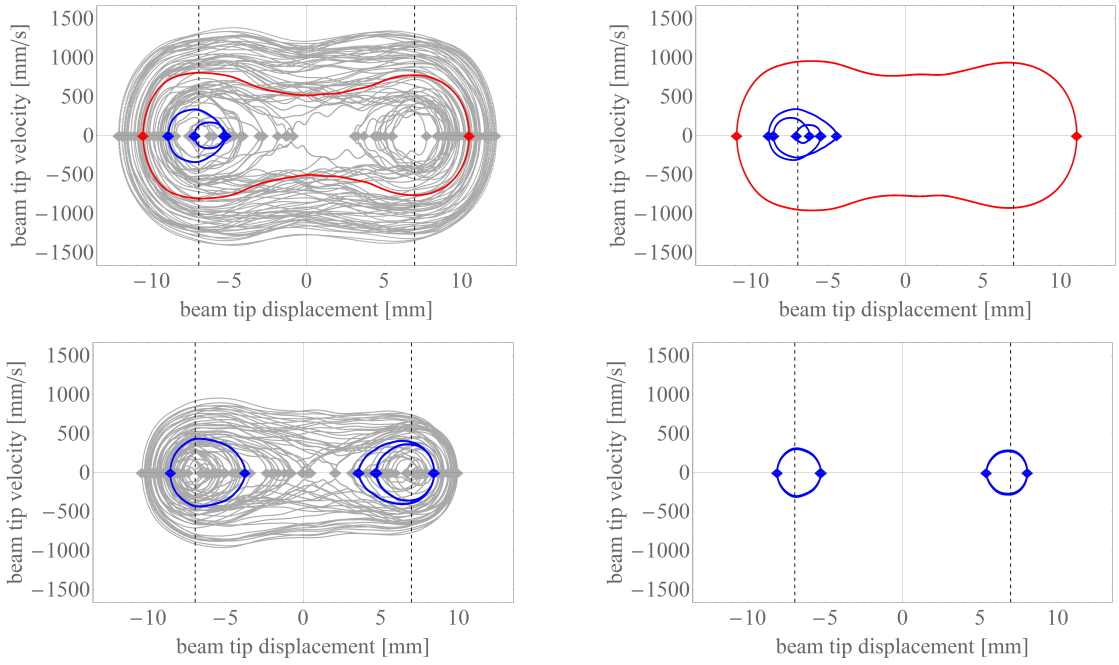

Fig. 5: Experimental phase diagrams and turning points (marker) of different solutions for a harmonic acceleration of amplitude $A = 3.81$ m/s^2 and different excitation frequencies. Upper left: 7 Hz / $\eta \approx 0.52$; upper right: 8.5 Hz / $\eta \approx 0.64$; lower left: 14 Hz / $\eta \approx 1.05$; lower right: 17 Hz / $\eta \approx 1.27$. Color code refers to the type of solution: intrawell solutions in blue, interwell solutions in red and chaotic solutions in gray.

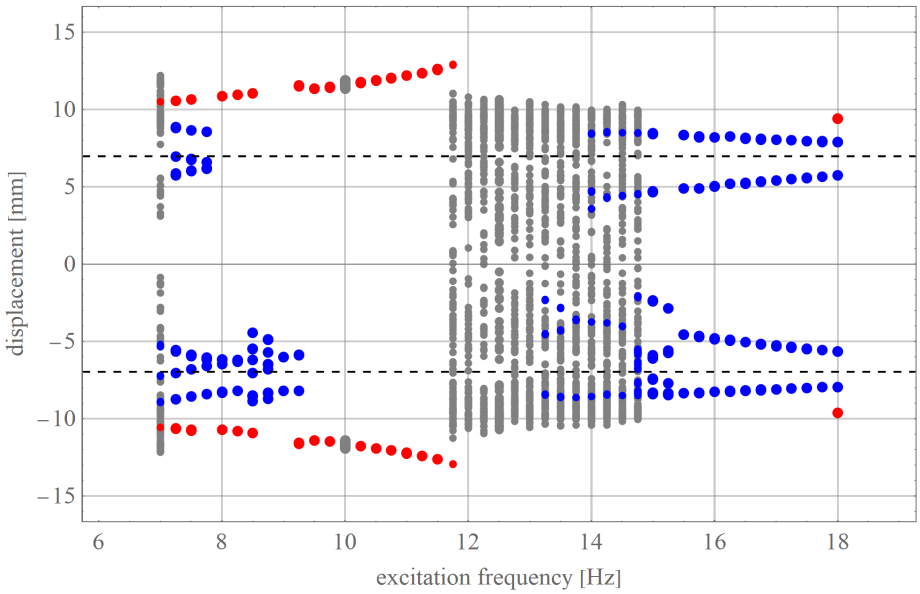

Fig. 6: Experimental results: turning points of the beam tip for parallel existing steady state solutions for harmonic acceleration of constant amplitude $A = 3.81\ \mathrm{m/s^2}$ and different excitation frequencies. Color code corresponding to figure 5.

Another possible way of displaying the occurring types of solutions is the system response diagram in figure 6, which is especially suitable to show the influence of the excitation frequency and is also used e.g. in [Lentz (2018)]. It shows all turning points of different solutions that exist in parallel for excitations of different frequency but constant amplitude. As it can be seen, there are different frequency ranges where more than one solution exists and some ranges, where only one solution has occurred during the different experimental repetitions. For each frequency ten experiments have been made, sometimes having the same final steady state and sometimes having different final steady states. The initial conditions of each experiment are not known nor reproducible, which means they cannot be controlled. Hence, it is not possible to directly reproduce each experiment numerically, making a comparison of the experiment to the Duffing model difficult. To deal with the lack of controllability of the entirety of the occurring solutions in the experiments (and also numerics), many trials with different initial conditions are done to increase the chances of various solutions, to allow a comparison between experimental and numerical results.
In figure 7, the results of numerical simulations of the model in equation (2) can be seen. It is found by a numerical integration using the NDSolve-function of MATHEMATICA 11 with no changes of the default settings with respect e.g. to the integration scheme, step size and precision goal. To get a better numerical conditioning, the differential equation for the modal coordinate x is transformed to be in the magnitude of millimeter $\tilde{x} = 10^{-3}x$ before solving for $\tilde{x}$ and transforming back. The sets of initial conditions in this case need to be chosen and are set to be 126 different equidistant values for $\tilde{x}$ for $t = 0$ between -15 and 15 and zero velocity. The integration time is 1000 seconds and the last ten seconds are used to be analyzed for their turning points analogous to the experimental data. For avoiding large arguments in the periodic cosine function and corresponding errors, the values are set back in the range between 0 and 2π when exceeding this range.

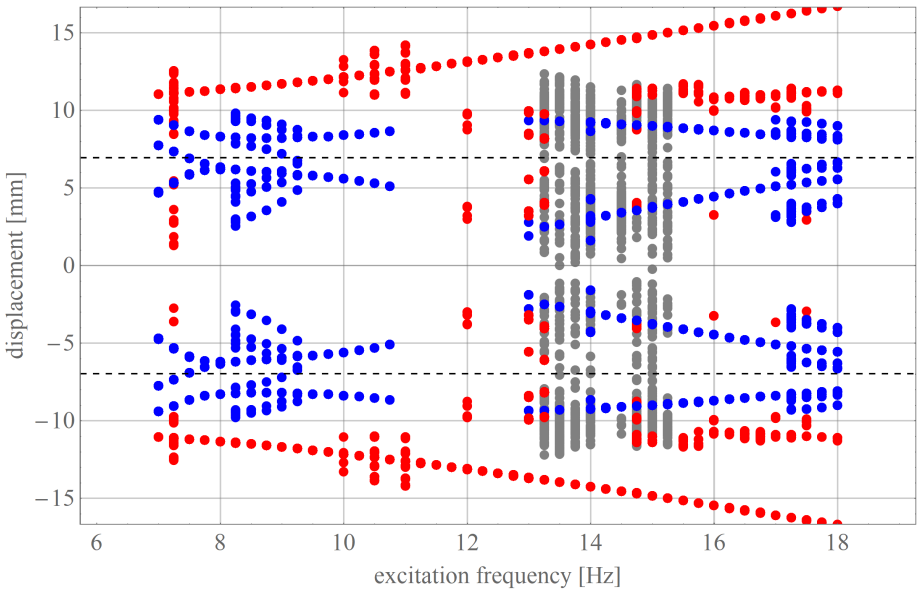

Fig. 7: Numerical results: system response diagram in Fig. 6 found by numerical integration of the Duffing model. Color code corresponding to figure 5.

When comparing both outcomes in figure 6 and 7 similar characteristics can be seen. In both diagrams, there are three main frequency ranges distinguishable: one at lower frequencies, where mostly intra- and interwell solutions (blue and red) occur in parallel, another range, where interwell solutions (only red) exist solely and a third where chaotic solutions are probable and also intrawell and interwell occur again. A difference between both diagrams is that in theory those three regions are shifted to higher frequencies. In the experiment lower excitation frequencies (around about 10 Hz / $\eta \approx 0.75$) lead to the preferred large interwell solutions and in theory, this range is slightly shifted to larger frequencies (around about 12 Hz / $\eta \approx 0.9$). The position of this range is of high interest due to its high potential for energy harvesting purposes since the beam undergoes large periodic deformations that cause high energy outputs. It is also noteworthy that the biggest region, where chaotic solutions were observed, in experiment is around the eigenfrequency of the beam (13.4 Hz / $\eta = 1$) and in theory again shifted to the right for larger frequencies (14Hz / $\eta \approx 1.05$). Another difference is that in theory large interwell solutions occur for every considered frequency but do not occur as often in the experiments. It shall be noted that the experimentally realized base excitation may differ from a harmonic excitation due to different reasons explained in section 2. A measure of the amplitude of each actual base acceleration is given by the Root Mean Square (RMS) value. The mean value of the acceleration amplitude A for all experiments (ten repetitions for each of the 45 frequencies) in figure 6 is 3.81 m/s^2 and the standard deviation of all values is 0.086 m/s^2.

The results shown so far were generated for one specific amplitude of the base excitation. In the next step, different amplitudes are considered. A map of the type of the solution (color code consistent to the figures above) that occurs for a single experiment with an excitation frequency and amplitude is shown in figure 8. Again, the experimentally realized initial conditions are uncontrollable and therefore again unknown. As it can be seen, the excitation amplitude is not uniformly distributed, due to influences of the vibrating table. The actual occurring base excitation amplitude is determined by the RMS value of the measured base excitation. The same rules to distinguish the type of solution are applied.

In figure 9 equivalent results of numerical simulations are shown. Again, time integration is performed using NDSolve in Mathematica 11 with default settings. For a 1:1 comparison of the results, the same excitation and initial conditions would need to be considered. This is impossible as described above as there are very restricted possibilities to control the initial conditions in the experimental setup. For this reason, again more simulations are done as experiments to cover a broader range of initial conditions. For simulations this is easier to perform as they are not as time consuming and can be done partly parallel.

For each excitation 25 simulations are performed, where the initial conditions are equidistant displacements $x(t = 0)$ in the range of $[-3x_1, 3x_1]$ with zero velocity. Only if always the same solution occurred, a filled squared marker of corresponding color is used. If the same solution occurs between 15 and 24 times out of 25, an diamond marker of the lighter color of the solution that occurred the most is used. Further, no marker is used, if no solution appeared more than at least 15 out of 25 times. Note that, for these criteria, chaotic solutions are less likely on the map and never occur 25 out of 25 times for a certain excitation. Consequently no squared grey marker can be found, but grey diamond markers are to be seen on the map in the same regions chaos appeared experimentally. Again, when comparing both results, similar characteristics can be found. Overall, the model is in general suitable to predict the experimental results, but in detail deviations can be found. In good agreement, for example, are the position of chaotic solutions (grey) and that for small excitation amplitudes (below 2 m/s^2), where mostly intrawell solutions exist. Differences are again shifts of the different regions to higher frequencies in the model results, as can be seen in the large red region. Similar theoretical investigations with maps of this kind can also be found in [Panyam et al. (2014)], which concur with the results of this paper.

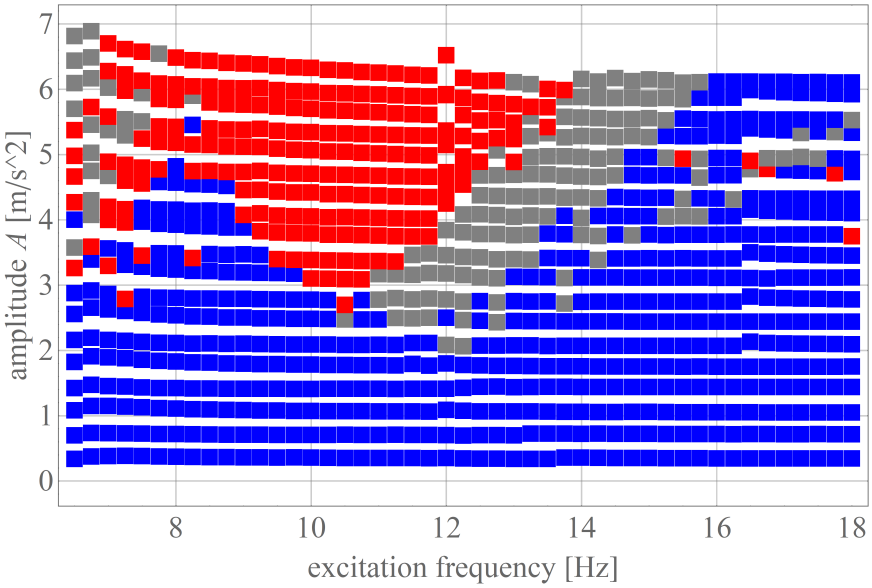

Fig. 8: Map of experimental results of the system response for different excitation frequencies and different amplitudes of harmonic acceleration. Only one experiment for each excitation is performed, wherefore only one solution occurred and uniquely defines the color of the marker. Color code corresponding to figure 5.

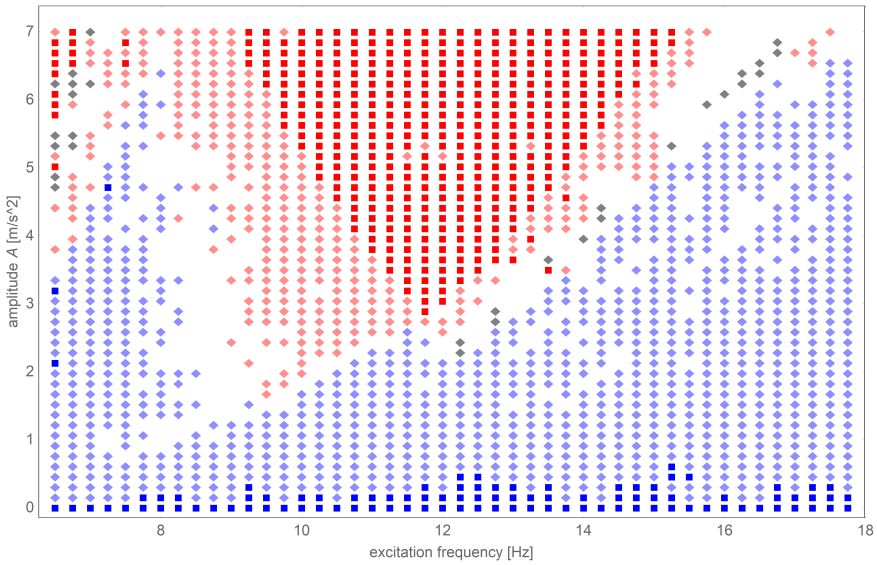

Fig. 9: Map of numerical results of the system responses found by time integration to be compared with figure 8. Color code corresponding to figure 5.

5 Conclusions

Energy harvesting performed by a bistable cantilever beam has attracted much attention in the past years. In most of the corresponding publications, the restoring force of the energy harvesting system is assumed to be of third degree, i.e. cubic. This modeling leads to the bistable Duffing equation. Corresponding model parameters are found heuristically.
In this paper, the assumption, that the restoring force is a cubic polynomial depending solely on the beam tip displacement, is investigated for suitability. Extensive experiments are performed to experimentally determine the system response for varying harmonic base excitations. A comparison to numerical results by time integration of the corresponding Duffing model is presented. The biggest issue is that the initial conditions cannot be controlled on the experimental setup that is used. Hence, the diversity of the solutions is probably not fully represented. To overcome this limitation several experiments and many simulations with varying initial conditions are done to increase the probability of occurrence of the respectively existing different solutions. In any case, the final steady solution of the system is in the focus of interest. Although there is no guarantee that all possible solutions are found, neither experimentally nor numerically, the occurring solutions are in good agreement and the results are broad enough for a comparison of the general characteristics. In fact the results show that in general the model covers most of the characteristics that can be seen in experiments but may have deviations. More specific, there might be a slight shift of the existence of solutions towards larger frequencies in theory. This might lead to false predictions when optimizing an energy harvesting system by tuning it to an existing harmonic excitation of a specific frequency. In general, the cubic restoring characteristics seems to be a good model, if the requirements on the accurateness of the model are not too high. On the other hand, as e.g. described in [Lentz (2018)] or [Noll et al. (2019a)], there may be specific cases where higher order approximations or in general extended modeling may be necessary.

6 Funding

This study was funded by Deutsche Forschungsgemeinschaft (DFG, German Research Foundation) - WA 1427/23-1,2.

Literatur

S. Adhikari, M. I. Friswell, and D. J. Inman. Piezoelectric energy harvesting from broadband random vibrations. *Smart Materials and Structures*, 18(11), 2009. ISSN 09641726. doi: 10.1088/0964-1726/18/11/115005.

Mohammed F. Daqaq, Ravindra Masana, Alper Erturk, and D. Dane Quinn. On the Role of Nonlinearities in Vibratory Energy Harvesting: A Critical Review and Discussion. *Applied Mechanics Reviews*, 66(4):40801, 2014. ISSN 0003-6900. doi: 10.1115/1.4026278. URL http://appliedmechanicsreviews.asmedigitalcollection.asme.org/article.aspx?doi=10.1115/1.4026278.

A. S. De Paula, D. J. Inman, and M. A. Savi. Energy harvesting in a nonlinear piezomagnetoelastic beam subjected to random excitation. *Mechanical Systems and Signal Processing*, 54:405–416, 2015. ISSN 10961216. doi: 10.1016/j.ymssp.2014.08.020. URL http://dx.doi.org/10.1016/j.ymssp.2014.08.020.

A. Erturk and D. J. Inman. Broadband piezoelectric power generation on high-energy orbits of the bistable Duffing oscillator with electromechanical coupling. *Journal of Sound and Vibration*, 330(10):2339–2353, 2011a. ISSN 0022460X. doi: 10.1016/j.jsv.2010.11.018. URL http://www.sciencedirect.com/science/article/pii/S0022460X10007807.

A. Erturk and D. J. Inman. *Piezoelectric Energy Harvesting*. John Wiley & Sons, Ltd, 2011b. doi: 10.1002/9781119991151.

A. Erturk, J. Hoffmann, and D. J. Inman. A piezomagnetoelastic structure for broadband vibration energy harvesting. *Applied Physics Letters*, 94(25):254102, 2009.

R. L. Harne and K. W. Wang. A review of the recent research on vibration energy harvesting via bistable systems. *Smart Materials and Structures*, 22(2), 2013. ISSN 09641726. doi: 10.1088/0964-1726/22/2/023001.

H. S. Kim, J. H. Kim, and J. Kim. A review of piezoelectric energy harvesting based on vibration. *International Journal of Precision Engineering and Manufacturing*, 12(6):1129–1141, 2011. ISSN 12298557. doi: 10.1007/s12541-011-0151-3.

C. Lan and W. Qin. Enhancing ability of harvesting energy from random vibration by decreasing the potential barrier of bistable harvester. *Mechanical Systems and Signal Processing*, 85:71–81, 2017. ISSN 10961216. doi: 10.1016/j.ymssp.2016.07.047. URL http://dx.doi.org/10.1016/j.ymssp.2016.07.047.

L. Lentz. Zur Modellbildung und Analyse von bistabilen Energy-Harvesting Systemen. *Dissertation, TU Berlin*, 2018.

L. Lentz and U. von Wagner. Multi-mode model of a piezomagnetoelastic energy harvester under random excitation. *Pamm*, 15(1): 259–260, 2015. doi: 10.1002/pamm.201510120.

L. Lentz, H. T. Nguyen, and U. von Wagner. Energy harvesting from bistable systems under random excitation. *Machine Dynamics Research*, 41, 2017.

G. Litak, M. I. Friswell, and S. Adhikari. Magnetopiezoelastic energy harvesting driven by random excitations. *Applied Physics Letters*, 96(21):12–15, 2010. ISSN 00036951. doi: 10.1063/1.3436553.

F. C. Moon and P. J. Holmes. A magnetoelastic strange attractor. *Journal of Sound and Vibration*, 65(2):275–296, 1979.

M.-U. Noll. Energy harvesting system. *figshare*, 2018. doi: https://doi.org/10.6084/m9.figshare.7492208.v1.

M.-U. Noll, L. Lentz, and U. von Wagner. On the Improved Modeling of the Magnetoelastic Force in a Vibrational Energy Harvesting System. *Journal of Vibrational Engineering and Technologies*, (0123456789), 2019a. ISSN 25233939. doi: 10.1007/s42417-019-00159-4. URL https://doi.org/10.1007/s42417-019-00159-4.

M.-U. Noll, L. Lentz, and U. von Wagner. on the Discretization of a Bistable Cantilever Beam With Application To Energy Harvesting. *Facta Universitatis, Series: Mechanical Engineering*, 17(2):125, 2019b. ISSN 0354-2025. doi: 10.22190/fume190301031n.

M. Panyam, R. Masana, and M. F. Daqaq. On approximating the effective bandwidth of bi-stable energy harvesters. *International Journal of Non-Linear Mechanics*, 67:153–163, 2014. ISSN 00207462. doi: 10.1016/j.ijnonlinmec.2014.09.002. URL http://dx.doi.org/10.1016/j.ijnonlinmec.2014.09.002.

S. P. Pellegrini, N. Tolou, M. Schenk, and J. L. Herder. Bistable vibration energy harvesters: A review. *Journal of Intelligent Material Systems and Structures*, 24(11):1303–1312, 2013. ISSN 1045389X. doi: 10.1177/1045389X12444940.

S. Priya. Advances in energy harvesting using low profile piezoelectric transducers. *Journal of Electroceramics*, 19(1):165–182, 2007. ISSN 13853449. doi: 10.1007/s10832-007-9043-4.

J. I. Tam and P. Holmes. Revisiting a magneto-elastic strange attractor. *Journal of Sound and Vibration*, 333(6):1767–1780, 2014. ISSN 0022460X. doi: 10.1016/j.jsv.2013.11.022. URL http://dx.doi.org/10.1016/j.jsv.2013.11.022.

C. Wei and X. Jing. A comprehensive review on vibration energy harvesting: Modelling and realization. *Renewable and Sustainable Energy Reviews*, 74(November 2016):1–18, 2017. ISSN 18790690. doi: 10.1016/j.rser.2017.01.073. URL http://dx.doi.org/10.1016/j.rser.2017.01.073.

H. Westermann, M. Neubauer, and J. Wallaschek. Modeling of a nonlinear vibration-based energy harvesting system as a Duffing oscillator. *Solid State Phenomena*, 198:663–668, 2013. ISSN 10120394. doi: 10.4028/www.scientific.net/SSP.198.663.

7 Further research

7.1 Three-dimensional magnetic force determination using COMSOL

The first publication [Noll et al., 2019a] is on the numerical computation of the magnetoelastic forces on the beam, to establish an alternative method to the heuristic method, to find the restoring force of the system. The results are compared to experimental results. As concluded in this publication, deviations exist between experiment and numerical results, which possibly result from two reasons described in the last part of the publication.

First is that in the modeling of the forces it is assumed that magnetic field can be computed approximately by a two-dimensional simulation. This assumption is only valid when the magnetic field is constant along this third dimension for the major part of the system's depth, so that the effects at the boundaries (facing in and out of the two-dimensional plane) can be neglected. However, when considering solely the magnetic field, it can be clearly seen the magnets do not produce a homogeneous magnetic field in the area where the beam is theoretically located, as shown in figure 8 of [Noll et al., 2019a]. This is likely to remain true in the presence of the beam, although the beam changes the magnetic field. Hence the force is not independent of the magnets as well as the beams's depth. This hypothesis is supported by experiments in [Vanegas Müller, 2018]. Therein, the force between different single magnets of different depths on the beam of constant depth is investigated to find out, if the individual depth of each magnet has an influence on the force exerted on the beam. The experiments show that the force is strongly depending on the magnet's depth, hence a three-dimensional magnetic field simulation is necessary, especially when the beam and the magnets are of the exact same depth. Therefore, in the following a three-dimensional simulation of the magnetic field is conducted to compare the results to those of the two-dimensional simulation presented in the first publication [Noll et al., 2019a]. The commercial software COMSOL is used for the stationary magnetic field simulation, as shown in figure 7. This software is able to perform a force determination by an implemented function that uses the Maxwell stress tensor. It is limited to global force computations concerning magnetoelastic forces. The validity of this simplification has been addressed in section 5.3. Although it may differ in the three-dimensional case, since it has also been applied in the first publication, it is consistently applied in the three-dimensional simulation as well. The three-dimensional simulation is meant to reproduce the results from the two-dimensional simulation in the first publication, with only the third dimension to be considered additionally. This means the geometry is alike, and only extended by the depth of the beam and magnets respectively. The materials are modeled analogously, but need to be defined differently in COMSOL. There, the remanent magnetic flux density B_r is to be entered to define the magnetic properties of the magnets. It is chosen as $B_\mathrm{r} = 1.3725$ T, which is within the range given by the magnet supplier and equivalent to the material definition done in the two-dimensional simulation in the first publication.

Note that there is a corrigendum to the first publication [Noll et al., 2019c], which corrects the value of the relative permeability of the steel beam. It has in both simulations been respected by the value of 1000, and not as 300 as falsely given in the table 1 of [Noll et al., 2019a].

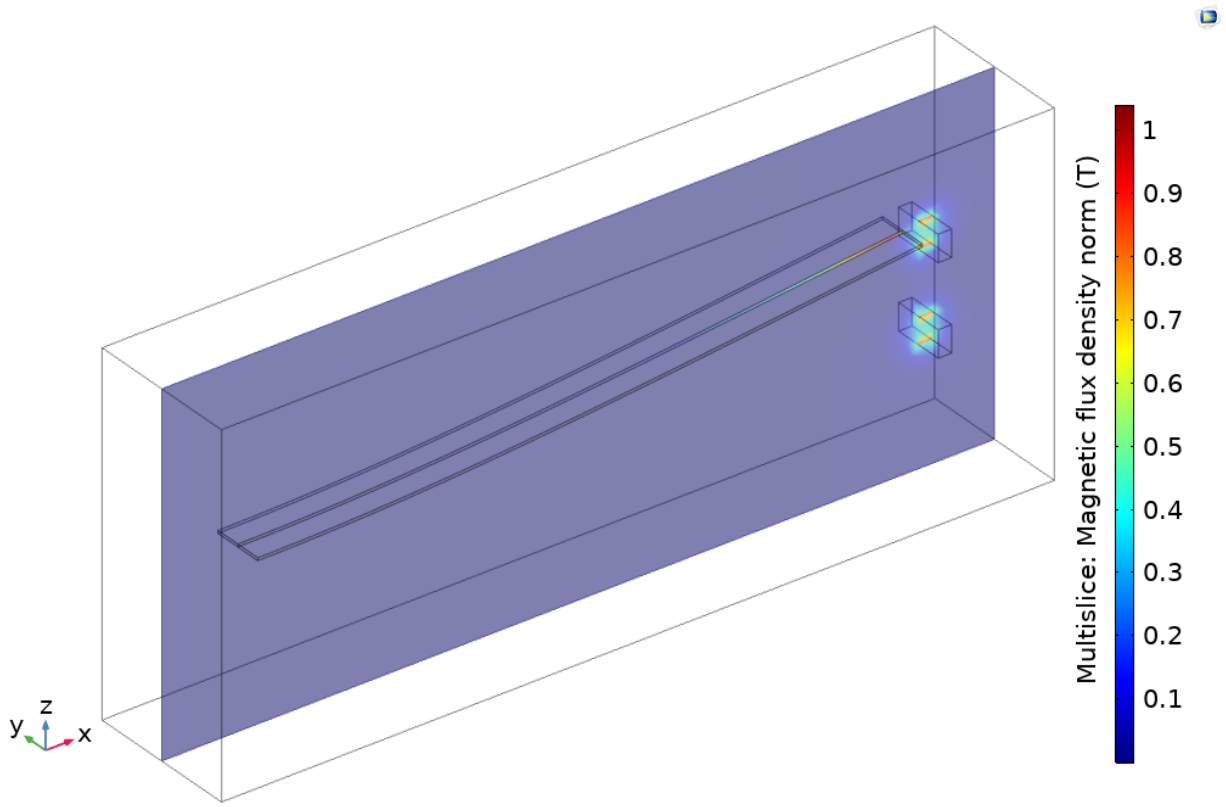

Fig. 7 Three-dimensional magnetic field simulation with COMSOL. To be seen is the geometry of the setup consisting of the magnets and the beam for an exemplary displacement of the beam. Additionally a slice (blue) is shown for the (normalized) magnetic flux density $\boldsymbol{B}$.

Computing the magnetoelastic force with COMSOL and processing the results analogous to the results in the first publication yields the following direct comparison of the bifurcation behavior of the equilibrium positions in figure 8 on the left and the corresponding frequencies in the same figure on the right. Note, that the results of the experiments and the two-dimensional force computation (taken from the first publication) are shown again to enable a direct comparison.

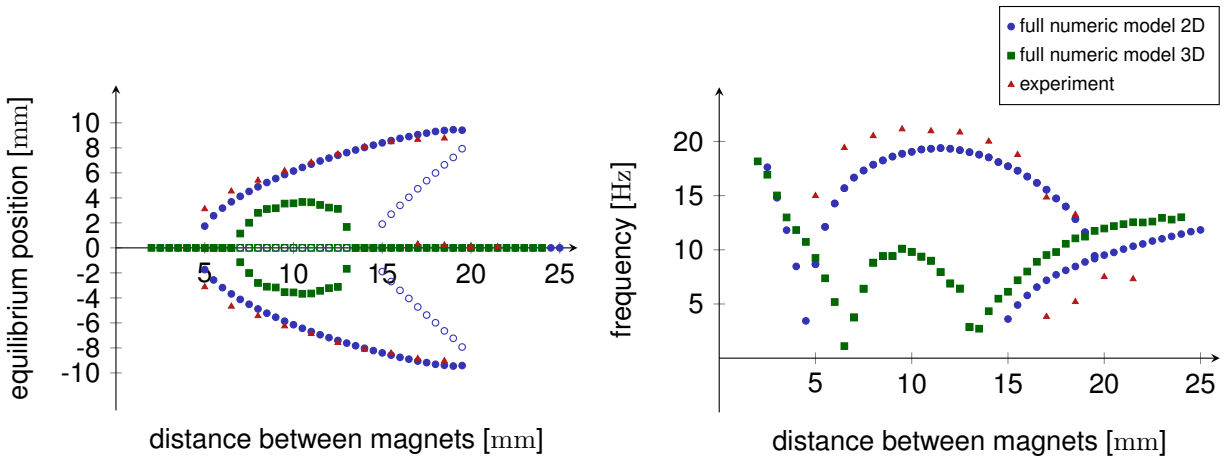

Fig. 8 Comparison of the results of the bifurcation behavior of the equilibrium positions (left) and frequencies (right) for different magnet distances for the two-dimensional case, the three-dimensional case and experiments.

As demonstrated, the deviations of the three-dimensional simulation to the experimental results are larger compared to those of the two-dimensional simulation. The magnet distances, where bistability exists, do not coincide with the experimentally determined magnet distances. Further, no tristability occurred in the three-dimensional force modeling. The equilibrium positions, as well as the corresponding frequencies are, in their absolute value, significantly smaller than found by experiments. The absolute values of the resulting forces are significantly smaller in the three-dimensional case. These surprisingly large deviations were discussed with the software support of COMSOL, which has confirmed the correct use of the software and the plausibility of the results.

A possible explanation of the fact that the two-dimensional simulation is providing better results than the three-dimensional simulation – without further investigation – is that the magnetic field in the two-dimensional case is assumed to be equally strong over the complete depth of the beam, but in the three-dimensional simulation decreases towards the edges, which results in smaller magnetic forces. Following this argumentation, it is possible that in both simulations the choice of the parameters for the magnetic materials is poor and coincidentally lead to better results in the two-dimensional case. Three different material parameters are to be considered, which are the remanent magnetic flux density (provided by the magnet supplier) and their relative permeability (taken from literature) and the relative permeability of the steel beam, which is the parameter of the highest uncertainty. Therefore, an adaptation of the permeability of the steel beam, by increasing its value, should result in larger forces and consequently a higher accordance of the three-dimensional case to the experiments. However, contrary to this perception, it does not yield results with higher accordance. Increasing the parameter, using double its value (2000), does not increase the forces significantly and consequently does not improve the accordance. There is a saturation of the force for large values of the permeability, a hypothesis which is also supported by the results in [Vanegas Müller, 2018]. There, different simulations of the force between magnet and beam are completed with varying permeability of the steel beam, showing that at some value for the permeability further increase of its value does not lead to larger forces. The threshold for this saturation is found to be significantly smaller than the initially used value of 1000, hence altering this value does not hold potential to improve the accordance to the experiments.

Other possible reasons for the deviations are that there are effects of the setup's reality, which are not covered by the linear stationary magnetic field simulation. So far not considered is the nonlinearity in the permeability of the beam material, which shows a pronounced hysteresis, as to be seen in figure 9 of [Noll et al., 2019a]. Once the beam is placed near the magnets it is retentive magnetized. Its previous magnetization due to an external magnetic field has an influence on its current magnetization. Further, deviations may result from the exact beam bending shape, or the assumption that the magnets are homogeneously magnetized with the constant exact remanent magnetic flux density and constant relative permeability. Additionally, uncertainties in the geometry of the experimental setup are not considered, especially its asymmetry and the size of the gap between beam tip and the upwards directed surface of the permanent. The setup does not allow a reproduction of a specific experiments with high accuracy, since the manual adjustment of magnet placement is imprecise.

7.2 Determination of the restoring force from measurements of forced vibrations

In the third publication, dynamic measurements are presented. The bistable beam, under the influence of a harmonic excitation, and its steady state, the stationary response, is captured and compared to predictions of the theoretical Duffing model found by the heuristic method, which is described in section 3.

The measurements conducted on the experimental setup can be used for more detailed investigations, particularly of the restoring force. The following approach explores an advanced heuristic method. In the basic heuristic method described in section 3, the position of the equilibria is determined, hence the states where the restoring force vanishes. In other words, the restoring is only known in these states (to be zero). In between the stable and unstable states, there is no information about the restoring force, which will be determined by considering dynamic measurements.This approach, where the restoring force is determined during dynamic experiments, was developed as well as performed in [Kienz, 2019] and also applied here. The equation of motion is reconsidered. A new notation is introduced, where the restoring term is not restricted to a cubic polynomial, but now kept a general nonlinear function R depending on the modal coordinate x, which is proportinal to the beam tip displacement. The other terms in the equation of motion can be determined using the measurements: x, $\dot{x}$ and the excitation $\ddot{b}$ are known (see [Noll et al., 2020]). Note that these quantities are measured as discrete values at distinct times t_i. Considering the equation of motion at certain discrete values of time, the values of the restoring term R_i can be found. Equation (2) of the third publication can be rewritten as

$$R_i(x_i) = g\ddot{b}_i - \ddot{x}_i - 2D\omega_1\dot{x}_i, \tag{15}$$

where the terms on the right side are all known from measurements and model assumptions, except the values of $\ddot{x}_i$, which can be determined numerical by a second derivation of x_i. These assumptions also regard the damping law, that is assumed to be a linear modal damping. In particular, there is a nonlinear damping expected, for instance due to the hysteresis of the magnetic material of the beam and its constant change of magnetization when moving through the external magnetic field. However, since the damping ration D of the system is small, the damping term is expected to be comparably small too.

The author has tried to determine $\ddot{x}_i$ by using the same approach as in the third publication, where the velocity $\dot{x}_i$ has been determined from a numerical differentiation of the time signal of the modal coordinate x_i. However, the results were not smooth enough unless when using a lowpass filter with such a small cut-off frequency that the characteristics of the original signal were changed drastically. Hence, another approach was used, which is more suitable. The time signal of the beam tip displacement is expanded in a Fourier series. This works well for periodic solutions, namely the intra- and (non chaotic) interwell solutions, but not for chaotic solutions. Thus, a restriction to periodic solutions only is made. When the signal is known as Fourier series, it is in the form of an analytic expression, which can easily be differentiated by time. This results in smooth signals, that can be evaluated at times t_i, and can be used as input for the right side of equation (15).

In the following steps, the equation of motion is, for reasons of simplicity, adapted so that the modal coordinate x_i is of the same value as the beam tip displacement $\hat{w}_i$, which means $\hat{w}_i = x_i\,\phi(L)$, where $\phi(L) = 1$ m. The continuous signal of the measured beam tip displacement is given by the following Fourier expansion

$$x(t) \approx \frac{\tilde{a}_0}{2} + \sum_{k\in K} \tilde{a}_k \cos\left(k\frac{2\pi}{T_0}\right) + \tilde{b}_k \sin\left(k\frac{2\pi}{T_0}\right), \tag{16}$$

which is a sum over specific $k \in K$ that are described later. T_0 is a base period to be chosen appropriately and the coefficients are given by

$$\tilde{a}_k = \frac{2(t_2 - t_1)}{T_0} \sum_i x_i \cos\left(k \frac{2\pi}{T_0} t_i\right) \tag{17}$$

$$\tilde{b}_k = \frac{2(t_2 - t_1)}{T_0} \sum_i x_i \sin\left(k \frac{2\pi}{T_0} t_i\right). \tag{18}$$

The choice of the frequencies to be considered is crucial to get a good approximation of the actual signal. Since the system is nonlinear, there are other frequencies probable besides the harmonic excitation frequency in the systems response. More precise, sub- and superharmonics are to be expected, which are even or uneven whole numbered fractions and multiples of the excitation frequency, depending on the kind of the solution (intra- or interwell). Therefore, consider the frequencies f_i

$$f_i = v_i \frac{\Omega}{2\pi}, \tag{19}$$

where all ratios v_i form a set V given as

$$V = \left\{ \frac{l}{m} \middle| 1 \leq l \leq 10 \text{ and } 1 \leq m \leq 7 \right\} = \left\{ \frac{1}{7}, \frac{1}{6}, ..., \frac{1}{3}, \frac{1}{2}, \frac{2}{7}, ..., 8, 9, 10 \right\}. \tag{20}$$

It includes many possible sub- and superharmonics, but also additional fractions of the excitation frequencies. This choice of V may seem arbitrary and very extensive, however it has produced very good results in the majority of the measurements. The set V contains 48 distinct fractions. In order to find K, which is the set of all k in equation (16), the greatest common divisor (GCD) is used and in the considered case given by

$$\mathrm{GCD}(V) = \frac{1}{420}. \tag{21}$$

The set K is then defined as

$$K = \left\{ \frac{v_i}{\mathrm{GCD}(V)} \middle| 1 \leq i \leq 48 \right\} = \left\{ 60, 70, 84, 105, ..., 3780, 4200 \right\}. \tag{22}$$

The largest period T_0, which is defined by the smallest considered frequency, is given by

$$T_0 = \min_i \left(\frac{2\pi}{v_i \Omega} \right) = \frac{14\pi}{\Omega}. \tag{23}$$

In the following figure 9 the measured (time discrete) signal of the beam tip displacement in blue and the continuous Fourier expansion of the signal in black of an exemplary intrawell solution are shown, where $T = 1/\Omega$. Both curves appear to be identical, due to their high consistency to each other.

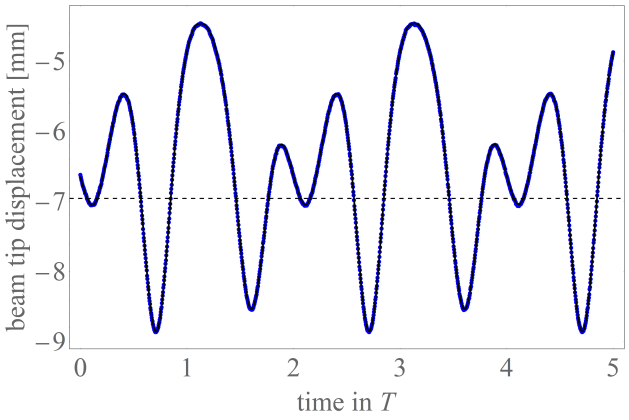

Fig. 9 Exemplary measured solution of the beam tip displacement during forced vibration (blue) for an harmonic excitation of amplitude $A = 3.81\ \mathrm{m/s^2}$ and excitation frequency of 8.5 Hz / $\eta \approx 0.64$ and corresponding Fourier expansion of the signal (black).

In the sets of figures 10 to 13, results of measurements are presented that correspond to the measurements shown in the third publication (in publication-figure 5). Left of these figures (in figures of this section), the phase diagram of each solution is shown again, when using the Fourier expanded signals, and on the right side of the figures, the corresponding restoring term, found by equation (15), is shown over the beam tip displacement. In the same figure, the restoring term according to the Duffing model is shown in black, which has been found by the heuristic method, described in section 3.
In the left figures, the phase diagrams, which can be compared to the phase diagrams found in the third publication, are shown. There, the signal of the velocity was found after a low pass filter and the numerical derivation of the discrete values of the beam tip displacement. As mentioned previously, in this section, a Fourier expansion of each signal with subsequent analytic differentiation is used. The phase diagrams look alike to the phase diagrams found in the third publication, which is an additional validation of the applied method.

Of particular interest are the figures on the right. There, a direct comparison of the restoring force found by the heuristic method to the restoring force found from the measurements is made. The results show the accordance of the heuristic restoring to the measured restoring force depends on the type of the solution that occurs.

When interwell solutions occur (red) the overall shape of the restoring term can be approximated by the heuristic model, which is a cubic polynomial. Especially towards large and also large negative displacements, both models have a fairly high accordance with each other. The equilibrium positions in the dynamic case concur with those static equilibria, thus the equilibria of the heuristic model. However, near to the trivial equilibrium (undeflected beam) the restoring shows larger deviations, and a tendency to change within this area for different solutions. It can be approximated by a polynomial, despite requiring a higher order than a cubic model.

Results for intrawell solutions (blue) are more complex. Not only that the restoring term shows some pronounced wavy forms, but it is also observed that it is not only a function of the displacement and others, as for specific displacements at different times, different restoring forces occur. Consequently, in the dynamic case there can be more than one position with a vanishing restoring force, which has never been observed in the static case by the author. Hence the restoring term cannot solely be described by a polynomial depending on the beam tip displacement. It might be, that the influence of the damping term, is higher in these cases. Possibly the large magnetic field close to the magnets causes intensive interactions that lead to a larger mismatch between theory and experiments and is to be investigated in more detail, which is not carried out in this dissertation.

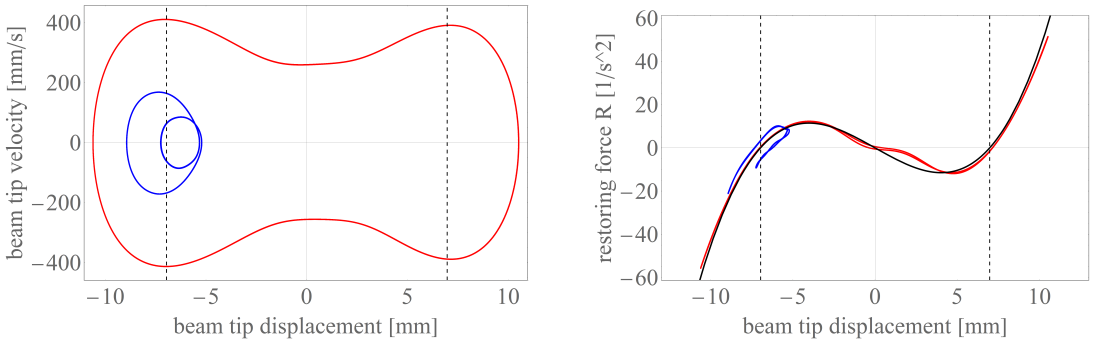

Fig. 10 Phase diagram (left) and restoring force (right) for harmonic excitation of frequency of 7 Hz / $\eta \approx 0.52$. Color code: intrawell in blue, interwell in red, heuristic cubic restoring force in black.

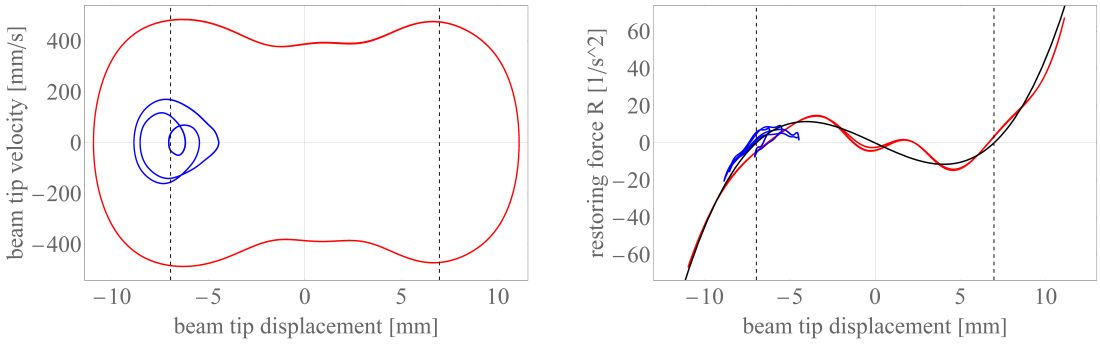

Fig. 11 Phase diagram (left) and restoring force (right) for a harmonic excitation of frequency of 8.5 Hz / $\eta \approx 0.64$. Color code: intrawell in blue, interwell in red, heuristic cubic restoring force in black.

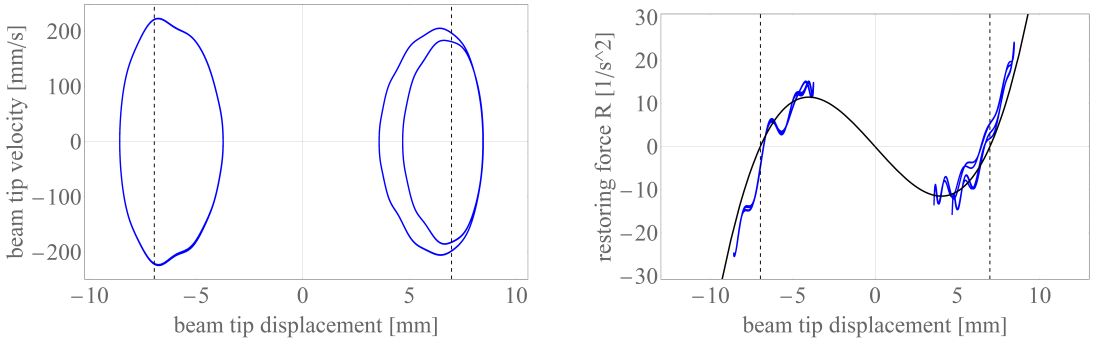

Fig. 12 Phase diagram (left) and restoring force (right) for a harmonic excitation of frequency of 14 Hz / $\eta \approx 1.05$. Color code: intrawell in blue, interwell in red, heuristic cubic restoring force in black.

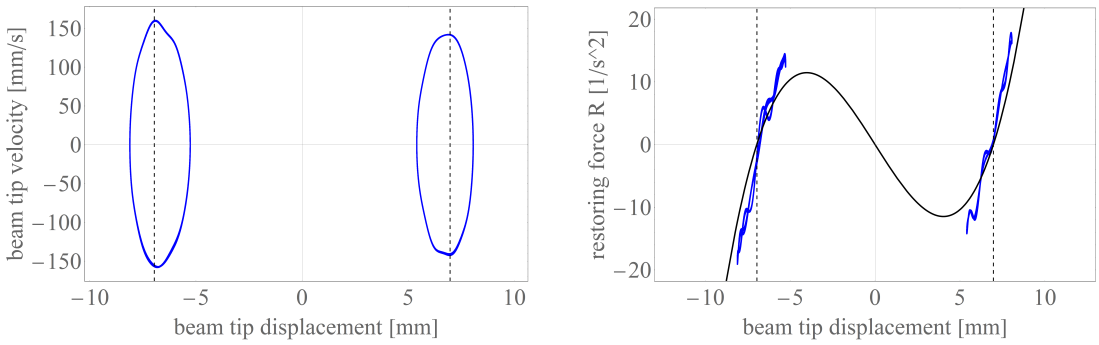

Fig. 13 Phase diagram (left) and restoring force (right) for a harmonic excitation of frequency of 17 Hz / $\eta \approx 1.27$. Color code: intrawell in blue, interwell in red, heuristic cubic restoring force in black.

8 Discussion and conclusions

This dissertation contributes to a more ambitious modeling of one popular nonlinear magnetoelastic energy harvesting system, whose main feature is the presence of two permanent magnets near the free end of a ferromagnetic beam. For simplicity's sake, only its mechanical part – without the piezos and the electrical circuit – is considered. The investigations presented give a deeper insight into the physical reality of an experimental setup of this subsystem, which is commonly modeled by the bistable Duffing oscillator. The cumulative dissertation, which encompasses three original publications, analyzes this specific type of model for suitability, and revisits model assumptions regarding the beam and the magnetoelastic forces exerted by the magnetic field of the permanent magnets. The dissertation furthermore endeavors to enable an optimization of the overall system through the establishment of a model based on the physical characteristics of the experimental setup, rather than heuristically derived model parameters, which are not directly connected to a considered setup.

In preparatory investigations prior to the three publications, the beam modeled on the basis of the linear Euler-Bernoulli beam theory is proven as suitable when it comes to describing its pure mechanical elastic restoring force. A further step examines the viability of accumulating the magnetoelastic force, which is distributed on the ferromagnetic beam in actual fact, at the beam's free end. This possibility is found to be applicable with negligible influence on the resulting model parameters. The publications, which are summarized in the following three paragraphs, treat both fundamental findings as underlying assumptions.

In the first publication, a procedure is shown to compute the magnetoelastic force numerically, in order to directly model the nonlinear restoring force of the setup. The intention was to find a method, other than the heuristic method, which gives a direct connection between the physical setup and the model originating from it, without necessitating the experimental setup to be built first. Here it is to be noted that, when comparing the accuracy of results found numerically to the results a heuristic model would provide, the accuracy of the heuristic model is, as expected, higher. This is due to the consideration of only the equilibrium positions and frequencies of the stable states, and the fact that the heuristic restoring force is defined to match these values. However, the restoring force determined numerically is not restricted to a cubic polynomial with only concurring equilibria and frequencies, but provides a more comprehensive model. Also it enables an optimizing of the energy harvesting system concerning its efficiency. In further research, a three-dimensional simulation, also linear and stationary, is completed to see if the accuracy of numerical results with the experimental results can be increased, which was so far not the case. The dissertation attributes the remaining discrepancies between the numerical and the experimental results to over-simplifications of the setup's reality, but does not investigate them in detail.

The second publication addresses the spatial discretization of the beam, and the assumption that the beam's deformation can be described only by the beam's first linear eigenfunction, which is commonly used to establish a single degree of freedom model. Therefore, experiments to determine the beam's shape are conducted. The beam during forced vibrations is captured in slow-motion video sequences, taken with a high-speed camera. Distinct markers are applied on the beam, and their movement is tracked over time. The resulting time signals of each beam marker are used to perform a Fast-Fourier analysis, in order to determine the frequencies of the beam's response. The vibration shape of the beam is determined for each frequency peak of the response. The results in the dynamic case, where no subharmonic responses of the harmonic excitation frequency occurred, show that the beam bends mostly in the shape of the first linear eigenfunction, and only has a small geometric share of the second eigenfunction in the case of superharmonic responses. For the part of the response in the same frequency as the excitation, the first eigenfunction is sufficient, at least in

the considered case, where the excitation frequency is close to the frequency of free vibrations of the beam in its stable equilibria. The results in general validate the choice of the beam model and justify the simplification that its bending shape is solely the beam's first eigenfunction. Furthermore, the results from the FEM simulations in the two-dimensional as well as the three-dimensional case remain significant (in both, the beam deformation shape is modeled by the first eigenfunction only). The geometric share of the second eigenfunction to the overall beam shape is smaller than the spatial discretization (characteristic length of the finite elements) in both simulations. The other initial question of interest answered in the second publication is whether nonlinear shape functions, depending, for instance, on the amplitude of the beam response, are needed and can possibly be used to reduce the required number of linear shape functions to sufficiently describe the beam deformation. In this respect, it is found that the dependency of the beam shape on the amplitude is covered by the first and second linear eigenfunction, and that it is not possible to eliminate the need of both by the use of a nonlinear shape function.

In the third paper, the predictions of the Duffing type model are compared to the results found on the experimental setup. Here, the focus is on the dynamic case of forced vibrations and the resulting steady state responses of the system. Therefore, extensive experiments with harmonic excitations of different but constant amplitude and frequency are done and compared to the results of numerical time integration. The theoretical model is the bistable Duffing model found by the heuristic method. It can be seen that, for excitations in a range around the frequency of free vibrations of the beam, the Duffing model is sufficient to cover most of the observed characteristics in the experiments, but there is a shift of the frequencies between numerics and experiment observable. This can cause errors when the Duffing model is used to predict frequencies of large orbit solutions with high energy output for the purpose of energy harvesting. In further investigations, the data obtained from the measurements is used to derive the nonlinear restoring force. This can be seen as an advanced heuristic method, since experimental data of a specific existing setup is considered to find the restoring force. The performed approach enables a determination of the restoring force for beam displacements other than the stable equilibrium positions, in contrast to static investigations done in the first publication. The results were two-sided: on the one hand, in general, the cubic restoring represented the overall restoring force in good agreement with the experimental data, especially towards large beam displacements. On the other hand, it can be seen that, especially for small beam displacements, the restoring force is not fixed. The shape of restoring force depends on the solution and is, in some cases, more complex than a simple cubic restoring function is able to represent. Also, it shows different behavior for different types of solutions. For intrawell solutions, where the beam is close to the magnets, a more complex restoring behavior can be observed with partly two beam tip positions with vanishing restoring force (on each side of the undeflected beam position), which has never been observed in the static case by the author.

Each of the publications contributes to an improvement of the overall model with its different aspects. The results give a deeper insight into the reality of the considered experimental setup. In most concerns, the Duffing oscillator, as a minimal model for the bistable beam, is capable of representing the main characteristics of the experimental data and the general model assumptions are a sufficient choice. A method to determine a model numerically, other than through a heuristic approach, is developed and constitutes a big step towards an optimization of the underlying energy harvesting system, although potential for an improvement of the accuracy of the numerically determined results remains.

References

[Adu-Manu et al., 2018] Adu-Manu, K. S., Adam, N., Tapparello, C., Ayatollahi, H., and Heinzelman, W. (2018). Energy-harvesting wireless sensor networks (eh-wsns): A review. *ACM Transactions on Sensor Networks (TOSN)*, 14(2):10.

[Anton and Sodano, 2007] Anton, S. R. and Sodano, H. A. (2007). A review of power harvesting using piezoelectric materials (2003–2006). *Smart materials and Structures*, 16(3):R1.

[Bard, 2019] Bard, S. (2019). Computation of the stationary probability density function of a stochastically excited bistable energy harvesting system. Master's thesis, TU Berlin.

[Bermúdez et al., 2016] Bermúdez, A., Rodriguez, A., and Villar, I. (2016). Extended formulas to compute resultant and contact electromagnetic force and torque from maxwell stress tensors. *IEEE Transactions on Magnetics*, 53(4):1–9.

[Bossavit, 2011] Bossavit, A. (2011). Virtual power principle and maxwell's tensor: which comes first? *COMPEL-The international journal for computation and mathematics in electrical and electronic engineering*, 30(6):1804–1814.

[Bossavit, 2014] Bossavit, A. (2014). On forces in magnetized matter. *IEEE Transactions on Magnetics*, 50(2):229–232.

[Brand et al., 2015] Brand, O., Fedder, G. K., Hierold, C., Korvink, J. G., and Tabata, O. (2015). *Micro energy harvesting*. John Wiley & Sons.

[Caliò et al., 2014] Caliò, R., Rongala, U. B., Camboni, D., Milazzo, M., Stefanini, C., De Petris, G., and Oddo, C. M. (2014). Piezoelectric energy harvesting solutions. *Sensors*, 14(3):4755–4790.

[Cao et al., 2015] Cao, J., Zhou, S., Wang, W., and Lin, J. (2015). Influence of potential well depth on nonlinear tristable energy harvesting. *Applied Physics Letters*, 106(17):173903.

[Carpenter, 1960] Carpenter, C. (1960). Surface-integral methods of calculating forces on magnetized iron parts. *Proceedings of the IEE-Part C: Monographs*, 107(11):19–28.

[Daqaq et al., 2014] Daqaq, M. F., Masana, R., Erturk, A., and Dane Quinn, D. (2014). On the role of nonlinearities in vibratory energy harvesting: a critical review and discussion. *Applied Mechanics Reviews*, 66(4).

[De Medeiros et al., 1998a] De Medeiros, L., Reyne, G., and Meunier, G. (1998a). Comparison of global force calculations on permanent magnets. *IEEE Transactions on magnetics*, 34(5):3560–3563.

[De Medeiros et al., 1999] De Medeiros, L., Reyne, G., and Meunier, G. (1999). About the distribution of forces in permanent magnets. *IEEE Transactions on Magnetics*, 35(3):1215–1218.

[De Medeiros et al., 1998b] De Medeiros, L., Reyne, G., Meunier, G., and Yonnet, J. (1998b). Distribution of electromagnetic force in permanent magnets. *IEEE transactions on magnetics*, 34(5):3012–3015.

[Derby and Olbert, 2010] Derby, N. and Olbert, S. (2010). Cylindrical magnets and ideal solenoids. *American Journal of Physics*, 78(3):229–235.

[Erturk et al., 2009] Erturk, A., Hoffmann, J., and Inman, D. J. (2009). A piezomagnetoelastic structure for broadband vibration energy harvesting. *Applied Physics Letters*, 94(25):254102.

[Erturk and Inman, 2011a] Erturk, A. and Inman, D. (2011a). Piezoelectric energy harvesting; John Wiley&Sons. *Ltd.: Chichester, UK*.

[Erturk and Inman, 2011b] Erturk, A. and Inman, D. J. (2011b). Broadband piezoelectric power generation on high-energy orbits of the bistable Duffing oscillator with electromechanical coupling. *Journal of Sound and Vibration*, 330(10):2339–2353.

[Fakhzan and Muthalif, 2013] Fakhzan, M. and Muthalif, A. G. (2013). Harvesting vibration energy using piezoelectric material: Modeling, simulation and experimental verifications. *Mechatronics*, 23(1):61–66.

[Gilbert and Balouchi, 2008] Gilbert, J. M. and Balouchi, F. (2008). Comparison of energy harvesting systems for wireless sensor networks. *International Journal of automation and computing*, 5(4):334–347.

[Griffiths and Reeves, 1999] Griffiths, D. J. and Reeves, A. (1999). Electrodynamics. *Introduction to Electrodynamics, 3rd ed., Prentice Hall, Upper Saddle River, New Jersey*, 301.

[Gross et al., 2011] Gross, D., Hauger, W., Schröder, J., Wall, W. A., and Bonet, J. (2011). *Engineering mechanics 2*. Springer.

[Hagedorn and DasGupta, 2007] Hagedorn, P. and DasGupta, A. (2007). *Vibrations and waves in continuous mechanical systems*. Wiley Online Library.

[Harb, 2011] Harb, A. (2011). Energy harvesting: State-of-the-art. *Renewable Energy*, 36(10):2641–2654.

[Harne and Wang, 2013] Harne, R. L. and Wang, K. (2013). A review of the recent research on vibration energy harvesting via bistable systems. *Smart materials and structures*, 22(2):023001.

[Ibrahim and Ali, 2012] Ibrahim, S. W. and Ali, W. G. (2012). A review on frequency tuning methods for piezoelectric energy harvesting systems. *Journal of renewable and sustainable energy*, 4(6):062703.

[Kienz, 2019] Kienz, P. (2019). Experimentelle Untersuchung des dynamischen Verhaltens eines bistabilen Energy Harvesting Systems unter harmonischer Anregung variabler Frequenz. Master's thesis, TU Berlin.

[Kim et al., 2011] Kim, H. S., Kim, J.-H., and Kim, J. (2011). A review of piezoelectric energy harvesting based on vibration. *International journal of precision engineering and manufacturing*, 12(6):1129–1141.

[Kim et al., 2015] Kim, M., Dugundji, J., and Wardle, B. L. (2015). Efficiency of piezoelectric mechanical vibration energy harvesting. *Smart Materials and Structures*, 24(5):055006.

[Kovacic and Brennan, 2011] Kovacic, I. and Brennan, M. J. (2011). *The Duffing equation: nonlinear oscillators and their behaviour*. John Wiley & Sons.

[Kumar et al., 2016] Kumar, A., Ali, S. F., and Arockiarajan, A. (2016). The Duffing-Holmes oscillator: A theoretical analysis of the magneto-elastic interactions. In *Conference on Nonlinear Systems & Dynamics IISER Kolkata*, volume 16, page 18.

[Kumar et al., 2015] Kumar, K. A., Ali, S., and Arockiarajan, A. (2015). Piezomagnetoelastic broadband energy harvester: Nonlinear modeling and characterization. *The European Physical Journal Special Topics*, 224(14-15):2803–2822.

[Lan and Qin, 2017] Lan, C. and Qin, W. (2017). Enhancing ability of harvesting energy from random vibration by decreasing the potential barrier of bistable harvester. *Mechanical Systems and Signal Processing*, 85:71–81.

[Lefevre et al., 1988] Lefevre, Y., Lajoie-Mazenc, M., and Davat, B. (1988). Force calculation in electromagnetic devices. In *Electromagnetic fields in electrical engineering*, pages 231–235. Springer.

[Leng et al., 2017] Leng, Y., Tan, D., Liu, J., Zhang, Y., and Fan, S. (2017). Magnetic force analysis and performance of a tri-stable piezoelectric energy harvester under random excitation. *Journal of Sound and Vibration*, 406:146–160.

[Lentz, 2018] Lentz, L. (2018). *Zur Modellbildung und Analyse von bistabilen Energy-Harvesting-Systemen*. PhD thesis, TU Berlin.

[Lentz et al., 2017] Lentz, L., Nguyen, H., and von Wagner, U. (2017). Energy harvesting from bistable systems under random excitation. *Machine Dynamics Research*, 41.

[Lentz and von Wagner, 2015] Lentz, L. and von Wagner, U. (2015). Multi-mode model of a piezomagnetoelastic energy harvester under random excitation. *PAMM*, 15(1):259–260.

[Litak et al., 2010] Litak, G., Friswell, M., and Adhikari, S. (2010). Magnetopiezoelastic energy harvesting driven by random excitations. *Applied Physics Letters*, 96(21):214103.

[Lumentut and Howard, 2013] Lumentut, M. and Howard, I. (2013). Analytical and experimental comparisons of electromechanical vibration response of a piezoelectric bimorph beam for power harvesting. *Mechanical Systems and Signal Processing*, 36(1):66–86.

[Maamer et al., 2019] Maamer, B., Boughamoura, A., El-Bab, A. M. F., Francis, L. A., and Tounsi, F. (2019). A review on design improvements and techniques for mechanical energy harvesting using piezoelectric and electromagnetic schemes. *Energy Conversion and Management*, 199:111973.

[Makarov and Rukhadze, 2009] Makarov, V. P. and Rukhadze, A. A. (2009). Force on matter in an electromagnetic field. *Physics-Uspekhi*, 52(9):937.

[Martens et al., 2013] Martens, W., von Wagner, U., and Litak, G. (2013). Stationary response of nonlinear magneto-piezoelectric energy harvester systems under stochastic excitation. *The European Physical Journal Special Topics*, 222(7):1665–1673.

[Matiko et al., 2013] Matiko, J., Grabham, N., Beeby, S., and Tudor, M. (2013). Review of the application of energy harvesting in buildings. *Measurement Science and Technology*, 25(1):012002.

[Moon, 1970] Moon, F. (1970). The mechanics of ferroelastic plates in a uniform magnetic field. *J. Appl. Mech.*

[Moon and Holmes, 1979] Moon, F. and Holmes, P. J. (1979). A magnetoelastic strange attractor. *Journal of Sound and Vibration*, 65(2):275–296.

[Moon and Pao, 1968] Moon, F. and Pao, Y.-H. (1968). Magnetoelastic buckling of a thin plate. *Journal of Applied Mechanics*, 35(1):53–58.

[Moon and Pao, 1969] Moon, F. and Pao, Y.-H. (1969). Vibration and dynamic instability of a beam-plate in a transverse magnetic field. *Journal of Applied Mechanics*, 36(1):92–100.

[Noll, 2016] Noll, M.-U. (2016). Entwicklung eines nichtlinearen Mehrfreiheitsgradmodells für einen bistabilen Schwinger unter Berücksichtigung eines stationären Magnetfeldes. Master's thesis, TU Berlin.

[Noll, 2018] Noll, M.-U. (2018). Energy harvesting system, figure. `https://figshare.com/articles/Energy_Harvesting_System/7492208/1`.

[Noll and Lentz, 2016] Noll, M.-U. and Lentz, L. (2016). On the refined modeling of the force distribution in a bistable magnetoelastic energy harvesting system due to a magnetic field. *PAMM*, 16(1):289–290.

[Noll and Lentz, 2017] Noll, M.-U. and Lentz, L. (2017). On the modeling of the distributed force in a bistable magnetoelastic energy harvesting system. Poster, presented in Oulu, Finland; to be found in the appendix.

[Noll et al., 2019a] Noll, M.-U., Lentz, L., and von Wagner, U. (2019a). On the improved modeling of the magnetoelastic force in a vibrational energy harvesting system. *Journal of Vibration Engineering & Technologies*, pages 1–11.

[Noll et al., 2019b] Noll, M.-U., Lentz, L., and von Wagner, U. (2019b). On the discretization of a bistable cantilever beam with application to energy harvesting. *Facta Universitatis, Series: Mechanical Engineering*, 17(2):125–139.

[Noll et al., 2019c] Noll, M.-U., Lentz, L., and von Wagner, U. (2019c). Correction to: On the improved modeling of the magnetoelastic force in a vibrational energy harvesting system. *Journal of Vibration Engineering & Technologies*, page 1.

[Noll et al., 2020] Noll, M.-U., Lentz, L., and von Wagner, U. (2020). Comparison of the dynamics of a Duffing equation model and experimental results for a bistable cantilever beam in magnetoelastic energy harvesting. submitted for publication in *Technische Mechanik. Scientific Journal for Fundamentals and Applications of Engineering Mechanics*.

[Overbeck, 2018] Overbeck, R. (2018). Generierung von Anregungsprozessen für ein Energy Harvesting System aus Messungen bei einer Fahrradfahrt. Bachelor's thesis, TU Berlin.

[Pankratov, 2019] Pankratov, I. (2019). Regelung eines elektrodynamischen Wandlers zur Erzeugung einer harmonischen Anregung eines Energy Harvesting Systems. Master's thesis, TU Berlin.

[Park et al., 2008] Park, G., Rosing, T., Todd, M. D., Farrar, C. R., and Hodgkiss, W. (2008). Energy harvesting for structural health monitoring sensor networks. *Journal of Infrastructure Systems*, 14(1):64–79.

[Paulo and Gaspar, 2010] Paulo, J. and Gaspar, P. D. (2010). Review and future trend of energy harvesting methods for portable medical devices. In *Proceedings of the world congress on engineering*, volume 2, pages 168–196.

[Pellegrini et al., 2013] Pellegrini, S. P., Tolou, N., Schenk, M., and Herder, J. L. (2013). Bistable vibration energy harvesters: a review. *Journal of Intelligent Material Systems and Structures*, 24(11):1303–1312.

[Rafique et al., 2018] Rafique, S., Rafique, and Quinn (2018). *Piezoelectric Vibration Energy Harvesting*. Springer.

[Reich, 2017] Reich, F. A. (2017). *Coupling of continuum mechanics and electrodynamics*. PhD thesis, TU Berlin.

[Reilly et al., 2009] Reilly, E. K., Miller, L. M., Fain, R., and Wright, P. (2009). A study of ambient vibrations for piezoelectric energy conversion. *Proc. PowerMEMS*, 2009:312–315.

[Reyne et al., 1987] Reyne, G., Sabonnadiere, J., Coulomb, J., and Brissonneau, P. (1987). A survey of the main aspects of magnetic forces and mechanical behaviour of ferromagnetic materials under magnetisation. *IEEE Transactions on magnetics*, 23(5):3765–3767.

[Rinaldi and Brenner, 2002] Rinaldi, C. and Brenner, H. (2002). Body versus surface forces in continuum mechanics: Is the Maxwell stress tensor a physically objective Cauchy stress? *Physical Review E*, 65(3):036615.

[Roundy et al., 2003] Roundy, S., Wright, P. K., and Rabaey, J. (2003). A study of low level vibrations as a power source for wireless sensor nodes. *Computer communications*, 26(11):1131–1144.

[Safaei et al., 2019] Safaei, M., Sodano, H. A., and Anton, S. R. (2019). A review of energy harvesting using piezoelectric materials: state-of-the-art a decade later (2008–2018). *Smart Materials and Structures*, 28(11):113001.

[Shaikh and Zeadally, 2016] Shaikh, F. K. and Zeadally, S. (2016). Energy harvesting in wireless sensor networks: A comprehensive review. *Renewable and Sustainable Energy Reviews*, 55:1041–1054.

[Tam, 2013a] Tam, J. I. (2013a). *Numerical and experimental investigations into the nonlinear dynamics of a magneto-elastic system*. PhD thesis, Princeton University.

[Tam, 2013b] Tam, J. I. (2013b). *Numerical and experimental investigations into the nonlinear dynamics of a magneto-elastic system*. Thesis poster, Princeton University.

[Tam and Holmes, 2014] Tam, J. I. and Holmes, P. (2014). Revisiting a magneto-elastic strange attractor. *Journal of Sound and Vibration*, 333(6):1767–1780.

[Tang et al., 2010] Tang, L., Yang, Y., and Soh, C. K. (2010). Toward broadband vibration-based energy harvesting. *Journal of intelligent material systems and structures*, 21(18):1867–1897.

[Tang et al., 2018] Tang, X., Wang, X., Cattley, R., Gu, F., and Ball, A. D. (2018). Energy harvesting technologies for achieving self-powered wireless sensor networks in machine condition monitoring: A review. *Sensors*, 18(12):4113.

[Toprak and Tigli, 2014] Toprak, A. and Tigli, O. (2014). Piezoelectric energy harvesting: State-of-the-art and challenges. *Applied Physics Reviews*, 1(3):031104.

[Tran et al., 2018] Tran, N., Ghayesh, M. H., and Arjomandi, M. (2018). Ambient vibration energy harvesters: A review on nonlinear techniques for performance enhancement. *International Journal of Engineering Science*, 127:162–185.

[Twiefel and Westermann, 2013] Twiefel, J. and Westermann, H. (2013). Survey on broadband techniques for vibration energy harvesting. *Journal of Intelligent Material Systems and Structures*, 24(11):1291–1302.

[Vanegas Müller, 2018] Vanegas Müller, E. A. (2018). Untersuchung der Kraftverteilung auf einen Balken innerhalb eines inhomogenen Magnetfeldes. Bachelor's thesis, TU Berlin.

[Wang and Meng, 2013] Wang, H. and Meng, Q. (2013). Analytical modeling and experimental verification of vibration-based piezoelectric bimorph beam with a tip-mass for power harvesting. *Mechanical Systems and Signal Processing*, 36(1):193–209.

[Wauer, 2014] Wauer, J. (2014). *Kontinuumsschwingungen*. Springer.

[Wei and Jing, 2017] Wei, C. and Jing, X. (2017). A comprehensive review on vibration energy harvesting: Modelling and realization. *Renewable and Sustainable Energy Reviews*, 74:1–18.

[Williams and Yates, 1996] Williams, C. and Yates, R. B. (1996). Analysis of a micro-electric generator for microsystems. *Sensors and Actuator's a: Physical*, 52(1-3):8–11.

[Wu et al., 2014] Wu, Y., Zuo, L., Zhou, W., Liang, C., and McCabe, M. (2014). Multi-source energy harvester for wildlife tracking. In *Active and Passive Smart Structures and Integrated Systems 2014*, volume 9057, page 905704. International Society for Optics and Photonics.

[Yildirim et al., 2017] Yildirim, T., Ghayesh, M. H., Li, W., and Alici, G. (2017). A review on performance enhancement techniques for ambient vibration energy harvesters. *Renewable and Sustainable Energy Reviews*, 71:435–449.

[Zhou et al., 2013] Zhou, S., Cao, J., Erturk, A., and Lin, J. (2013). Enhanced broadband piezoelectric energy harvesting using rotatable magnets. *Applied Physics Letters*, 102(17):173901.

[Zhou et al., 2014] Zhou, S., Cao, J., Inman, D. J., Lin, J., Liu, S., and Wang, Z. (2014). Broadband tristable energy harvester: modeling and experiment verification. *Applied Energy*, 133:33–39.

[Zhou and Zuo, 2018] Zhou, S. and Zuo, L. (2018). Nonlinear dynamic analysis of asymmetric tristable energy harvesters for enhanced energy harvesting. *Communications in Nonlinear Science and Numerical Simulation*, 61:271–284.

[Zhou et al., 2018] Zhou, Z., Qin, W., and Zhu, P. (2018). Harvesting performance of quad-stable piezoelectric energy harvester: Modeling and experiment. *Mechanical Systems and Signal Processing*, 110:260–272.

[Zhou et al., 2016] Zhou, Z.-Y., Qin, W.-Y., and Zhu, P. (2016). Energy harvesting in a quad-stable harvester subjected to random excitation. *AIP Advances*, 6(2):025022.

Appendix [Noll and Lentz, 2017]

Energy Harvesting
M. Sc. Max-Uwe Noll, M. Sc. Lukas Lentz
MMD Mechatronische Maschinendynamik
Prof. Dr.-Ing. Utz von Wagner
berlin

On the Modeling of the Distributed Force in a Bistable Magnetoelastic Energy Harvesting System

The performance of linear vibrational Energy Harvesting systems is best when the excitation frequency is close to the systems resonant frequency. To overcome this limitation nonlinearities are introduced. The system shown in figure 1 is investigated. Its modeling is usually done by representing the influence of the magnets by a cubic single load. The current work presents an improved model where a distributed transverse and a distributed lateral magnetoelastic load are considered.

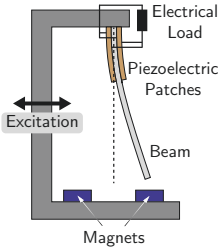

Fig. 1: Energy Harvester [1]

Modeling

I Mechanical Model

- The PDE of a prestressed Euler-Bernoulli beam is given by

$$\mu\ddot{w} + EIw'''' = q + [Nw']'$$

where q is a distributed transverse load and N a resultant of a distributed normal load, both depending on the position on the beam and its displacement.

- A single mode approximation for the beam tip displacement w_L in a Galerkin scheme yields

$$\ddot{w}_\mathrm{L} + \underbrace{\omega_0^2\, w_\mathrm{L}}_{\mathrm{F_{el}}} = \underbrace{\phi(L)\int_0^L q\,\phi\,\mathrm{d}x}_{\mathrm{F_{m1}}} \underbrace{- w_\mathrm{L}\int_0^L N\,\phi'^2\,\mathrm{d}x}_{\mathrm{F_{m2}}},$$

where $\mathrm{F_{el}}$ is the elastic restoring force and $\mathrm{F_{m1}}$ as well as $\mathrm{F_{m2}}$ the load due to the transverse and the lateral forces.

II Magnetic Field

- The magnetic field is computed for a large number of possible beam displacements by a stationary 2D-FEM simulation.
- The displaced beam is in contrast to [2] considered in each simulation to regard its feedback effects on the magnetic field.

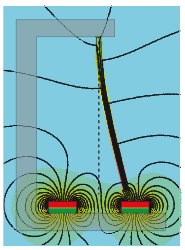
Fig. 2: Magnetic Field

III Distributed Force

- The force is determined using the Maxwell stress tensor $\boldsymbol{T}$ given by

$$T_{ij} = B_i H_j - \frac{1}{2}\,\delta_{ij}\,\boldsymbol{B}\cdot\boldsymbol{H}.$$

- The force on a finite beam element is as stated in [3] computed by a limit process from outside the element towards its boundary by

$$\boldsymbol{F} = \oint_{\partial\Omega} \boldsymbol{T}\,\boldsymbol{n}\,\mathrm{d}x.$$

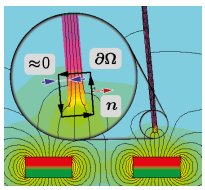

Fig. 3: Force on Element

Results

- The resultant load is a nonlinear function of the position on the beam, its displacement and the shape of the deflected beam.
- The major influence of the distributed load is observed at the beam tip.
- The distributed load is reduced to an equivalent single load for different distances between the magnets.
- The distance between the magnets changes the systems characteristics regarding its equilibrium positions as well as the corresponding "linearized frequencies".
- The minimal polynomial degree of a nonlinear approximation of the load capable to represent all equilibrium positions is three or five depending on the distance between the magnets.

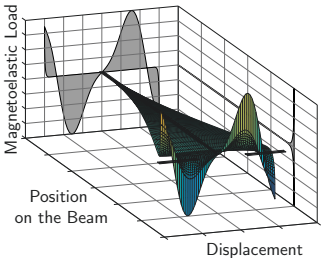

Fig. 4: Distributed Load

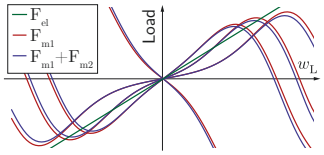

Fig. 5: Single Load

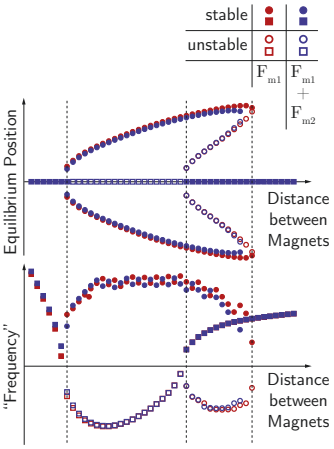

Fig. 6: Bifurcation Behavior

Future Work

- The next step is an investigation of the influence of the chosen underlying beams bending form on the load.
- Furthermore, an experimental validation of the computed magnetoelastic force will be done.

Key References

[1] A. Erturk, J. Hoffmann and D. J. Inman, A Piezomagnetoelastic Structure for Broadband Vibration Energy Harvesting, Applied Physics Letters 94, 254102 (2009)

[2] J. I. Tam and P. J. Holmes, Revisiting a Magneto-Elastic Strange Attractor, Journal of Sound and Vibration 333, 1767-1780 (2014)

[3] A. Bermúdez, A. L. Rodríguez and I. Villar, Extended Formulas to Compute Resultant and Contact Electromagnetic Force and Torque from Maxwell Stress Tensors, IEEE Transactions on Magnetics (2016)

Funded by
DFG Deutsche Forschungsgemeinschaft
Project-Nr.: WA 1427/23-1,2

Institut of Applied Mechanics, Chair of Mechatronics and Machine Dynamics, Technische Universität Berlin, Einsteinufer 5, 10587 Berlin, Germany